RESOLV
RUHR EXPLORES SOLVATION
CLUSTER OF EXCELLENCE - EXC 2033

RUB

Analyzing Solvent Effects on Halogen-bonded Ion Pairs with Wavefunction Methods Combined with COSMO

by

Sarah Karbalaei Khani

Dissertation submitted in partial fulfillment
of the requirements for
the degree of a Doctor in Natural Sciences (Dr. rer. nat.)

RUHR-UNIVERSITÄT BOCHUM

FAKULTÄT FÜR CHEMIE UND BIOCHEMIE

LEHRSTUHL FÜR THEORETISCHE CHEMIE

Acknowledgment

First, I would like to express my deep gratitude to my supervisor Prof. Dr. Christof Hättig for all the support, encourage and opportunities he has given me. I appreciate all his contributions of time, ideas and funding in my PhD studies to make it a great and rich experience for me.

I would like to acknowledge my committee members: Prof. Dr. Lars Schäfer, who is also my second supervisor, and Prof. Dr. Sonia Coriani for their time, interest and insightful comments. I have had the pleasure to work in the group of Prof. Coriani during my internship at DTU in 2018 and I very much appreciate our collaboration in the MCD project.

I give thanks to the Cluster of Excellence RESOLV for funding my PhD studies and for organizing practical events which helped me to enhance my skills.

I am grateful to my colleagues in the group of Christof Hättig who have been a source of friendship and joy for me. They have contributed highly in my personal and professional improvements.

Lastly, I would like to highly thank my loving, supporting and encouraging husband, Alireza, and my parents, siblings and nieces.

Sarah K. Khani

Ruhr Universität Bochum

July 2019

Contents

1 Introduction **4**

1.1 Continuum Solvent Models 8

1.2 Reaction Field Theory 12

1.3 The Wavefunction-based Methods 15

1.3.1 Algebraic Diagrammatic Construction ADC 16

1.3.2 Second-order Approximate Coupled Cluster Singles and Doubles Model CC2 19

1.4 Electronic Spectroscopy 21

2 COSMO-RI-ADC(2) excitation energies and excited state gradients **30**

3 UV absorption and magnetic circular dichroism spectra of purine, adenine, and guanine: A coupled cluster study in vacuo and in aqueous solution **41**

4 Solvent effects on the absorption and fluorescence of halogen-bonded ion pairs **56**

5 Comparison of reaction field schemes for coupling continuum solvation models with wavefunction methods for excitation energies **80**

6 Outlook **102**

Appendices **104**

1 Introduction

Ab initio methods are divided into wavefunction-based methods (single-reference methods including Møller-Plesset Perturbation Theory (MPPT), Configuration Interaction (CI) and Coupled cluster (CC), and multi-reference methods and new approaches including Quantum Monte Carlo and density matrix renormalization group (DMRG)) and electron-density-based methods (density functional theory (DFT)). Since for DFT the exact XC functional is unknown, approximate ones must be employed to account for the electron correlation. Also, in case of wavefunction methods, since achieving the exact solution is computationally too expensive, approximate methods have to be used instead. In general, there are two possibilities for the calculation of excitation energies: one possibility is to optimize the wavefunction for the ground and excited states and calculate the difference as the excitation energy and the other one is to calculate excitation energies from the response of the ground state using response theory. The former approach usually requires multi-reference methods, which are from the onset more expensive than single-reference methods, while the latter approach does not necessarily need multi-reference methods and can also be applied for DFT, which is then called time-dependent DFT (TDDFT). However, a disadvantage of response theory arises from the strong dependence of the accuracy and applicability on the excitation level (single, double, etc.).

Configuration interaction singles (CIS), coupled cluster singles (CCS) and time-dependent Hartree-Fock (TDHF) are old methods that have been widely used to treat excited states where TDHF is also known as random phase approximation (RPA) and CIS and CCS as the

Tamm-Dancoff approximation (TDA). [1] TDDFT has become today one of the most well-known methods for the calculation of excited states of medium-sized to large molecules. [2] On the other hand, TDDFT with semi-local functionals (LDA, GGA, mGGA, etc.) cannot accurately describe non-local excitations like charge transfer (CT) and Rydberg excitations. For that purpose, DFT requires functionals with 100% long-range exchange. Furthermore, if the adiabatic approximation is used, DFT is limited to single excitations. [3,4] Within the wavefunction-based methods electron correlation is accounted for by including successively higher excited determinants in the wavefunction ansatz. Configuration interaction (CI) methods can be applied at a truncated level (configuration interaction singles and doubles (CISD), configuration interaction singles, doubles and triples (CISDT), etc.) but show a slow convergence towards the full CI (FCI) limit. In contrast to CI, coupled cluster (CC) is a size extensive method that can treat dynamic electron correlation in a very accurate way for both ground and excited states and is widely used for the computation of atomic and molecular properties for single reference systems. The systematic hierarchy of the CC approach with increasing accuracy is given as CC singles (CCS), approximate CC singles and doubles (CC2), CC singles and doubles (CCSD), approximate CC singles, doubles and triples (CC3), etc., for which the response theory to treat excited state energies and properties has been implemented. [5] Along with CC methods, the algebraic diagrammatic construction (ADC) scheme for the polarization propagator delivers a series of *ab initio* methods for the calculation of excited states based on perturbation theory. [6, 7]

Many spectroscopic experiments are conducted in the condensed phase. Even though in many cases the absorption and emission of the solute is the matter of interest, solvents

may influence these processes. For instance, electronic states with larger dipole moments are more stabilized by polar solvents than states with small dipole moments and also the solvent-induced changes of the lifetime of excited states may lead to different relaxation pathways. In quantum chemical calculations of molecular properties, however, describing the whole system in solution is not so straightforward since the dynamics of the system play often a more significant role than in the gas phase and a large number of configurations of the solvent have to be sampled to produce representative results. For instance, in case of polarizable embedding (PE) calculations for molecules in solution, a few hundreds of configurations should be used. [8–10]

There are various approaches to account for solvent effects into the reaction media. *Ab initio* molecular dynamics (AIMD) is computationally a demanding approach which treats the full (solute+solvent) system at the quantum mechanical (QM) level, but is mainly restricted to DFT (TDDFT is challenging to use in AIMD). QM/MM with a polarizable molecular mechanics (MM) system coupled with molecular dynamics (MD) is another approach that, although computationally more affordable than AIMD, is still very costly. Besides the computational cost, the parametrization of the MM part, which for electronic transitions should preferably be polarizable, can be complicated for this approach. Continuum solvation models (CSMs) are significantly more affordable than the other two approaches while they do not require sampling and are easier to parametrize. CSMs have, on the other hand, problems to describe specific solute-solvent interactions like hydrogen bonds and also solute-solvent interactions beyond electrostatics such as dispersion and Pauli repulsion. For the present study, in order to treat the problem at a QM level beyond

DFT, the conductor-like screening model (COSMO) as a CSM was selected as a suitable approach to take the solvent effects into account.

The principal objective of this Ph.D. thesis is to study solvent effects on photochemistry such as photo-excitation and photo-deexcitation mechanisms of organic molecules, in particular halogen-bonded systems. Towards this end, we aimed to take advantage of COSMO as a computationally affordable approach for taking the averaged effect of the solvent into account. Given the deficiencies of TDDFT mentioned above, using the currently available PCM-TDDFT methods was not an appropriate choice for our studies on electronic excitations. Also the PCM-CCSD approach, which goes beyond the HF method, imposes high computational cost even for medium-sized molecules and does not produce good geometries. Hence, by the implementation of COSMO-RI-CC2 (RI stands for the resolution of identity approximation) and COSMO-RI-ADC(2) (ADC(2) stands for the polarization propagator in second order of perturbation theory) for electronic excitation energies and excited state analytic gradients in the TURBOMOLE program package, [11] we have provided new computational tools that surpasses DFT particularly for CT electronic states in accuracy and yet with affordable computational cost for small- and medium-sized molecules.

In the following subsections, I explain the concept of continuum solvent models and then the reaction field scheme we selected and implemented in the TURBOMOLE software to combine the continuum solvent model with coupled cluster theory and algebraic diagrammatic construction as the QM methods. Furthermore, as an application of the new computational tools mentioned above, we analyzed the spectroscopic properties of DNA nucleobases and halogen-bonded complexes in solution.

1.1 Continuum Solvent Models

As indicated in the previous section, for different applications different solvation models and QM methods are used in order to achieve the required accuracy at a reasonable computational cost. One type of approach is based on a discrete molecular (explicit) description of the medium, *e.g.* a molecular mechanics (MM) description for the environment. Another approach, called 3D-RISM, [12] is based on the molecular integral equation (IE) [13] theory that unlike molecular dynamics-based approaches is fast and noise-free but still incorporates the microscopic nature of solute-solvent interactions. The third type is the continuum (or implicit) description of the solvent according to which the microscopic nature of the environment is withdrawn and it is replaced by a dielectric.

There are two principal advantages of continuum solvation models. The first is the reduced number of degrees of freedom that have to be treated explicitly and the second advantage is the limited number of parameters such as nuclear radii, dielectric constant and refractive index.

In all continuum models the solute (a molecule or few molecules) forms a cavity within the dielectric medium imitating the solvent. It is generally accepted that the cavity shape should reproduce the molecular shape; otherwise this may lead to deformations in the charge distribution after solvent polarization with large unrealistic effects on the results, especially for properties. Cavities are generally adopted as interlocked spheres with van der Waals (vdW) radii, each centered on a selected atom of the solute. The solute-solvent interaction is explained by a mutual polarization of the solute charge distribution inside

the cavity and the dielectric continuum. In order to solve the electrostatic problem, in 1994 Tomasi and Persico introduced six different approaches, namely, apparent surface charge (ASC) methods, the multipole expansion (MPE) methods, the generalized Born approximation (GBA), the image charge (IMC) methods, the finite element methods (FEM), and the finite difference methods (FDM). [14] From these approaches, the apparent surface charge (ASC) models comprise the most popular subclass of dielectric continuum approaches to accounts for the potential operator, which describes the electrostatic interaction of the solute with the solvent. Among continuum models, the so-called polarizable continuum model (PCM) was originally developed to combine with *ab initio* QM methods for the description of solvent effects on isolated molecules. This model was initially developed in Pisa in 1981 by Miertuš *et al.* [15] In the first formulation, the PCM surface charge approach (indicated as dielectric PCM or DPCM) was calculated by defining the electrostatic charge appearing at the surface of molecular cavity, which separates two regions with dielectric permittivity 1 inside the cavity and ε outside the cavity (ε is the dielectric constant). [15, 16] This model requires the solution of a classical electrostatic Poisson problem for the potential

$$-\vec{\nabla} \times [\varepsilon(\vec{r})\vec{\nabla}V(\vec{r})] = 4\pi\rho_M(\vec{r}) \ , \tag{1}$$

where ρ_M is the solute charge distribution and $\varepsilon(\vec{r})$ is the general Poisson-dependent permittivity. The electrostatic potential in equation 1 can be solved with regard to another potential V, which is the sum of the electrostatic potential generated by the solute charge distribution ($V_M(\vec{r})$) and the one generated by the polarization of the dielectric medium

($V_\sigma(\vec{r})$), [17]

$$V(\vec{r}) = V_M(\vec{r}) + V_\sigma(\vec{r}) \ . \tag{2}$$

The first formulation of the apparent charge distribution $\sigma(\vec{s})$, which is applied for the DPCM model, was

$$\sigma(\vec{s}) = \frac{\varepsilon - 1}{4\pi\varepsilon} \frac{\partial}{\partial n}(V_M + V_\sigma) \ . \tag{3}$$

An alternative definition of the PCM charge distribution was devised by Klamt and Schüürmann in 1993 [18], in which the dielectric constant of the solvent is changed from the specific finite value ε for each solvent to infinity. The value corresponds to that of a conductor and the model is called conductor-like screening model (COSMO). The fundamental difference between COSMO and other apparent surface charge dielectric models is the adoption of a scaled conductor boundary condition rather than the exact dielectric boundary condition. Based on this assumption, the solution of the PCM electrostatic equation is no longer needed because the sum of the two potentials mentioned above cancels out on the cavity surface ($V(\vec{r}) = V_M(\vec{r}) + V_\sigma(\vec{r}) = 0$). [19, 20] Inspired by the notations introduced in the both PCM and COSMO literature, the COSMO boundary condition is formulated as

$$0 = f(\varepsilon)V_M(\vec{s}) + \mathcal{A}S\sigma(\vec{s}) \ , \tag{4}$$

where S is a diagonal matrix with the cavity segment areas as elements and $V_M(\vec{s})$ is the vector of the solute electrostatic potential on the cavity segments. $\mathcal{A}$ is the symmetric Coulomb interaction matrix of the charges on the segments with diagonal elements

representing the self-interactions and is defined as

$$\mathcal{A}_{ij} = \begin{cases} 1/(\mathbf{t}_i - \mathbf{t}_j) & \text{for} \quad i \neq j \\ \\ 3.8\sqrt{S_i} & \text{for} \quad i = j \ , \end{cases} \tag{5}$$

where $\mathbf{t_i}$ and S_i are the center and the area of segment i, respectively. Figure 1 shows an example of the segments on the COSMO cavity. [18] The scaling factor $f(\varepsilon)$, which assures that we are modeling a dielectric and not a conductor, can be written as

$$f(\varepsilon) = \frac{\varepsilon - 1}{\varepsilon + x} \ . \tag{6}$$

In the original implementation of COSMO, for neutral compounds the value of $x = 0.5$ gave the most accurate results while for ions in low dielectric solvents the choice of $x = 0$ is preferable [19, 21]. Within the PCM model family, the $x = 0$ choice has been preferred for neutral compounds and the model is known as CPCM. [22]

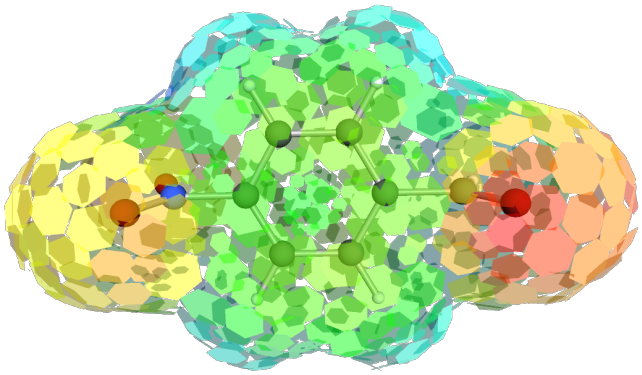


Figure 1: An example of the discretization of COSMO cavity into hexagonal and/or trigonal segments.

One of the advantages of COSMO over other dielectric continuum solvation models is its

stability with regard to artifacts coming from the small percentage of solute charge density that reaches out of the cavity, the so-called outlying charge correction. The outlying charge errors (OCEs) have been a significant problem for the DPCM. [17] For the interpretation of the apparent surface charge distribution, an alternative algorithm was introduced by Cancès and Mennucci, [23, 24] the so-called integral equation formalism IEF-PCM, which reduces the OCEs of the original DPCM formulation. This model has been derived within a more mathematically founded framework than the DPCM and CPCM alternatives, while at the same time, it contains both DPCM and CPCM as its subcases. Later on, in 2000, another method called SS(V)PE was offered by Chipman [25], which is identical with IEF-PCM. Since IEF-PCM is the name of the method in Gaussian 09, some people denote the SS(V)PE/IEF-PCM shortly as IEF-PCM method. The results for IEF-PCM and CPCM can be almost identical for neutral compounds and ions if $x = 0.5$ and $x = 0$ are applied in the COSMO scaling function. Furthermore, the comparison of COSMO, IEF-PCM and SS(V)PE reveals that the deviations for solvation energy are in the range of 0.3 kJ$\cdot$ mol^{-1}. [21]

1.2 Reaction Field Theory

In the previous section, I have introduced different continuum solvent models and explained how the electrostatic equations are solved within the framework of our target model, COSMO. This section briefly describes how to combine the solvent contributions with the quantum mechanical description of the solute.

The reaction field is generated from a solute charge distribution. The coupling of a continuum description of a solvent, like PCM and COSMO, with a QM description of a solute is based on the definition of an effective Hamiltonian leading to a nonlinear Schrödinger equation [26] as

$$\{\hat{H}^{\text{vac}} + \langle\Psi|\hat{Q}|\Psi\rangle \cdot \hat{V}\}|\Psi\rangle = E|\Psi\rangle \ , \tag{7}$$

where $\hat{H}^{\text{vac}}$ is the vacuum Hamiltonian, the operator $\hat{V}$ measures the solute potential on the cavity surface and the operator $\hat{Q}$ measures the surface charge. Since the continuum model averages over the configurational space of the solvent, the electrostatic energy for COSMO for variational methods, like HF, represents free energies. For the free energies the work associated with polarizing the continuum should be taken into account, which equals to the half of the electrostatic energy. Thus, for the equilibrated system in the ground state the free energy is

$$G^{\text{solv}} = \langle\Psi|\hat{H}^{\text{vac}} + \frac{1}{2}\langle\Psi|\hat{Q}|\Psi\rangle \cdot \hat{V}|\Psi\rangle \ . \tag{8}$$

Regarding the definition of the reaction field, the more accurate the charge distribution, the more accurate the reaction field. This indicates that the charge distribution from correlated methods will provide higher accuracy. Different levels of integration of the continuum model and the QM method can be categorized in four main groups including the perturbation to energy (PTE) scheme, the perturbation to density (PTD) scheme [27], post-SCF [28] and the iterative perturbation to energy and density (PTED) scheme [26]. In the PTED approach, the self-consistent reaction field of a selected ground- or excited state is determined by iterating the solution of the Hartree-Fock (HF) and post-HF wavefunction

and the corresponding density until the surface charges achieved from the relaxed density converged within a numerical threshold to self-consistent values. On the other hand, the simplest non-iterative PTE approach engages the polarized HF molecular orbitals for the subsequent post-HF calculations. The PTD approach involves the computation of SCF orbitals and the ground state post-HF density in vacuum follow by the calculation of solvation energy with correlated gas-phase density. In case of excitation energies and transition moments, PTED is a more accepted approach for the fast (electronic) polarizability of the environment as it takes both the equilibrium and non-equilibrium solvent effects into account. However, for the slow (nuclear or orientational) polarizability of the environment, especially if the investigated process is faster than the solvent nuclear relaxation, the environment cannot equilibrate and the PTED scheme becomes problematic. The PTED scheme is computationally more involved compared to the PTE and PTD. Furthermore, for the implementation of molecular geometries in the electronic excited state the entire PTED scheme becomes challenging. On the other hand, the PTE scheme, which is computationally more affordable, does not provide a proper description of the excited state as it only uses the reaction field calculated from the HF density.

In the current thesis, the principal aim is to combine the COSMO and the post-HF ADC(2) and CC2 methods for the computation of excited state energies and analytic gradients. For this purpose, we have adopted the post-SCF scheme [28] as an alternative approach to the more accepted but computationally expensive PTED scheme by producing a reaction field that goes beyond the less accurate PTE and PTD schemes with about the same computational cost.

The next section describes the QM methods we have combined with COSMO to calculate the ground- and excited state properties of organic molecules in an isotropic environment.

1.3 The Wavefunction-based Methods

After having selected the reaction field to account for the polarizable isotropic environment, we have to choose a theoretical method which is computationally efficient and at the same time accurate enough to deliver a conclusive solution to the investigated photochemical problem. In the case of large molecules, this can be particularly difficult because their excited states are usually close in energy but carry very different electronic structures (*e.g.* $\pi\pi^*$, $n\pi^*$, charge transfer, Rydberg, or doubly excited). Nowadays, for medium-sized and large molecules accurate benchmarks are mostly generated by wavefunction-based *ab initio* methods, comprising well-known methods like complete-active space self-consistent field (CASSCF) in combination with second-order perturbation theory (CASPT2), the approximate coupled-cluster schemes of second and third order, CC2 and CC3, and the algebraic diagrammatic construction (ADC) scheme of the polarization propagator in second and third order of perturbation theory, ADC(2) and ADC(3). Among these methods, we applied, for both method development and applications, the second-order methods ADC(2) and CC2. The following subsections briefly introduce these methods and their relations to each other.

1.3.1 Algebraic Diagrammatic Construction ADC

The ADC scheme of the polarization propagator for electronically excited states arises from many-body Green's function theory and describes the time evolution of the polarization of a many-electron system. [7, 29] For the electronic Hamiltonian of molecules, the latter function includes building blocks called propagators. The one-electron propagator represents the probability of an electron moving within a certain time t from one place to another. The two-electron propagator accounts for two correlated electrons. The polarization propagator implicitly incorporates information about the electronically excited states of the system, as it is apparent in the corresponding spectral representation of the propagator

$$\Pi_{pq,rs}(\omega) = \sum_{n\neq 0} \frac{\langle \Psi_0 | c_q^\dagger c_p | \Psi_n \rangle \langle \Psi_n | c_r^\dagger c_s | \Psi_0 \rangle}{\omega + E_0^N - E_n^N} + \sum_{n\neq 0} \frac{\langle \Psi_0 | c_r^\dagger c_s | \Psi_n \rangle \langle \Psi_n | c_q^\dagger c_p | \Psi_0 \rangle}{-\omega + E_0^N - E_n^N} \ , \tag{9}$$

where Ψ_0 is the electronic ground state of the molecule with energy E_0^N and $c_q^\dagger$ and c_p, respectively, denote creation and annihilation operators of second quantization. The sum is carried over all electronically excited states Ψ_n with total energy E_n^N. In equation 9 both sums on the right-hand side account for identical physical information, hence, it is sufficient to consider only one of them

$$\Pi_{pq,rs}(\omega) = \Pi^+_{pq,rs}(\omega) + \Pi^-_{pqrs}(\omega) \ \text{ and,} \tag{10}$$

$$\Pi^-_{pq,rs}(\omega) = \Pi^+_{pq,rs}(-\omega) \ .$$

In the ADC scheme, the non-diagonal polarization propagator $\Pi^+(\omega)$ is written as

$$\Pi^+_{pq,rs}(\omega) = \mathbf{f}^\dagger_{pq}(\omega - \mathbf{M})^{-1}\mathbf{f}_{rs} \ . \tag{11}$$

For the derivation of the approximate ADC(n) schemes, the matrices $\mathbf{M}$ and $\mathbf{f}$ are expanded in a power series using the Møller-Plesset perturbation partitioning. Each pair $\mathbf{f}^{(n)}$ and $\mathbf{M}^{(n)}$, $n = 0, 1, 2, ...$, defines an approximation for the transition function and for the polarization propagator. These approximations are named the *nth* order ADC scheme. It is worthwhile to note that the ADC(n) methods converge to full-CI with increasing order. The matrix $\mathbf{M}^{(n)}$ allows for the calculation of vertical excitation energies as poles of the polarization propagator by solving the Hermitian eigenvalue problem

$$\mathbf{MY} = \mathbf{Y}\Omega \quad , \quad \mathbf{Y}^{\dagger}\mathbf{Y} = 1 \; , \tag{12}$$

where Ω and $\mathbf{Y}$ denote the diagonal matrix of eigenvalues and the eigenvector matrix, respectively. The combination of the eigenvectors $\mathbf{Y}_n$ with the spectral amplitude vector $\mathbf{f}_{pq}^{(n)}$ can give one-electron densities, transition densities and difference densities. [7,29] The lack of a generic definition of the ground state treatment should be noted as a limitation of the individual ADC schemes and in general of propagator methods for excitation energies. Regarding that all ADC schemes are structured by perturbation theory in coherence with Møller-Plesset perturbation theory, the electronic ground state can be treated by the corresponding MP(n) method with a similar accuracy/cost balance as the excited states. The ADC schemes vary in the order of perturbation theory to which the matrix elements of each single block are expanded, where ADC(1) has a smaller matrix than ADC(2) and ADC(3). The matrices of ADC(4) include triple blocks, Table 1. First order models ADC(1), CCS and CIS are identical in the calculation of zeroth order properties. ADC(2) configuration space comprises singly excited, so-called particle-hole (p-h), states

Table 1: Comparison of the properties of ADC schemes.

Method	Configuration Space	E_0	p-h	2p-2h	Response Properties	Scaling
ADC(1)	p-h	1	1	-	1	n^4
ADC(2)	2p-2h	2	2	0	2	n^5
ADC(3)	2p-2h	3	3	1	3	n^6

and doubly-excited, so-called two particle-two hole (2p-2h), intermediate states. The (p-h) block is expanded to second order of perturbation theory, the (p-h,2p-2h) coupling block to first order and the (2p-2h) block to zeroth order with the orbital energy differences as the diagonal elements. On the other hand, for the third-order ADC(3) scheme, the matrix elements of all blocks are treated consistently at one order of perturbation theory higher than in ADC(2), where the (p-h) block is treated in third order, and the (p-h, 2p-2h) coupling block and the (2p-2h) block are treated at the second and first order, respectively. The second order methods CIS(D), ADC(2) and CC2 are closely related, both from the theoretical and computational point of view. The ADC(2) matrix $\mathbf{M}^{\mathrm{ADC(2)}}$ can be constructed from the corresponding non-symmetric CC2 Jacobian matrix $\mathbf{A}^{\mathrm{CC2}}$. Ignoring the t_1 amplitudes of the CC2 Jacobian returns the CIS(D_∞) Jacobian $\mathbf{A}^{\mathrm{CIS(D_\infty)}}$. The secular matrix used in ADC(2) is symmetric since it only includes the hermitian part of that for CIS(D_∞). [30] The second order approach ADC(2) is a robust and reliable excited-state method with mean errors (±standard deviation) of 0.22±0.38 eV and 0.12±0.16 eV for the singlet and triplet excitation energies, respectively. [31, 32] In cases where no states with

obvious double excitation character interfere with the investigated excitations, ADC(2) and CC2 should be the method of choice for the calculation of spectra if the molecules are not too large and if the accuracy is sufficient. [33]

1.3.2 Second-order Approximate Coupled Cluster Singles and Doubles Model CC2

Among non-variational methods, coupled cluster (CC) theory is one of the most commonly used approaches in obtaining both the correlation energies and frequency-dependent molecular properties. Including the approximate models CC2 and CC3, we obtain a hierarchy for CC models as: CCS(N^4), CC2(N^5), CCSD(N^6), CC3(N^7), CCSDT(N^8), etc. where N is the number of electrons. Due to the exponential ansatz, CC methods include all higher-order terms within a given excitation manifold, therefore, the convergence towards full configuration interaction (FCI) is considerably improved compared to perturbational approaches. The CC2 model is an approximation to CCSD and the CC3 model is an approximation to CCSDT.

Although the total energy of CC2 is of second-order Møller-Plesset peturbation theory (MP2) quality, unlike MP2, excitation energies and transition moments can be computed as poles and residues of the corresponding linear response function.

In the absence of an external perturbation the CCSD energy is determined as

$$E^{\mathrm{CCSD}} = \langle \mathrm{HF}|\hat{H}\exp(\hat{T}_1 + \hat{T}_2)|\mathrm{HF}\rangle \ , \tag{13}$$

and the CCSD amplitude equations are

$$\Omega_1 = \langle \mu_1 | \hat{\bar{H}} + [\hat{\bar{H}}, \hat{T}_2] | \mathrm{HF} \rangle = 0 \tag{14}$$

$$\Omega_2 = \langle \mu_2 | \hat{\bar{H}} + [\hat{\bar{H}}, \hat{T}_2] + \frac{1}{2}[[\hat{\bar{H}}, \hat{T}_2], \hat{T}_2] | \mathrm{HF} \rangle = 0 \ , \tag{15}$$

where the Hamiltonian is partitioned into a Fock operator F and a fluctuation operator W, $H = F + W$. $\hat{\bar{H}}$ is a similarity transformed Hamiltonian and is defined as $\hat{\bar{H}} = \exp(-\hat{T}_1)\hat{H}\exp(\hat{T}_1)$. Since the CCSD energy is correct through third order, to obtain the energy correct through second order the double amplitudes need to be included for the fluctuation potential only to first order. Thus, for CC2 the singles equation remain as the ones for CCSD, Eq. 14, while the doubles equation are approximated as [5]

$$\Omega_2 = \langle \mu_2 | \hat{\bar{H}} + [\hat{F}, \hat{T}_2] | \mathrm{HF} \rangle = 0 \ . \tag{16}$$

Because of their importance in response theory with one-electron perturbations, the singles amplitudes are here, in contrast to ordinary Møller-Plesset perturbation theory, counted as zeroth-order parameters.

The resolution of the identity (RI) approximation reduces the computational demand of the CC2 model by lowering the computational cost as well as the scaling of the disk and memory space for the calculation and transformation of two-electron integrals from $\mathcal{O}(n^2N^2)$ to $\mathcal{O}(nN^2)$ and $\mathcal{O}(N^2)$, respectively, where n is the number of correlated electrons and N is the size of the basis set. [34] Therefore, by exploiting the RI approximation the applicability of the CC2 model for the calculation of excitation energies can be expanded to molecules 2-3 times larger than those that can be treated with conventional CC2 implementations.

1.4 Electronic Spectroscopy

One important application of spectroscopy is to study the properties of molecules including nuclear structure, electronic structure and reactivity by analyzing the absorption, emission and scattering of electromagnetic radiation. Different parts of the electromagnetic spectrum are sensitive to different parts of the molecular wavefunction.

In UV-vis absorption spectroscopy the electromagnetic radiation in the visible and ultraviolet regime induces transitions between different electronic states; usually by exciting electrons from valence orbitals. The excitation of a molecule from its ground state to an excited electronic state due to the absorption of one photon is referred to as *one-photon absorption* (OPA). In very intense laser fields the electronic excitation can happen by concurrent absorption of two photons with half of the excitation energy which is referred to as *two-photon absorption* (TPA). In case of OPA, within the Franck-Condon principle, which says that transitions from one electronic state to another happen so quickly that a slow nuclear vibration of a heavy nucleus cannot follow, the transition moment $\langle \Psi_f | \hat{\mu}_\alpha | \Psi_0 \rangle$ will only be nonzero if the transition is electric dipole-allowed. In other words, the direct product of the irreducible representations involved must be equal to the totally symmetric representation

$$\Gamma(\Psi_f) \otimes \Gamma(\hat{\mu}_\alpha) \otimes \Gamma(\Psi_0) = \Gamma(\hat{E}) \ . \tag{17}$$

In an absorption spectrum absorption lines occur at different energies equal to dipole-allowed excitations and the intensity of the lines is proportional to the associated oscillator strength. The oscillator strength for an excitation $0 \rightarrow n$ is a dimensionless value referring

to the number of oscillators associated with a given frequency ω_{0n} [35]

$$f_{n0}^{\alpha} = \frac{2m_e\omega_{n0}}{\hbar e^2}|\langle 0|\hat{\mu}_\alpha|n\rangle|^2 \ . \tag{18}$$

In general, only dipole-allowed transitions can be observed in absorption spectroscopy. In TPA the simultaneous absorption of two photons allows the electrons to reach electronic states that are dipole forbidden in OPA via dipole-allowed intermediate states. The TPA transition matrix elements can be written as [35]

$$M_{0f} = \frac{1}{\hbar}\sum_n \left[\frac{\langle 0|\hat{\mu}_\alpha|n\rangle\langle n|\hat{\mu}_\beta|f\rangle}{\omega_{n0}-\omega_1} + \frac{\langle 0|\hat{\mu}_\beta|n\rangle\langle n|\hat{\mu}_\alpha|f\rangle}{\omega_{n0}-\omega_2}\right] , \tag{19}$$

where $|0\rangle$, $|f\rangle$ and $|n\rangle$ are the initial, final and intermediate states, α and β are Cartesian coordinates, $\hbar$ is Planck's constant and ω_{n0} is the total energy of the two photons, $\omega_{n0} = \omega_1+\omega_2$. For instance, in the case of molecules with a center of inversion the g↔u transitions are allowed in OPA and forbidden in TPA spectra, while the g↔g (and u↔u) transitions are allowed in TPA but forbidden in OPA spectra. In molecules the absorption band can be broadened by several factors comprising the rotational and vibrational motions of the molecule, temperature effects, molecular collisions, solvent, and finite lifetime of the excited electronic states. The vertical transition energy $\Delta E_{\rm ve}$ is obtained by neglecting the nuclear motion and assuming that the excitations are occurring at the equilibrium geometry. The 0-0 transition, which is also experimentally observable in well-resolved gas-phase absorption spectra, corresponds to the excitation from the lowest vibrational state of the electronic ground state to the lowest vibrational state of the excited state and is usually denoted as ΔE_{00}. The adiabatic excitation energy, $\Delta E_{\rm ad}$, is the electronic energy difference between the ground and excited electronic states at their equilibrium geometries.

Magnetic circular dichroism (MCD) spectroscopy is another type of electronic spectroscopy that provides insights into the electronic structure of molecules and complexes, which, in contrast to CD, can even be highly symmetric. The UV-vis absorption and MCD spectra of a molecule carry the same set of spectral bands but the band morphologies are different due to the magnetic field applied in MCD. The MCD signal intensity is proportional to the external magnetic field strength. Although all CD, VCD and MCD spectroscopies measure the difference in absorption of left and right polarized light, the origin of these spectroscopic techniques is quit different.

A CD spectrum is the difference in the absorption of left-handed circularly polarized light (lcp) and right-handed circularly polarized light (rcp) when cp light passes through molecules, which are intrinsically chiral, and interacts to different extents with L and R enantiomers. Sterioisomers of a chiral molecule absorb preferentially either left or right circularly polarized light. In the case of non-chiral molecules, the absorption of lcp and rcp would in general be equal and no dichroism or birefringence would be observed. However, an external magnetic field perturbs the wavefunctions for ground- and excited states (the Zeeman effect) such that an optical activity is also induced in non-chiral molecules. This phenomenon is the basis of MCD spectroscopy and was first observed by Michael Faraday in 1845. [36] The MCD spectral data is usually expressed, based on Beer-Lambert law, in terms of the difference between extinction coefficients ϵ (M^{-1} cm^{-1}) divided by the

magnetic field strength, $\Delta\epsilon$ (M^{-1} cm^{-1} T^{-1}):

$$\Delta\epsilon = -\frac{8\pi^2 N_A \omega}{3 \times 1000 \times ln(10)(4\pi\epsilon_0)\hbar c_0} B_{ext} \times \sum_n \left\{ \frac{1}{\hbar} \frac{\partial a_{0n}(\omega)}{\partial \omega} \mathcal{A}_{0n} + a_{0n}(\omega) \left[\mathcal{B}_{0n} + \frac{\mathcal{C}_{0n}}{kT} \right] \right\} , \tag{20}$$

where ω is the circular frequency of the radiation, N_A is the Avogadro number, c_0 is the speed of light in vacuum, ϵ_0 is the dielectric constant, $a_{0n}(\omega)$ is a Lorentzian lineshape function for spectral broadening, k is the Boltzmann constant and T is the temperature. $\mathcal{A}$, $\mathcal{B}$ and $\mathcal{C}$ are three contributions with different physical origins for the analysis of MCD spectra.

The $\mathcal{A}$ term appears when the molecule has either an orbitally degenerate ground- or excited electronic states and is defined as [35]

$$\mathcal{A}_{0n} = \frac{1}{2g} \sum_{0_\alpha n_\beta} \sum_{(0'_\alpha n'_\beta) \neq 0} \mathrm{Im}[(\langle n'_\beta | \hat{\mathbf{m}} | n_\beta \rangle \delta_{0'_\alpha 0_\alpha} - \langle 0_\alpha | \hat{\mathbf{m}} | 0'_\alpha \rangle) \cdot \langle 0'_\alpha | \hat{\mu} | n'_\beta \rangle \times \langle n_\beta | \hat{\mu} | 0_\alpha \rangle] , \tag{21}$$

where the ($\prime$) symbol represents the degenerate state. g is the degree of degeneracy of the electronic states, 0 and n are the electronic ground- and excited states, $\hat{\mathbf{m}}$ and $\hat{\mu}$ are the magnetic and electric dipole moment operators and α and β are the different magnetic components of the degenerate states. The $\mathcal{A}$ term represents the difference in the induced magnetic moments by the external magnetic field, weighted by the electric dipole transition moments associated with the absorption of lcp and rcp.

The $\mathcal{B}$ term, which exists irrespective of the degeneracy of the ground and excited states, arises from the electronic states perturbed by the external magnetic fields that have dif-

ferent polarization [35]

$$\mathcal{B}_{0n} = \sum_{0_\alpha n_\beta} \mathrm{Im}\left(\sum_{k\neq 0} \frac{\langle k|\hat{\mathbf{m}}|0_\alpha\rangle \cdot \langle n_\beta|\hat{\mu}|k\rangle \times \langle 0_\alpha|\hat{\mu}|n_\beta\rangle}{\omega_{k0}} + \sum_{k\neq n} \frac{\langle n_\beta|\hat{\mathbf{m}}|k\rangle \cdot \langle k|\hat{\mu}|0_\alpha\rangle \times \langle 0_\alpha|\hat{\mu}|n_\beta\rangle}{\omega_{kn}} \right), \tag{22}$$

where k is an electronic intermediate state. By looking at the $\mathcal{B}$ term, in order to have MCD spectrum, there have to be perpendicular components between the two electronic transition moments $\langle 0|\hat{\mu}|n_\beta\rangle$ and $\langle k|\hat{\mu}|0_\alpha\rangle$ and there has to be a parallel component between the magnetic transition moment $\langle n_\beta|\hat{\mathbf{m}}|k\rangle$ and the vector product of the electronic transition moments.

The $\mathcal{C}$ term originates from the Boltzmann distribution among the components of a degenerated ground state and, consequently, depends on the temperature by $1/kT$ [35]

$$\mathcal{C}_{0n} = \frac{1}{2g} \sum_{0_\alpha n_\beta} \sum_{0'} \mathrm{Im}[\langle 0_\alpha|\hat{\mathbf{m}}|0'_\alpha\rangle \cdot (\langle 0'_\alpha|\hat{\mu}|n_\beta\rangle \times \langle n_\beta|\hat{\mu}|0_\alpha\rangle)] \ . \tag{23}$$

At very low temperatures, the lowest state contributes most to the MCD intensity and results in a symmetric Gaussian shaped Faraday $\mathcal{C}$ term, while by increasing the temperature higher states become populated and, due to the separation of band centers of electronic transitions absorbing the lcp and rcp, the shape of the $\mathcal{C}$ term becomes asymmetric. [35]

Outline Of Dissertation

The main motivation of this dissertation is the incorporation of solvent effects as an isotropic polarizable environment into the calculation of vertical excitation energies and excited state properties of molecules in solution.

The next chapters of this dissertation are organized as follows. Chapter 2 introduces the theoretical details and the implementation for combining the COSMO solvent model and the second-order wavefunction method ADC(2) for excited state analytic gradients as well as two example applications. The theoretical details and implementation of the COSMO-RI-CC2 method for vertical excitation energies, transition moments and Faraday $\mathcal{B}$ terms along with the calculated OPA and MCD spectra of purine, adenine and guanine are explained in Chapter 3. In chapter 4, solvent effects on the photoexcitation and deexcitation mechanisms of three halogen-bonded complexes in solution are described. In order to analyze the performance of different reaction field schemes at the COSMO-ADC(2) level and also the performance of the COSMO-CC2(post-SCF), in Chapter 5, we have calculated the solvent shifts for two experimental data sets. Finally, in the last chapter I discuss the research limitations and propose possible solutions for them.

References

[1] A. L. Fetter and J. D. Walecka. *Quantum Chemistry of many-particle systems.* McGraw-Hill: New York, 1971.

[2] E. K. U. Gross and W. Kohn, Phys. Rev. Lett. **21**, 2850 (1985).

[3] A. Dreuw, J. L. Weisman and M. Head-Gordon, J. Chem. Phys. **119**, 2943 (2003).

[4] A. Dreuw and M. Head-Gordon, Chem. Rev. **105**, 4009 (2005).

[5] O. Christiansen, H. Koch and P. Jørgensen, Chem. Phys. Lett. **243**, 409 (1995).

[6] A. Szabo and N. S. Ostlund. *Modern Quantum Chemistry: Introduction to Advanced Electronic Structure Theory.* New York: Dover, 1989.

[7] J. Schirmer, Phys. Rev. A. **26**, 2395 (1982).

[8] J. M. Olsen, K. Aidas, K. V. Mikkelsen and J. Kongsted, J. Chem. Theory Comput. **6**, 249 (2010).

[9] D. Hršak, A. M. Khah, O. Christiansen and C. Hättig, J. Chem. Theory Comput. **11**, 3669 (2015).

[10] A. M. Khah, S. K. Khani and C. Hättig, J. Chem. Theory Comput. **114**, 4640 (2018).

[11] TURBOMOLE V7.2 2017, a development of University of Karlsruhe and Forschungszentrum Karlsruhe GmbH, 1989-2007, TURBOMOLE GmbH, since 2007; available from `http://www.turbomole.com`.

[12] J. Heil and S. M. Kast, J. Chem. Phys. **142**, 114107 (2015).

[13] D. Beglov and B. Roux, J. Chem. Phys. **104**, 8678 (1996).

[14] J. Tomasi and M. Persico, Chem. Rev. **94**, 2027 (1994).

[15] S. Miertuš, E. Scrocco and J. Tomasi, Chem. Phys. **55**, 117 (1981).

[16] B. Mennucci, WIREs Comput. Mol. Sci. **2**, 386 (2012).

[17] J. Tomasi, B. Mennucci and R. Cammi, Chem. Rev. **105**, 2999 (2005).

[18] A. Klamt and G. Schüürmann, J. Chem. Soc. Perkin Trans. 2. 799 (1993).

[19] A. Klamt, WIREs Comput. Mol. Sci. **1**, 699 (2011).

[20] A. Klamt, WIREs Comput. Mol. Sci. **8**, e1338 (2017).

[21] A. Klamt, C. Moya and J. Palomar, J. Chem. Theory Comput. **11**, 4220 (2015).

[22] V. Barone and M. Cossi, J. Phys. Chem. A. **102**, 1995 (1998).

[23] E. Cancès, B. Mennucci and J. Tomasi, J. Chem. Phys. **107**, 3032 (1997).

[24] B. Mennucci, R. Cammi and J. Tomasi, J. Chem. Phys. **109**, 2798 (1998).

[25] D. M. Chipman, J. Chem. Phys. **112**, 5558 (2000).

[26] B. Lunkenheimer and A. Köhn, J. Chem. Theory Comput. **9**, 977 (2013).

[27] J. M. Mewes, Z. Q. You, M. Wormit, T. Kriesche, J. M. Herbert and A. Dreuw, J. Phys. Chem. A. **119**, 5446 (2015).

[28] T. Schwabe, K. Sneskov, J. M. H. Olsen, J. Kongsted, O. Christiansen and C. Hättig, J. Chem. Theory Comput. **8**, 3274 (2012).

[29] A. B. Trofimov and J. Schirmer, J. Phys. B: At. Mol. Opt. Phys. **28**, 2299 (1995).

[30] C. Hättig, Adv. Quantum Chem. **50**, 37 (2005).

[31] J. H. Starcke, M. Wormit, J. Schirmer and A. Dreuw, Chem. Phys. **329**, 39 (2006).

[32] M. Wormit, D. R. Rehn, P. H. P. Harbach, J. Wenzel, C. M. Krauter, E. Epifanovsky and A. Dreuw, Mol. Phys. **112**, 774 (2014).

[33] A. Dreuw and M. Wormit, WIREs Comput. Mol. Sci. **5**, 82 (2015).

[34] C. Hättig and F. Weigend, J. Chem. Phys. **113**, 5154 (2000).

[35] P. Norman, K. Ruud and T. Saue. *Principles and Practices of Molecular Properties.* John Wiley & Sons, 2018.

[36] N. Kobayashi, A. Muranaka and J. Mack. *Circular Dichroism and Magnetic Circular Dichroism Spectroscopy for Organic Chemists.* Royal Society of Chemistry, 2012.

2 COSMO-RI-ADC(2) excitation energies and excited state gradients

The incorporation of COSMO into the ADC(2) approach as a sub-project in the present thesis provides us with a reliable and affordable computational tool that allows to introduce the isotropic environment effects into the electronic excitation and deexcitation mechanisms of organic dyes.[1] An implementation of COSMO-ADC(2) for excitation energies has already been carried out by Lunkenheimer, Köhn, Dreuw and coworkers. [26, 27] Herein, for the first time, we present the theory development and implementation of COSMO-ADC(2) for excited state analytic gradients for molecules in solution. The application of the implemented code for two cases; 4-(N,N-dimethylamino)benzonitrile and 2-Iodobenzimidazolium·OTf has also been shown.[2,3]

My contribution to this project comprises the major portion of theory development and modification of the code under the supervision of Christof Hättig and in case of applications, I have performed all the calculations and compiled the numbers, tables and figures. Since the polarizable embedding (PE) theory and COSMO share some subroutines in TURBOMOLE program, Alireza Marefat Khah contributed partially to the theory development and implementation where the two solvent models have a common structure. The first draft of the manuscript was written by me and further developed together with my co-authors.

[1] References are shared with Chapter 1.

[2] Article: https://pubs.rsc.org/en/content/articlepdf/2018/cp/c8cp00643a

[3] ESI: http://www.rsc.org/suppdata/c8/cp/c8cp00643a/c8cp00643a7.pdf

PCCP

PAPER

View Article Online
View Journal | View Issue

Check for updates

Cite this: *Phys. Chem. Chem. Phys.*, 2018, **20**, 16354

COSMO-RI-ADC(2) excitation energies and excited state gradients†

Sarah Karbalaei Khani,* Alireza Marefat Khah and Christof Hättig

Received 29th January 2018,
Accepted 19th April 2018

DOI: 10.1039/c8cp00643a

rsc.li/pccp

We present an implementation of analytic gradients for electronically excited states for the algebraic-diagrammatic construction through second order, ADC(2), in combination with the conductor-like screening model (COSMO) as an implicit solvent model. The implementation uses a post-SCF reaction field scheme for the coupling between the environment and the quantum system which retains the computational efficiency of the gas-phase RI-ADC(2) calculations. Applying this approach, we computed solvatochromic shifts for UV absorption and fluorescence transitions of 4-(*N*,*N*-dimethylamino)benzonitrile using equilibrium geometries for the ground and the first excited states optimized in the presence of acetonitrile as solvent. Furthermore, we investigated the excited state energies and geometries of the 2-iodobenzimidazolium·triflate ion pair in aqueous solution as an example where solvent effects have a large influence on the structure and the UV spectrum.

Published on 20 April 2018. Downloaded by Ruhr Universitat Bochum on 6/20/2018 12:17:46 PM.

1 Introduction

The inclusion of solvent effects not only on the absorption and emission processes but also on the geometrical structure in ground and excited states are essential for a detailed understanding of the photophysics and photochemistry of molecular systems in solution. A potentially very accurate strategy to compute excitation energies of molecules in solution consists of the inclusion of a large number of explicit solvent molecules combined with a sampling over a statistically representative number of configurations to reproduce bulk and fluctuation effects. However, if this approach is used with accurate quantum mechanical (QM) methods the sampling triggers even for a relatively small number of explicit solvent molecules high computational costs.

The main effects of solute–solvent interactions on electronic excitations are generally of electrostatic origin and related to the solvent polarity. The importance of elucidating these electrostatic effects using a computationally affordable approach gave rise to the formulation of continuum solvation models (CSMs) which use an implicit average description of solute–solvent interactions and are nowadays widely used in combination with different quantum chemical methods.[1–4] One of the most popular CSM approaches used in combination with electronic spectra is the Polarizable Continuum Model (PCM)[5] in different parameterizations.[6] The PCM model has been implemented for excited state energies and analytic gradients in solution at the configuration interaction singles (CIS) level,[7] as well as for time-dependent density functional theory (TDDFT) and the coupled-cluster singles and doubles (CCSD) model.[8–13] In the context of QM continuum solvation or in general for QM reaction field methods, there exist different approaches to compute electronic excitation energies. Two of them are the state specific (SS) and the linear response (LR) approach. The state specific strategy solves the non-linear Schrödinger equations for the states of interest assuming that the excitation energies are the differences between the corresponding total solute–solvent free energies,[14,15] while the linear-response strategy avoids the explicit calculation of the excited state wave functions and computes the excitation energies as the poles of the linear response function using a common eigenvalue equation for all excited states.[16,17] For a QM system in vacuum the two approaches are equivalent as long as the equivalence is not broken by approximations in the wavefunction ansatz. This is no longer true for a QM system embedded in a polarizable environment (reaction field), where the partitioning of the full system into separately treated subsystems—the QM system and the environment—coupled by a wavefunction- or density-dependent interaction leads to a non-linear Schrödinger equation. In this case the SS and LR approaches differ from the onset unless the full supermolecular solution is recovered. Both approaches along with a corrected LR (cLR) approach to reduce the gap between the SS and LR formalisms have been used *e.g.* within the TDDFT framework.[18–21] In the context of reaction field schemes for correlated wavefunction methods these issues have been reviewed at the example of COSMO-ADC(2) by Lunkenheimer and Köhn.[22]

Arbeitsgruppe Quantenchemie, Ruhr-Universität, Bochum 44780, Germany. E-mail: Sarah.KarbalaeiKhani@rub.de, Alireza.MarefatKhah@rub.de, Christof.Haettig@rub.de

† Electronic supplementary information (ESI) available. See DOI: 10.1039/c8cp00643a

This journal is © the Owner Societies 2018

Published on 20 April 2018. Downloaded by Ruhr Universitat Bochum on 6/20/2018 12:17:46 PM.

Implementations of PCM for excitation energies have also been reported for coupled-cluster (CC) methods which can provide more accurate results than TDDFT especially for charge-transfer transitions. For correlated wavefunction methods that use orbitals from preceding *e.g.* Hartree–Fock (HF) calculations and do not optimize them simultaneously with the correlated wavefunction, the non-linearity of the Schrödinger equation for a QM system in a reaction field produces complications already for the ground state. Among different approaches proposed to deal with this problem in an approximate manner in CC and other correlated wavefunction methods,[23,24] there are two approximations called PTED (perturbation theory with self-consistent energy and density) and PTE, using the HF reaction field. The latter scheme neglects post-Hartree–Fock contributions to the reaction field and introduces solute–solvent interactions only through the Fock operator and the polarization of the molecular orbitals (MOs) while the former scheme (PTED) is considered to be a more complete form in which the correlated electronic density is used to calculate a self-consistent reaction field. Beside the aforementioned schemes, two intermediate approximations between PTE and PTED called PTE(S) and PTES (where S stands for singles) have been proposed for CCSD by Caricato[25] to calculate free energies and analytic gradients to improve upon the PTE approximation towards the PTED results with less computational efforts than the latter. However, CCSD often gives molecular structures that are not very accurate and is computationally expensive.

The conductor-like screening model (COSMO)[26] is another extensively used CSM which shares many features with PCM, in particular with the C-PCM variant of the latter. COSMO has been implemented by Lunkenheimer and Köhn[22] for electronic excitation energies with the ADC(2) (algebraic diagrammatic construction through second-order)[27] method, which is based on second-order Møller–Plesset perturbation theory, in the ricc2[28] module of TURBOMOLE.[29,30] For long-lived states (the ground state or the lowest excited states) this implementation applies SS approaches and the reaction field is calculated fully self-consistently in an iterative PTED scheme. For short-lived states where only the fast part of the reaction field can respond to the changes in the electron density a cLR scheme is adopted, based on the PTED reaction field of the reference state. Although PTED is in certain aspects the most complete scheme, its high computational costs for post-HF and post-KS methods as well as the complication to extend it for analytic gradients make it a less preferred choice.

In the current work we report an implementation of COSMO-ADC(2) with a reaction field scheme that was originally developed in the context of the PERI-CC2[31] method (where PE stands for polarizable embedding) as an approach that is an intermediate between PTE and PTED. This scheme, which we will denote in the following as post-SCF, has some similarities to the PTES scheme proposed by Caricato,[25] but was especially designed to compute electronic excitation energies and other response properties in solution in such a way that it retains the computational efficiency of the vacuum RI-CC2 or RI-ADC(2) methods while capturing all important solvent effects on excited state energies at the LR level of the correlated wavefunction.[31] This reaction field scheme allows for a straight-forward implementation of the corresponding analytic gradients for the excited state energies which we report in the current work for COSMO-RI-ADC(2). It avoids the self-consistent iterations of the PTED scheme around the Hartree–Fock and post-HF calculations as well as the accompanied danger of numerical instabilities if the reaction field is not converged tightly enough. As long as no state-specific corrections are included, it provides excited state potential energy surfaces (PES) with a consistent behavior at avoided crossings and conical intersections.

2 Theory

2.1 The conductor-like screening model

The dielectric continuum approach assumes the solvent as a structureless continuum in which the solute is surrounded by a molecule-shaped cavity. The cavity is discretized into small surface segments. COSMO is an apparent surface charge (ASC) model with polarized charges created by the mutual polarization of the solvent and the solute which are spread on the cavity surface.[26] In the COSMO picture of isotropic solution, the solvent reaction field is obtained as an integral over the surface charge distribution which in the actual implementation is represented by point charges placed at the centers of the cavity surface segments. The free energy $\mathscr{G}$ of the solute embedded in a dielectric continuum is within the COSMO model in an equilibrium situation given by:

$$\mathscr{G} = \langle \hat{H}^{\mathrm{QM}} \rangle - \frac{1}{2} f(\varepsilon) \sum_{\mu\nu} V_\mu \left[\mathscr{A}^{-1}\right]_{\mu\nu} V_\nu. \tag{1}$$

In the above equation $\mathscr{A}$ is the response kernel for COSMO,[26] $f(\varepsilon)$ a scaling factor depending on the dielectric constant of the solvent ε and V_μ the value of the electrostatic potential at the center of the surface segment μ which is given by:

$$V_\mu = \left\langle \frac{\hat{Q}(\mathbf{r})}{|\mathbf{t}_\mu - r|} \right\rangle, \tag{2}$$

where $\mathbf{t}_\mu$ is the center of segment μ and $\hat{Q}(\mathbf{r})$ the charge density operator. The angle brackets $\langle\,\rangle$ denote the quantum mechanical expectation value. The polarization charges induced by the solute on the cavity segments are obtained as:

$$Q_\mu = -f(\varepsilon) \sum_{\nu} \left[\mathscr{A}^{-1}\right]_{\mu\nu} V_\nu. \tag{3}$$

2.2 ADC(2) and its relation to CC2

The second order methods CIS(D),[32] CC2[33] and ADC(2)[27] provide excitation energies for singly excited states with similar accuracy as those obtained with the computationally more demanding CCSD method. The non-perturbative CC2 and ADC(2) methods are also found to give equilibrium structures and vibrational frequencies which for main group single-reference molecules usually are superior to those from CCSD which is, however, more robust with respect to strong correlation effect.[34] An advantage of ADC(2) over CC2 for excited state calculations is that for ADC(2) the excitation energies are obtained as the eigenvalues of

Published on 20 April 2018. Downloaded by Ruhr Universitat Bochum on 6/20/2018 12:17:46 PM.

a Hermitian secular matrix[34] while in coupled-cluster response theory the excitation energies are computed as eigenvalues of a non-Hermitian Jacobi matrix.[28] This guarantees for ADC(2) a qualitatively correct description of conical intersections between states of the same symmetry. In addition, it reduces the computational costs for analytic gradients by almost a factor of four since no separate equations need to be solved for left and right eigenvectors and the first-order ground state amplitudes and the corresponding Lagrange multipliers can in a canonical basis be calculated without solving coupled equations.

In contrast to the CC2 model,[33] ADC(2) is not derived from the response function of a ground state method. Therefore, there is no unique definition of the total energy for it. To be consistent with the order to which correlation effects are included as well as for computational convenience, second order Møller–Plesset perturbation (MP2) theory is applied to define the ground state energy. From technical and practical points of view ADC(2) and CC2 are, however, very similar. If we consider the CC2 Jacobi matrix as a function of the ground state singles and doubles amplitudes, $\mathbf{A}(T_1,T_2)$, its relation to the secular matrix of the ADC(2) model can be expressed as[34]

$$\mathbf{A}^{\mathrm{ADC(2)}} = \frac{1}{2}\left(\mathbf{A}\left(0, T_2^{\mathrm{MP1}}\right) + \mathbf{A}\left(0, T_2^{\mathrm{MP1}}\right)^{\dagger}\right) \tag{4}$$

where the CC2 cluster amplitudes are replaced by those from first-order perturbation theory and only the Hermitian part of the matrix is included.

2.3 COSMO-ADC(2) with the post-SCF coupling scheme

As pointed out in the introduction, for correlated wavefunction methods or in general for post-SCF methods, there are different possibilities to couple the QM system to the environment for the reaction field calculation:

• The perturbation at the energy (PTE) scheme uses the reaction field obtained from the ground state HF density. The disadvantage of this scheme is that the environment does not respond to electronic excitation processes in the QM system and therefore important contributions for the coupling between the excitation process in the QM system and the reaction field are missing if the QM system is not chosen large enough. The computational costs for this scheme are comparable to those for the corresponding gas-phase calculations.

• The perturbation at the energy and density (PTED) scheme is the most expensive one. It makes the post-HF density and the solvent reaction field self-consistent; usually in a loop over the HF and the post-HF calculation which is terminated once the remaining changes are below certain thresholds. The PTED scheme has already been implemented for COSMO-MP2 and COSMO-ADC(2) in the TURBOMOLE[22,29,30] package. However, it is not the method of choice for potential energy surfaces because of the dependence of the excited state energies on the choice of the reference state for the reaction field. The state-specific reaction field contributions lead to a qualitatively wrong behavior of the excited state potential energy surfaces in the vicinity of near degeneracies and state intersection. Furthermore, the self-consistency iterations lead to high computational costs and can affect the numerical stability of geometry optimizations if the convergence thresholds are not tight enough. These issues motivated us to apply an alternative scheme for the coupling between the reaction field and the solute.

• The post-SCF scheme that we implemented for COSMO-RI-CC2 excitation energies and COSMO-RI-ADC(2) excitation energies and excited state gradients evaluates the post-HF contributions to the solvent reaction field with an approximate post-HF contribution to the density, ($\mathbf{D}^{\Delta}$), which is calculated only from the single excitation parts of the cluster amplitudes, Lagrange multipliers or eigenvectors. This scheme has already been applied for the implementation of PERI-CC2 excitation energies, and one- and two-photon transition moments.[31,35] The computational costs of this scheme are comparable to the corresponding gas-phase calculations and the energies for all excited states are obtained from a single eigenvalue equation so that the obtained potential energy surfaces show a consistent behavior at avoided crossings and conical intersections.

Furthermore, for excited state one can combine the linear response approach with state-specific perturbative corrections to account for the response of the reaction field to the difference between the ground and the excited state charge density (see *e.g.* ref. 22 for a related discussion at the COSMO-ADC(2) level). While from a practical point of view, perturbative state-specific corrections are very useful for computing excitation energies for given structures, they are very problematic for excited state geometry optimizations. As all non-degenerate perturbation theories (for example CIS(D)), such state-specific corrections will again lead to potential energy surfaces (PES) which behave qualitatively wrong in the vicinity of near degeneracies and intersections. Since the latter are ubiquitous in polyatomic molecules, perturbative methods are usually not applicable for studying their excited state PES.

The post-SCF scheme used for RI-CC2 and RI-ADC(2) can be derived from the general free energy Lagrangian for the full CC model in a self-consistent reaction field framework as:[36]

$$L_{\text{COSMO-CC}}(t,\bar{t}) = \langle \Lambda | \hat{H}^{\mathrm{QM}} | \mathrm{CC} \rangle + \frac{1}{2}\sum_{\kappa\lambda} Q_{\kappa}\left(\mathbf{D}^{\mathrm{CC}}\right) V_{\lambda}\left(\mathbf{D}^{\mathrm{CC}}\right) \tag{5}$$

$$= \left\langle \Lambda \middle| \hat{H}^{\mathrm{QM}} + \frac{1}{2}\hat{G}^{\mathrm{pol}} \middle| \mathrm{CC} \right\rangle \tag{6}$$

where the Λ state is defined as

$$\langle \Lambda | = \left(\langle \mathrm{HF} | + \sum_{\mu_i} \sum_{i} \bar{t}_{\mu_i} \langle \mu_i | \right) \exp(-\hat{T}). \tag{7}$$

In eqn (5) and (6), $\hat{H}^{\mathrm{QM}}$ is the vacuum electronic Hamiltonian, $\hat{G}^{\mathrm{pol}}$ is the electronic interaction operator between the QM system and the reaction field—in the case of COSMO with the cavity surface charges—and $\mathbf{D}^{\mathrm{CC}}$ is the unrelaxed CC density which is defined as

$$\mathbf{D}^{\mathrm{CC}}_{pq} = \langle \Lambda | \hat{E}_{pq} | \mathrm{CC} \rangle \tag{8}$$

 This journal is © the Owner Societies 2018

Published on 20 April 2018. Downloaded by Ruhr Universitat Bochum on 6/20/2018 12:17:46 PM.

where $\hat{E}_{pq}$ are the spin-free one-particle operators. For implicit solvent models, like PCM and COSMO, the different time scales for the relaxation of the nuclear and the electronic polarization of the environment should be taken into account by replacing $f(\varepsilon)$ (see eqn (1)) by a frequency-dependent factor. Also in the current implementation we allow that f is chosen as a step function which in the static limit and at low frequencies (*i.e.* equilibrium situations) is defined as $f(\varepsilon)$, where ε is the static dielectric constant while in the optical range it changes to $f(n^2)$ where n is the refractive index.

From the general ansatz introduced in eqn (6) the corresponding free energy Lagrangian for the CC2 model is derived by skipping all contributions beyond second order in the fluctuation potential, but counting the singles amplitudes as zeroth-order because of their special role in response theory:

$$\begin{aligned} L = \mathscr{G}_{\mathrm{HF}} &+ \left\langle \mathrm{HF} \middle| \hat{\tilde{F}}_{\mathrm{N}}^{\mathrm{pol}} + \hat{\tilde{W}}_{\mathrm{N}}^{\mathrm{QM}} + \left[\hat{\tilde{W}}_{\mathrm{N}}^{\mathrm{QM}}, \hat{T}_2\right] + \frac{1}{2}\hat{\tilde{G}}(\mathbf{D}^{\Delta}) \middle| \mathrm{HF} \right\rangle \\ &+ \left\langle \bar{t}_1 \middle| \hat{\tilde{F}}_{\mathrm{N}}^{\mathrm{pol}} + \hat{\tilde{W}}_{\mathrm{N}}^{\mathrm{QM}} + \left[\hat{F}_{\mathrm{N}}^{\mathrm{pol}} + \hat{\tilde{W}}_{\mathrm{N}}^{\mathrm{QM}}, \hat{T}_2\right] \middle| \mathrm{HF} \right\rangle \\ &+ \left\langle \bar{t}_2 \middle| \left[\hat{F}_{\mathrm{N}}^{\mathrm{pol}}, \hat{T}_2\right] + \hat{\tilde{W}}_{\mathrm{N}}^{\mathrm{QM}} \middle| \mathrm{HF} \right\rangle. \end{aligned} \tag{9}$$

In the above equation operators are introduced in their normal ordered form with respect to the HF wave function.

$$\hat{O}_{\mathrm{N}} = \hat{O} - \langle \mathrm{HF}|\hat{O}|\mathrm{HF}\rangle \tag{10}$$

Furthermore, double excitation amplitudes and Lagrange multipliers are neglected for the density from which the post-HF contribution to the reaction field is calculated as:

$$\mathbf{D}^{\Delta}_{pq} = \langle \mathrm{HF} + \bar{t}_1 | \mathrm{e}^{-\hat{T}_1}\hat{E}_{pq}\mathrm{e}^{\hat{T}_1}|\mathrm{HF}\rangle - \langle \mathrm{HF}|\hat{E}_{pq}|\mathrm{HF}\rangle. \tag{11}$$

In eqn (9) we introduced the Fock operator for the embedded system, $\hat{F}^{\mathrm{pol}} = \hat{F}^{\mathrm{QM}} + \hat{G}^{\mathrm{pol,HF}}$ and the fluctuation potential $\hat{W}^{\mathrm{QM}} = \hat{H}^{\mathrm{QM}} - \hat{F}^{\mathrm{QM}}$. With a tilde we denote operators dressed with the ground state singles amplitudes as $\hat{\tilde{O}} = \exp(-\hat{T}_1)\hat{O}\exp(\hat{T}_1)$. The density-dependent reaction field operators for COSMO are defined as:

$$\hat{G}(\mathbf{D}) = \sum_{\mu} Q_{\mu}(\mathbf{D}) V_{pq,\mu}\hat{E}_{pq}, \tag{12}$$

$$Q_{\mu}(\mathbf{D}) = -f\sum_{\nu}\left[\mathbf{A}^{-1}\right]_{\mu\nu}\sum_{pq} V_{pq,\nu}D_{pq}, \tag{13}$$

$$V_{pq,\nu} = -\left\langle p \middle| \frac{1}{|\mathbf{t}_{\nu} - \mathbf{r}|} \middle| q \right\rangle. \tag{14}$$

In eqn (13) the frequency-dependence of the reaction field polarization enters through $\hat{G}(\mathbf{D}^{\Delta})$ *via* the scaling factor f.

For COSMO-MP2, which is used as the ground state for COSMO-ADC(2), density $\mathbf{D}^{\Delta}$ vanishes if the Hartree–Fock wavefunction fulfills the Brillouin condition. Then the singles amplitudes t_{μ_1} and Lagrange multipliers $\bar{t}_{\mu_1}$ become zero in first-order perturbation theory so that the above approach reduces at the MP2 level to PTE-COSMO-MP2. The expressions for the polarization contributions to the CC2 Jacobian have been discussed for the atomistic polarizable embedding (PE) in ref. 31. Given those expressions along with the relation (4), the polarization contributions to the ADC(2) secular matrix are obtained as:

$$\mathbf{A}^{\mathrm{pol}}_{\mu_1,\nu_1} = \langle \mu_1 | \left[\hat{G}^{\mathrm{pol,HF}}, \tau_{\nu_1}\right] + \hat{G}^{\nu_1} | \mathrm{HF}\rangle \tag{15}$$

$$\mathbf{A}^{\mathrm{pol}}_{\mu_1,\nu_2} = 0 \tag{16}$$

$$\mathbf{A}^{\mathrm{pol}}_{\mu_2,\nu_1} = 0 \tag{17}$$

$$\mathbf{A}^{\mathrm{pol}}_{\mu_2,\nu_2} = \langle \mu_2 | \left[\hat{G}^{\mathrm{pol,HF}}, \tau_{\nu_2}\right] | \mathrm{HF}\rangle, \tag{18}$$

where

$$\hat{G}^{\mathrm{pol,HF}} = \sum_{\mu} \left\langle \mathrm{HF} \middle| \hat{Q}_{\mu} \middle| \mathrm{HF} \right\rangle \hat{V}_{\mu}. \tag{19}$$

The operator in the last term of eqn (15) for the singles-singles block $\mathbf{A}^{\mathrm{pol}}_{\mu_1\nu_1}$ is defined as the derivative of $\hat{G}(\mathbf{D}^{\Delta})$ with respect to the cluster amplitudes. Its contribution to the linear transformation of the secular matrix with a vector R_{ν} are evaluated through an auxiliary density $\mathbf{D}^{\eta}$ defined *via* the derivative of $\mathbf{D}^{\Delta}$ with respect to t_{ν_1}:

$$\mathbf{D}^{\eta} = \sum_{\nu_1} \frac{\partial \mathbf{D}^{\Delta}}{\partial t_{\nu_1}} R_{\nu_1}, \tag{20}$$

$$\sum_{\nu_1} \langle \mu_1 | \hat{G}^{\nu_1} | \mathrm{HF}\rangle R_{\nu_1} = \langle \mu_1 | \hat{G}(\mathbf{D}^{\eta}) | \mathrm{HF}\rangle. \tag{21}$$

In the same way, its contribution to left transformations are evaluated as:

$$\sum_{\mu_1} L_{\mu_1} \langle \mu_1 | \hat{G}^{\nu_1} | \mathrm{HF}\rangle = \langle \mathrm{HF} | \left[\hat{G}(\mathbf{D}^{\xi}), \tau_{\mu_1}\right] | \mathrm{HF}\rangle \tag{22}$$

with the auxiliary density

$$\mathbf{D}^{\xi} = \sum_{\mu_1} L_{\mu_1} \frac{\partial \mathbf{D}^{\Delta}}{\partial \bar{t}_{\mu_1}}. \tag{23}$$

For CC2, the auxiliary transition densities $\mathbf{D}^{\eta}$ and $\mathbf{D}^{\xi}$ differ in terms that depend on t_1 and $\bar{t}_1$ while for ADC(2) the difference reduces to a factor of 2 from spin summation in the spin-free closed shell case when a biorthonormal basis for the single excitation manifold with $|ck\rangle = \hat{E}_{ck}|\mathrm{HF}\rangle$ and $\langle ck| = \frac{1}{2}\langle \mathrm{HF}|\hat{E}^{\dagger}_{ck}$ is used. In the non-equilibrium limit, *i.e.* for vertical electronic transitions and for short time scales after the transition, $\hat{G}(\mathbf{D}^{\eta})$ and $\hat{G}(\mathbf{D}^{\xi})$ should be evaluated with $f(n^2)$, while in equilibrium situations, *i.e.* for time scales long compared to the solvent relaxation time, they should be evaluated with $f(\varepsilon)$.

2.4 Excited state gradient theory for COSMO-RI-ADC(2)

As pointed out above, ADC(2) technically differs from CC2 in two aspects: the ground state singles and doubles amplitudes $\hat{T}_1$ and $\hat{T}_2$ are those from first-order Møller–Plesset perturbation theory, where the ground state singles amplitudes $\hat{T}_1$ vanish if $|\mathrm{HF}\rangle$ fulfills the Brillouin condition. Furthermore, ADC(2) has a symmetric secular matrix in contrast to the non-hermitian CC2 Jacobian.

Published on 20 April 2018. Downloaded by Ruhr Universitat Bochum on 6/20/2018 12:17:46 PM.

2.4.1 The relaxed excited state Lagrange function. The orbital-relaxed Lagrange function for the total energy of an excited state f at the COSMO-RI-ADC(2) level of theory is formulated as:

$$\begin{aligned} L^{\mathrm{f}} &= \langle \mathrm{HF}|\hat{F}^{\mathrm{QM}} + \hat{W}^{\mathrm{QM}} + [\hat{W}^{\mathrm{QM}}, \hat{T}_2]|\mathrm{HF}\rangle \\ &+ \sum_{\mu_2} \bar{t}^{\mathrm{f}}_{\mu_2} \langle \mu_2|[\hat{F}^{\mathrm{pol}}, \hat{T}_2] + \hat{W}^{\mathrm{QM}}|\mathrm{HF}\rangle \\ &+ \sum_{i,j=1}^{2} \sum_{\mu_i\nu_j} \bar{E}^{\mathrm{f}}_{\mu_i} A_{\mu_i\nu_j} E^{\mathrm{f}}_{\nu_j} + \bar{\omega}^{\mathrm{f}} \left(1 - \sum_{i=1}^{2} \sum_{\mu_i} \bar{E}^{\mathrm{f}}_{\mu_i} E^{\mathrm{f}}_{\mu_i}\right) \\ &+ \frac{1}{2} \sum_{\mu} \left\langle \mathrm{HF}|\hat{Q}_\mu|\mathrm{HF}\right\rangle \langle \mathrm{HF}|\hat{V}_\mu|\mathrm{HF}\rangle + \sum_{\mu_0} \bar{\kappa}_{\mu_0} F^{\mathrm{pol}}_{\mu_0}. \end{aligned} \tag{24}$$

The first term in eqn (24) represents the HF and MP2 ground state energy, the second term accounts for the first order amplitude equations for $\hat{T}_2$ and the third term gives the excitation energy. $\bar{E}^{\mathrm{f}}$ and E^{f} are formally the left and right eigenvectors of **A** (for ADC(2) they are equivalent). The fourth term accounts for the normalization of the eigenvectors and the sixth term for the Hartree–Fock equations. The fifth term represents the polarization energy for the HF ground state. Thus, explicit effects of the polarizable continuum environment on the electronic excited states enter in the Lagrange function through the secular matrix **A**, the Fock matrix $\mathbf{F}^{\mathrm{pol}}$ and the HF polarization energy.

Requiring the Lagrangian to be stationary with respect to variations of the amplitudes t_{μ_2} gives the equations for the Lagrange multipliers $\bar{t}_{\mu_2}$:

$$\begin{aligned} \frac{\mathrm{d}L^{\mathrm{f}}}{\mathrm{d}t^{\mathrm{f}}_{\mu_2}} &= \langle \mathrm{HF}|[\hat{W}^{\mathrm{QM}}, \tau_{\mu_2}]|\mathrm{HF}\rangle + \langle E_1|[[\hat{W}^{\mathrm{QM}}, E_1], \tau_{\mu_2}]|\mathrm{HF}\rangle \\ &+ \left\langle \bar{t}^{\mathrm{f}}_{\mu_2}|[\hat{F}^{\mathrm{pol}}, \tau_{\mu_2}]|\mathrm{HF}\right\rangle = 0, \end{aligned} \tag{25}$$

which in a canonical MO basis can be directly inverted (cmp. ref. 34). In the same way, requiring stationarity with respect to orbital variations leads to the CPHF (or Z-vector) equations:

$$\sum_{AI} \bar{\kappa}_{AI} \left(A^{\kappa}_{AIBJ} - \delta_{AB}\varepsilon_A - \delta_{IJ}\varepsilon_I\right) = -\eta^{\kappa,\mathrm{f}}_{BJ}. \tag{26}$$

The capital indices refer to both active and frozen orbitals and ε_{p} are the orbital energies. The matrix A^{κ} on the left-hand side of eqn (26) is for COSMO defined as:

$$\begin{aligned} A^{\kappa}_{pqrs} &= \left\langle \mathrm{HF}\left|\left[\left[\hat{W}^{\mathrm{QM}}, E^{-}_{pq}\right], E^{-}_{rs}\right]\right|\mathrm{HF}\right\rangle \\ &+ \sum_{\mu} \left\langle \mathrm{HF}\left|\left[\hat{Q}_\mu, E^{-}_{pq}\right]\right|\mathrm{HF}\right\rangle \langle \mathrm{HF}|[\hat{V}_\mu, E^{-}_{rs}]|\mathrm{HF}\rangle. \end{aligned} \tag{27}$$

The expression for the right-hand-side (RHS) vector $\eta^{\kappa,\mathrm{f}}_{BJ}$ will be discussed below.

2.4.2 Excited state relaxed one- and two-electron densities. Our implementation of COSMO-RI-ADC(2) exploits the resolution of the identity (RI) approximation which allows for a fast atomic orbital (AO) to molecular orbital (MO) transformation at the level of three-index integrals and subsequent fast formation of the four-index integrals in the MO basis. The HF calculations can be done with or without applying the RI approximation. Therefore, we distinguish in the following between exact four-index integrals, $(pq|rs)$, from the HF energy and the Fock matrix and four-index integrals in the post-HF part which are always calculated within the RI approximation $(pq|rs)^{\mathrm{RI}}$.

Since we distinguished above between the charge density that couples the reaction field to the QM system and the exact charge density of the QM system, we obtain no explicit polarization contribution to the expression for the post-HF contributions to the (normal) one- and two-electron densities. Detailed expressions for the one-electron and the non-separable two-electron densities, $\mathbf{D}^{\mathrm{F,ex}}$ and $\mathbf{d}^{\mathrm{nsep,ex}}_{pqrs}$, that are used for the RI-ADC(2) gradients are given in ref. 34 and will not be repeated here. With them the RHS vector $\eta^{\kappa,\mathrm{f}}_{BJ}$ for COSMO-RI-ADC(2) can be calculated as:

$$\begin{aligned} \eta^{\kappa,\mathrm{f}}_{AI} &= \frac{1}{2}\left(D^{\mathrm{F,ex}}_{AI} + D^{\mathrm{F,ex}}_{IA}\right)(\varepsilon_I - \varepsilon_A) - \frac{1}{4}\sum_{pq}\left(D^{\mathrm{F,ex}}_{pq} + D^{\mathrm{F,ex}}_{qp}\right) A_{pqAI} \\ &+ \sum_{prs}\Big[\left(d^{\mathrm{nsep,ex}}_{pArs} + d^{\mathrm{nsep,ex}}_{Aprs}\right)(pI|rs)^{\mathrm{RI}} \\ &- \left(d^{\mathrm{nsep,ex}}_{pIrs} + d^{\mathrm{nsep,ex}}_{Iprs}\right)(Ap|rs)^{\mathrm{RI}}\Big] \\ &+ 2\sum_{i}\Big[G_{Ai}(\mathbf{D}^{\eta}(E_1))\left(D^{\xi}_{iI}(E_1) + D^{\xi}_{Ii}(E_1)\right) \\ &- G_{Ii}(\mathbf{D}^{\eta}(E_1))\left(D^{\xi}_{iA}(E_1) + D^{\xi}_{Ai}(E_1)\right)\Big]. \end{aligned} \tag{28}$$

After solution of the CPHF equations the gradients for the excited state can be evaluated as:

$$\begin{aligned} \frac{\mathrm{d}L}{\mathrm{d}x} &= \sum_{\alpha\beta} D^{\mathrm{eff,ao}}_{\alpha\beta} h^{[x]}_{\alpha\beta} + \frac{1}{2}\sum_{\alpha\beta\gamma\delta} d^{\mathrm{sep,ao}}_{\alpha\beta\gamma\delta} (\alpha\beta|\gamma\delta)^{[x]} \\ &- \sum_{\alpha\beta} F^{\mathrm{eff,ao}}_{\alpha\beta} S^{[x]}_{\alpha\beta} + \sum_{\alpha\beta P} \Lambda^{\mathrm{ao},P}_{\alpha\beta} (\alpha\beta|P)^{[x]} \\ &- \sum_{PQ} \gamma_{PQ} V^{[x]}_{PQ} + \frac{\mathrm{d}\Delta L^{\mathrm{pol,ex}}}{\mathrm{d}x}. \end{aligned} \tag{29}$$

We refer again to ref. 34 for detailed expressions of the AO and auxiliary densities. In the non-equlibrium limit the matrix $G(\mathbf{D}^{\eta})$ has to be computed with the screening function $f(n^2)$ for the optical range.

The explicit contributions from the reaction field to the analytic first derivatives of the excited state energy with respect to an external parameter x is:

$$\begin{aligned} \frac{\mathrm{d}\Delta L^{\mathrm{pol,ex}}}{\mathrm{d}x} &= \sum_{\kappa} Q^{\mathrm{HF}}_{\kappa}\left(\sum_{pq} D^{\mathrm{eff}}_{pq} V^{[x]}_{pq,\kappa} + V^{\mathrm{nuc},[x]}_{\kappa}\right) \\ &+ \sum_{\kappa}\left(Q^{\mathrm{eff}}_{\kappa} - Q^{\mathrm{HF}}_{\kappa}\right)\left(\sum_{pq} D^{\mathrm{HF}}_{pq} V^{[x]}_{pq,\kappa} + V^{\mathrm{nuc},[x]}_{\kappa}\right) \\ &+ \frac{1}{f(\varepsilon)}\sum_{\kappa\lambda} Q^{\mathrm{HF}}_{\kappa} \mathcal{A}^{[x]}_{\kappa\lambda}\left(Q^{\mathrm{eff}}_{\lambda} - \frac{1}{2}Q^{\mathrm{HF}}_{\lambda}\right) \\ &+ \sum_{\kappa\lambda} Q^{\xi}_{\kappa} \sum_{pq} D^{\eta}_{pq} V^{[x]}_{pq,\lambda} + \sum_{\kappa\lambda} Q^{\eta}_{\kappa} \sum_{pq} D^{\xi}_{pq} V^{[x]}_{pq,\lambda} \\ &+ \frac{1}{f(\varepsilon)}\sum_{\kappa\lambda} Q^{\xi}_{\kappa} \mathcal{A}^{[x]}_{\kappa\lambda} Q^{\eta}_{\lambda}. \end{aligned} \tag{30}$$

This journal is © the Owner Societies 2018

Published on 20 April 2018. Downloaded by Ruhr Universitat Bochum on 6/20/2018 12:17:46 PM.

In the last equation Q_κ^{HF}, Q_κ^ξ, Q_λ^η, and Q_κ^{eff} are the surface charges induced by the electron densities $\mathbf{D}^{\mathrm{HF}}$, $\mathbf{D}^\xi$, $\mathbf{D}^\eta$, and $\mathbf{D}^{\mathrm{eff}}$, respectively. For ADC(2) the contributions from Q_κ^η and $\mathbf{D}^\xi$ and from Q_κ^ξ and $\mathbf{D}^\eta$ are identical so that only one needs to be evaluated if the other is multiplied by a factor of 2. For expression for $\mathbf{D}^{\mathrm{eff}}$ we refer to ref. 34. $\mathscr{A}^{[x]}_{\kappa\lambda}$ is the derivative of the COSMO response kernel (cmp. (1)), $V^{[x]}_{pq,\kappa}$ are the derivatives of the potential energy integrals, and $V^{\mathrm{nuc},[x]}_\kappa$ the respective nuclear counterparts. Here, the charges Q_κ^ξ and Q_λ^η are in the non-equilibrium limit calculated with $f(n^2)$ and in the equilibrium limit with $f(\varepsilon)$.

The COSMO-RI-ADC(2) excitation energies and excited state gradients have been implemented in a development version of the ricc2[28] module of the TURBOMOLE package.[29]

3 Applications

In the current section we present as application of the implemented code described above solvatochromatic shifts of the UV and fluorescence spectra in two molecular systems where a qualitatively correct simultaneous description of charge transfer excitations and solvent effects is important. Their structures are shown in Fig. 1. The first one is 4-(*N*,*N*-dimethyl-amino)-benzonitrile (DMABN) and the second one the intermolecular complex formed by the 2-iodo-benzimidazolium cation with the triflate anion.

All ground state geometry optimizations have been done at the MP2/def2-TZVPP (vacuum) and/or COSMO-MP2/def2-TZVPP (solution) level of theory. The vertical excitation energies as well as the excited state geometry optimizations are calculated at the COSMO-RI-ADC(2) level with def2-TZVPP orbital[37] and auxiliary[38] basis sets and the corresponding effective core potential[37] for iodine. The frozen core approximation was applied with the $1s^2$ orbitals kept frozen for all C, O, and N atoms. For iodine, all orbitals were frozen up to and including the $4s^24p^6$ shell. The post-SCF reaction field scheme was applied to couple the QM system to the environment. Cartesian coordinates are provided as Supporting Information. All MP2 and ADC(2) calculations were done with the ricc2[28] module of the TURBOMOLE[29,30] package.

3.1 Solvatochromic shifts of vertical excitation energies

4-(*N*,*N*-Dimethylamino)benzonitrile (DMABN) is a paradigmatic example of a phenomenon called dual fluorescence, because depending on the experimental conditions, *e.g.* in a polar solvent, it fluoresces at two different energies. This organic donor–acceptor compound has been studied extensively by theoretical and computational groups over the last decades. It shows in addition to a band from a locally excited (LE) state, which dominates the fluorescence spectra of DMABN in both vacuum and polar solvents, a low-energy fluorescence band from a state termed intramolecular charge transfer (ICT) state, which is only observed in polar solvents.

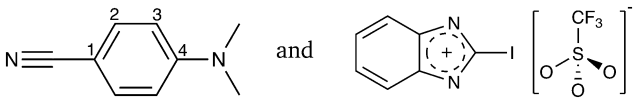


Fig. 1 Schematic structures of the investigated compounds.

Despite several computational studies on the spectroscopic properties of DMABN,[39–41] the solvent effects on the excited state energies and structures have not yet been investigated thoroughly at a correlated level of theory. In the following, we will discuss the excitation energies of DMABN at the ADC(2)/def2-TZVPP level in vacuum as well as in acetonitrile (non-equilibrium limit with ε = 36.7, n^2 = 1.81) as an example of a polar solvent, where we have used COSMO with both the PTED and the post-SCF reaction field schemes. Furthermore, we have used the gradient implementation for the post-SCF-COSMO-ADC(2)/def2-TZVPP approach to obtain the fully optimized equilibrium structure for the ICT state of DMABN in acetonitrile solution. Acetonitrile has been chosen as a solvent because a large amount of available computational and experimental data.[39,42–44]

According to ref. 45 and 46, the vertical excitations in vacuum and in the Franck–Condon region for the first excited state (LE) (also known as L_b state) is dominated by the one-electron HOMO → LUMO+1 transition and for the second excited state (ICT) (also known as L_a state) by the one-electron HOMO → LUMO transition. The results obtained for the vertical excitation energies, transition moments and excited state dipole moments in acetonitrile solution with COSMO-ADC(2) using the PTED and post-SCF reaction field schemes are listed together with the vacuum results in Table 1.

The PTED scheme predicts the second excited state as the bright state (f_2 = 0.63) and solvent induced shifts for the first and second excited state (LE and ICT, respectively) of −0.12 and −0.38 eV in acetonitrile, respectively. On the other hand, from the values for the oscillator strengths obtained with the post-SCF scheme we can conclude that this reaction field scheme predicts the bright state (f_2 = 0.71) to be the lowest excited state at 4.22 eV (with a solvatochromic shift of −0.46 eV). The analysis of the natural transition orbitals (NTOs) for the first two excited states,

Table 1 Calculated solvent shifts for the vertical excitation energies Δ^{sol} (eV), transition moments f and dipole moments μ (D) for the first two excited states of DMABN[a]

	Reaction field		
	In vacuo	PTED	Post-SCF
$\Delta\mathscr{G}_{1,0}$	4.42	4.29	4.31
$\Delta^{\mathrm{sol}}_{1,0}$		−0.12	−0.11
f_1	0.03	0.03	0.05
μ_1	9.30	12.08	12.82
$\Delta\mathscr{G}_{2,0}$	4.69	4.30	4.22
$\Delta^{\mathrm{sol}}_{2,0}$		−0.38	−0.46
f_2	0.55	0.63	0.71
μ_2	12.19	15.06	17.14

[a] All calculations are carried out at the COSMO-RI-ADC(2)/def2-TZVPP level using geometries optimized at the PTE-COSMO-MP2/def2-TZVPP level. Excited state energies are reported in different environments: '*in vacuo*' refers to the gas phase, for both PTED and post-SCF reaction field schemes acetonitrile has been used as the solvent (post-SCF reaction field has been used in the non-equilibrium solvation limit, ε = 36.7 and n^2 = 1.81). The PTED calculations are equilibrated for the ground state and include state-specific excited state non-equilibrium corrections.

Published on 20 April 2018. Downloaded by Ruhr Universitat Bochum on 6/20/2018 12:17:46 PM.

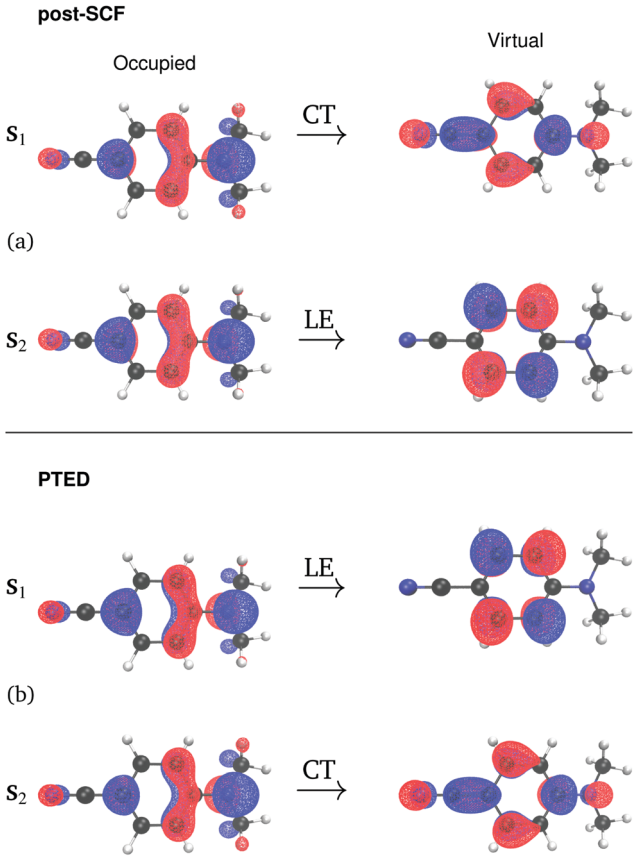


Fig. 2 Natural transition orbitals of DMABN calculated at the COSMO-ADC(2)/def2-TZVPP level in acetonitrile solution using (a) the post-SCF and (b) the PTED reaction field scheme.

Fig. 2, shows that S_1 and S_2 for the PTED scheme have LE and ICT characters, respectively, while for the post-SCF scheme the order is reversed. Table 1 shows that both schemes predict an increase of the dipole moments for both excited states with respect to the ground state (the ground state dipole moment in vacuum and solution are 7.41 and 9.94 D, respectively). The larger solvent shift for the L_a or ICT state in comparison to that for the L_b or LE state can be rationalized by the fact that the ICT state has a larger dipole moment (17.14 D with post-SCF and 15.06 D with PTED) compared to the LE state, and is thus more stabilized in a polar solvent like acetonitrile. An inversion of the order of the LE and ICT states in acetonitrile was also obtained by Scalmani[9] with PCM-TDDFT using a completely equilibrated response of the solvent for the calculation of vertical excitation energies.

With the post-SCF reaction field scheme the wall-time for the calculation of the vertical excitation energies plus the transition and dipole moments is very close to that of a corresponding calculation for the vacuum case and about five times shorter than for the PTED scheme.

To demonstrate the applicability of the developed COSMO-RI-ADC(2) excited state gradients to study the solvent effects on excited state structures, we studied the equilibrium geometry of the ICT state of DMABN in acetonitrile. According to the results reported in ref. 45, in the gas phase the LE state has a shallow

Table 2 Main geometrical parameters for the ground state (G.S.) and the ICT state in acetonitrile solution. The ground state geometry is optimized at the COSMO-MP2/def2-TZVPP and the excited ICT state at the COSMO-RI-ADC(2)/def2-TZVPP level (ε = 36.7, for the non-equilibrium limit n^2 = 1.81)

		ICT state		
	G.S.	COSMO eq.	COSMO non-eq.	Gas phase[a]
N–C_4[b]	1.36	1.42	1.42	1.44
C_3–C_4	1.42	1.44	1.44	1.45
C_2–C_3	1.38	1.37	1.37	1.37
C_1–C_2	1.40	1.44	1.44	1.43
C_1–C	1.42	1.40	1.40	1.41
C≡N	1.16	1.19	1.19	1.19
τ	0°	56°	65°	90°
ϕ	0°	32°	33°	41°

[a] Geometrical parameters of the ICT state with the C_s structure reported from ref. 45. [b] All the bond lengths are reported in Å. Atom numbers are the same as Fig. 1.

double minimum with a small twisting angle of $\tau = \pm 19°$ (τ is defined as the average of the dihedral angles $C_{Me}NC_4C_3$ and $C_{Me}'NC_4'C_3'$) with a small barrier of <0.05 eV. Some characteristic geometrical parameters of the ICT structures in acetonitrile solvent are collected in Table 2. Similar as in the gas phase studies,[45] the equilibrium geometry of the ICT state obtained at the RI-ADC(2)/def2-TZVPP level in acetonitrile solution, Fig. 3, has a twisted structure. The equilibrium geometry for the ICT state in the gas phase is found to have a twisted structure with a torsion angle of $\tau = 90°$ and an out-of-plane angle of $\phi = 41°$ (ϕ is defined as the angle of the C_4N bond with respect to a plane given by C_4, C_3 and C_3', cmp. Fig. 1). The torsion angles τ for the equilibrium geometries of the ICT state computed in the equilibrium and non-equilibrium solvation limits differ by only $\approx 9°$. All other internal coordinates are for the two structures nearly the same (cmp. Table 2). The torsion angle of the amino group is, however, with $\tau = 65°$ (non-eq) and $\tau = 56°$ (eq) smaller than in the gas phase. Also the out-of-plane angle of the dimethyl-amino group in solution is with $\phi \approx 33°$ smaller than in the gas phase study. Similar as in the gas phase, we find also in solution besides the twisting of the dimethyl-amino group, an increase of the C≡N and the N–C_4 bond lengths accompanied by a shortening of the C_1–C bond length from ground to the excited state. *I.e.* the phenyl moiety shows in the ICT state a quinoidal distortion. This is an expected consequence of the charge transfer from the lone-pair of the amino group to the benzene ring. The dipole moment of the ICT minimum in both

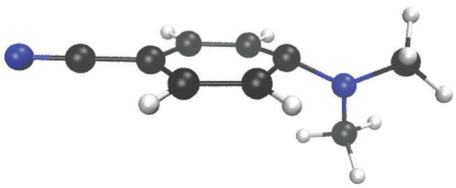


Fig. 3 Optimized geometry of the ICT state of DMABN at COSMO-RI-ADC(2)/def2-TZVPP level in the framework of post-SCF reaction field approach (non-equilibrium limit, ε = 36.7 and n^2 = 1.81).

This journal is © the Owner Societies 2018

Published on 20 April 2018. Downloaded by Ruhr Universitat Bochum on 6/20/2018 12:17:46 PM.

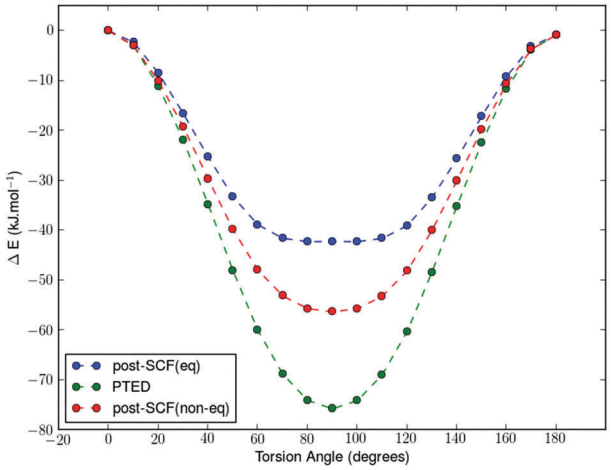


Fig. 4 Calculated potential energy curves for the ICT state of DMABN at the COSMO-ADC(2)/def2-TZVPP level as a function of the torsion angle τ. For further details see the text.

the equilibrium and the non-equilibrium solvation limits do not change much relative to the corresponding value for the ICT state at the Franck–Condon point (from 17.1 D to 17.5 D and 18.0 D, respectively).

To analyze the importance of state-specific reaction field contributions for the PES of charge transfer states we calculated unrelaxed PES scans for the ICT state of DMABN along the torsion angle defined by the atoms $C_{Me}NC_4C_3$ (cmp. Fig. 1) with all other internal coordinates constrained to their values in the PTE-COSMO-MP2 ground state geometry. The results for the equilibrium and non-equilibrium post-SCF and the PTED reaction field scheme from ref. 22 are shown in Fig. 4. For all three reaction field schemes increasing the torsion angle leads initially to a fast decrease in energy and agree well in the regime of $\pm 40^\circ$ around Franck–Condon point which is important for the short-time dynamics. For the post-SCF (eq) the potential reaches a flat minimum with a width of $\approx \pm 25^\circ$, while the post-SCF (noneq) and the PTED curves reach deeper sharp minima with essentially fully twisted geometries. Thus, an accurate description of the ICT minimum requires a reaction field scheme which includes a state-specific response to the excited state electron density. As pointed out above, such schemes are not suited for geometry optimization starting from the Franck–Condon point if one does not know that there will be no state intersections along the relaxation path on the excited state PES. DMABN, where S_1 and S_2 have, depending on the solvent polarity, an avoided crossing and/or conical intersection between the Franck–Condon point and the ICT or LE minimum, is a typical example for such a situation.

3.2 The 2-iodo-benzimidazolium·OTF ion pair in water

The 2-iodo-benzimidazolium·OTF ion pair is used as a second test system to study solvent effects on electronic excitation energies and geometries of excited states in solution. The Lewis acid character of the 2-iodo-benzimidazolium cation and the Lewis base character of the triflate anion lead in the ground state to the formation of a halogen-bonded 2-iodo-benzimidazolium·OTF complex. It is noteworthy that the solvent has significant effects on the geometry of the ion pair, in particular on the length of the halogen bond which shrinks in solution by ≈ 0.38 Å compared to the corresponding bond length in vacuum, as well as on the binding energy in the ground state where the structure with stacking interaction between the triflate anion and the five-membered ring is energetically more favored over the halogen-bonded structure by about 3.7 kcal mol^{-1}. We have investigated the vertical excitation energies and analyzed the natural transition orbitals for the three lowest transitions in vacuum and in aqueous solution. Water is usually the worst-case scenario for continuum solvation models. In vacuum, the first transition at 4.55 eV has a mixed inter- and intramolecular CT character (see the ESI† for the NTOs in the vacuum case). The second and third states in vacuum at 4.67 eV and 5.15 eV are, respectively, inter- and intramolecular CT transitions. Table 3 summarizes the excitation energies, transition moments and the changes of dipole moments with respect to the ground state obtained in vacuum and in aqueous solution within the post-SCF and PTED schemes.

Table 3 Calculated vertical excitation energies $\Delta\mathscr{G}$ (eV), transition moments f and the changes of dipole moments $\Delta\mu$ (D) for the first three electronic excited states of the halogen-bonded 2-iodo-benzimidazolium·OTF ion pair in vacuum and aqueous solution (in the non-equilibrium solvation limit, ε = 80.4 and n^2 = 1.78)[b]

	Reaction field		
	In vacuo	PTED	Post-SCF
$\Delta\mathscr{G}_{1,0}$	4.55	4.75	4.70
f_1	0.41	0.46	0.55
$\Delta\mu_1$[a]	−7.82	1.27	1.28
$\Delta\mathscr{G}_{2,0}$	4.67	5.15	5.17
f_2	0.08	0.08	0.13
$\Delta\mu_2$	−19.33	5.97	6.94
$\Delta\mathscr{G}_{3,0}$	5.15	5.61	5.64
f_3	0.00	0.00	0.00
$\Delta\mu_3$	−10.19	5.62	5.99

[a] $\Delta\mu_i = \mu_i - \mu_0$ with μ_0 as the dipole moment of the ground state. [b] All calculations are carried out at the COSMO-RI-ADC(2)/def2-TZVPP level using geometries optimized at the PTE-COSMO-MP2/def2-TZVPP level. Excited state energies are reported in different environments: '*in vacuo*' refers to the gas phase, for both PTED and post-SCF reaction field schemes water has been used as the solvent (post-SCF reaction field has been used in the non-equilibrium solvation limit, ε = 80.4 and n^2 = 1.78). The PTED calculations are equilibrated for the ground state and include state-specific excited state non-equilibrium corrections.

The characters of the excited states predicted by the post-SCF reaction field scheme for the three lowest states agree with those obtained with the more costly PTED scheme. Also the vertical excitation energies obtained with the two reaction field schemes are in good agreement. The results from the post-SCF scheme for the second and third states are only marginally higher by about 0.02 and 0.03 eV, respectively, and for the first excited state slightly lower by 0.05 eV. The values of the transition moments calculated in both approaches predict that in the UV spectrum of 2-iodo-benzimidazolium·OTF the first excited state is a bright state.

The stabilization of the local charges on the triflate anion and the benzimidazolium rings by the polar solvent and the corresponding weakening of the ionic interaction results in

Published on 20 April 2018. Downloaded by Ruhr Universitat Bochum on 6/20/2018 12:17:46 PM.

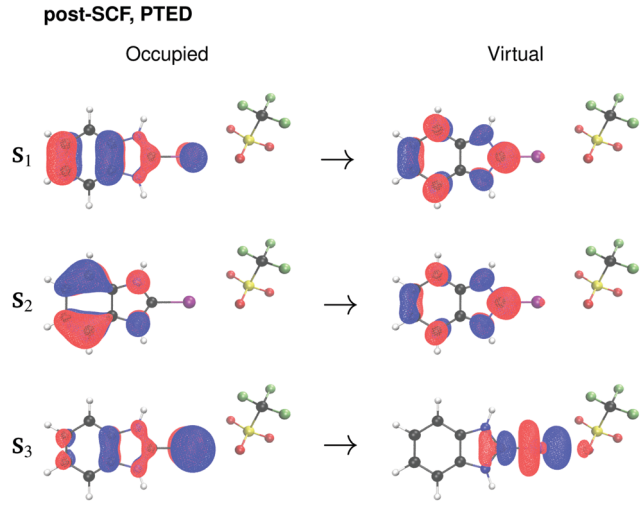


Fig. 5 Natural transition orbitals of 2-iodo-benzimidazolium·OTF calculated at COSMO-RI-ADC(2)/def2-TZVPP level within the post-SCF scheme (the same as for PTED) in aqueous solution (ε = 80.4 and n^2 = 1.78).

different characters for the electronic transitions in water compared to the vacuum case, especially for the second and third states. In accord with this, the values for the changes of the dipole moment upon excitation, $\Delta\mu$, predicted for these three states are negative in vacuum due to the decrease of the dipole moment in the excited states, while in aqueous solution both reaction field schemes predict positive values for $\Delta\mu$, *i.e.* an increase of the dipole moment upon excitation.

As shown in Fig. 5, both, the post-SCF and the PTED reaction field schemes, predict in aqueous solution a locally $\pi \rightarrow \pi^*$ excited character for the S_1 state with a small intramolecular CT from the iodine atom to the conjugated rings. Also they give with 5.17 eV (post-SCF) and 5.15 eV (PTED) very close excitation energies for the second excited state with $\pi \rightarrow \pi^*$ character and also agree well with 5.64 eV (post-SCF) and 5.61 eV (PTED) for the excitation energies of the third excited state with $n \rightarrow \sigma^*$ character (from a lone pair of the iodine atom to the σ^* orbital of the C–I bond).

Also for the 2-iodo-benzimidazolium·OTF ion pair we applied the newly developed gradient implementation for COSMO-RI-ADC(2) to determine the equilibrium geometry of the lowest singlet excited state S_1 using the def2-TZVPP basis set, Fig. 6.

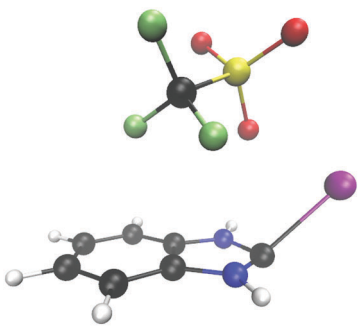


Fig. 6 The equilibrium structure of the S_1 state in aqueous solution at COSMO-RI-ADC(2)/def2-TZVPP level within the post-SCF reaction field scheme (non-equilibrium limit, ε^2 = 80.4 and n^2 = 1.78).

The striking difference between the S_1 and the S_0 equilibrium structures is that in the S_1 state the attraction between the CF_3 group and the π-system of the benzimidazolium rings dominates over the I–O halogen bond interaction. The charge transfer from the p_π orbital of iodine to the benzimidazolium gives rise to a C–I bond elongation by $\approx$0.4 Å and an out-of-plane bending of the C–I bond by $\approx 46^\circ$ similar as observed for the amino group in the ICT state of DMABN.

4 Summary and conclusions

In this work we applied a post-SCF reaction field scheme, which is intermediate between the PTE and PTED reaction field schemes, for combining the COSMO polarizable continuum model with the correlated wavefunction method ADC(2) for calculations on electronically excited states including solvent effects. The theory for analytic excited state gradients for the post-SCF variant of COSMO-ADC(2) has been derived and implemented for equilibrium and non-equilibrium situations so that solvent effects on excited state relaxation dynamics, equilibrium geometries and potential energy surfaces can be studied at this level of theory. The post-SCF reaction field scheme goes beyond PTE by including linear response contributions to the reaction field at the correlated, *i.e.* here the ADC(2) level, but it avoids perturbative corrections and waives the state-specific self-consistent construction of the reaction field for the excited states of the PTED scheme. Both would prevent a qualitative correct description of avoided crossings and conical intersections of the excited states and the PTED scheme would increase the computational costs by a large factor and diminish the numerical stability of the molecular gradients. With the post-SCF reaction field scheme the additional computational costs for including solvent effects at the correlated wavefunction level on excitation energies and excited state molecular gradients are only a small fraction of the costs for the corresponding gas phase calculation.

We demonstrated the capability of COSMO-RI-ADC(2) to provide solvent-induced shifts for UV spectra and excited state equilibrium structures within the post-SCF scheme for two different compounds: DMABN and 2-iodo-benzimidazolium·OTF. Although in the first case we observe an inversion in the order of the lowest two excited states between the post-SCF and the PTED scheme in acetonitrile solution where the two states are very close in energy, the two reaction field schemes agree in general well for solvent shifts of excitation energies, transition and dipole moments. For both sample applications we investigated the relaxation of the excited state structures for the first singlet excited states starting from the Franck–Condon geometries at the COSMO-RI-ADC(2) level of theory within the post-SCF scheme.

In conclusion, COSMO-RI-ADC(2) with the post-SCF reaction field scheme with its consistent description of the excited state PES, which are obtained from a common eigenvalue problem, is a highly attractive method to calculate not only vertical excitation energies but also properties related to the PES like

 This journal is © the Owner Societies 2018

Published on 20 April 2018. Downloaded by Ruhr Universitat Bochum on 6/20/2018 12:17:46 PM.

equilibrium geometries, deexcitation pathways and Stoke shifts in solution beyond the TDDFT level. The implementation of analytic excited state gradients for this approach provides the possibility to obtain useful insights into photophysical properties and photochemical pathways in solution at the correlated wavefunction level. The price that is paid to obtain PES which retain a physically correct structure in the vicinity of (near) degeneracies is the exclusion of state-specific corrections that account for changes of the reaction field induced by the change of density upon excitation is a limited applicability for states with large charge transfer. This is a dilemma for reaction field methods which is difficult to resolve.

The reported COSMO-RI-ADC(2) functionalities have been implemented in a development version of the TURBOMOLE program package[29,30] and will be made available in forthcoming releases of the package.

Conflicts of interest

There are no conflicts to declare.

Acknowledgements

We gratefully acknowledge financial support from the Cluster of Excellence RESOLV (EXC 1069) and project Ha 2588/8-1 funded by the Deutsche Forschungsgemeinschaft.

References

1 J. Tomasi, B. Mennucci and R. Cammi, *Chem. Rev.*, 2005, **105**, 2999–3093.
2 C. Cramer and D. Truhlar, *Chem. Rev.*, 1999, **99**, 2161–2200.
3 A. Klamt, *Wiley Interdiscip. Rev.: Comput. Mol. Sci.*, 2011, **1**, 699–709.
4 A. Klamt, *J. Phys. Chem.*, 1996, **100**, 3349–3353.
5 J. Tomasi, B. Mennucci and R. Cammi, *Chem. Rev.*, 2005, **105**, 2999–3094.
6 B. Mennucci, *Wiley Interdiscip. Rev.: Comput. Mol. Sci.*, 2012, **2**, 386–404.
7 R. Cammi, B. Mennucci and J. Tomasi, *J. Phys. Chem. A*, 2000, **104**, 5631–5637.
8 M. Cossi and V. Barone, *J. Chem. Phys.*, 2001, **115**, 4708–4717.
9 G. Scalmani, M. J. Frisch, B. Mennucci, J. Tomasi, R. Cammi and V. Barone, *J. Chem. Phys.*, 2006, **124**, 094107.
10 R. Cammi, *J. Chem. Phys.*, 2009, **131**, 164104.
11 R. Cammi, *Int. J. Quantum Chem.*, 2010, **110**, 3040–3052.
12 R. Cammi, *Int. J. Quantum Chem.*, 2012, **112**, 2547–2560.
13 M. Caricato, *J. Chem. Theory Comput.*, 2012, **8**, 5081–5091.
14 S. Yomosa, *J. Phys. Soc. Jpn.*, 1974, **36**, 1655.
15 B. Mennucci, R. Cammi and J. Tomasi, *J. Chem. Phys.*, 1998, **109**, 2798–2807.
16 K. V. Mikkelsen, P. Jrrgensen and H. J. A. Jensen, *J. Chem. Phys.*, 1994, **100**, 6597–6607.
17 O. Christiansen, T. Nymand and K. V. Mikkelsen, *J. Chem. Phys.*, 2000, **113**, 8101–8112.
18 R. Cammi, S. Corni, B. Mennucci and J. Tomasi, *J. Chem. Phys.*, 2005, **122**, 104513.
19 S. Corni, R. Cammi, B. Mennucci and J. Tomasi, *J. Chem. Phys.*, 2005, **123**, 134512.
20 R. Improta, V. Barone, G. Scalmani and M. J. Frisch, *J. Chem. Phys.*, 2006, **125**, 054103.
21 M. Caricato, B. Mennucci, J. Tomasi, F. Ingrosso, S. Corni and G. Scalmani, *J. Chem. Phys.*, 2006, **124**, 124520.
22 B. Lunkenheimer and A. Köhn, *J. Chem. Theory Comput.*, 2013, **9**, 977–994.
23 O. Christiansen and K. V. Mikkelsen, *J. Chem. Phys.*, 1999, **110**, 8348.
24 R. Cammi, *J. Chem. Phys.*, 2009, **131**, 164104.
25 M. Caricato, *J. Chem. Phys.*, 2011, **135**, 074113.
26 A. Klamt and G. Schüürmann, *J. Chem. Soc., Perkin Trans. 2*, 1993, 799–805.
27 J. Schirmer, *Phys. Rev. A: At., Mol., Opt. Phys.*, 1982, **26**, 2395–2416.
28 C. Hättig and F. Weigend, *J. Chem. Phys.*, 2000, **113**, 5154–5161.
29 TURBOMOLE V7.2 2017, a development of University of Karlsruhe and Forschungszentrum Karlsruhe GmbH, 1989–2007, TURBOMOLE GmbH, since 2007, available from http://www.turbomole.com.
30 F. Furche, R. Ahlrichs, C. Hättig, W. Klopper, M. Sierka and F. Weigend, *Wiley Interdiscip. Rev.: Comput. Mol. Sci.*, 2014, **4**, 91–100.
31 T. Schwabe, K. Sneskov, J. M. H. Olsen, J. Kongsted, O. Christiansen and C. Hättig, *J. Chem. Theory Comput.*, 2012, **8**, 3274–3283.
32 M. Head-Gordon, R. J. Rico, M. Oumi and T. J. Lee, *Chem. Phys. Lett.*, 1994, **219**, 21–29.
33 O. Christiansen, H. Koch and P. Jørgensen, *Chem. Phys. Lett.*, 1995, **243**, 409–418.
34 C. Hättig, *Adv. Quantum Chem.*, 2005, **50**, 37–60.
35 D. Hrsak, A. M. Khah, O. Christiansen and C. Hättig, *J. Chem. Theory Comput.*, 2015, **11**, 3669–3678.
36 K. Sneskov, T. Schwabe, J. Kongsted and O. Christiansen, *J. Chem. Phys.*, 2011, **134**, 104108.
37 F. Weigend and R. Ahlrichs, *Phys. Chem. Chem. Phys.*, 2005, **7**, 3297–3305.
38 A. Hellweg, C. Hättig, S. Höfener and W. Klopper, *Theor. Chem. Acc.*, 2007, **117**, 587–597.
39 I. Georgieva, A. J. A. Aquino, F. Plasser, N. Trendafilova, A. Köhn and H. Lischka, *J. Phys. Chem. A*, 2015, **119**, 6232–6243.
40 N. Dozova, R. Kumar, T. Pradhan, F. Lacombat, B. Valeur, J. S. Kim and P. Plaza, *Chem. Commun.*, 2015, **51**, 14859–14861.
41 B. F. E. Curchod, A. Sisto and T. J. Martínez, *J. Phys. Chem. A*, 2017, **121**, 265–276.
42 K. A. Zachariasse, M. Grobys and E. Tauer, *Chem. Phys. Lett.*, 1997, **274**, 372–382.
43 S. I. Druzhinin, N. P. Ernsting, S. A. Kovalenko, L. P. Lustres, T. A. Senyushkima and K. A. Zachariasse, *J. Phys. Chem. A*, 2006, **110**, 2955–2969.
44 V. A. Galievsky and K. A. Zachariasse, *Acta Phys. Pol., A*, 2007, **112**, S39–S56.
45 A. Köhn and C. Hättig, *J. Am. Chem. Soc.*, 2004, **126**, 7399–7410.
46 C. Hättig, A. Hellweg and A. Köhn, *J. Am. Chem. Soc.*, 2006, **128**, 15672–15682.

3 UV absorption and magnetic circular dichroism spectra of purine, adenine, and guanine: A coupled cluster study in vacuo and in aqueous solution

Reprinted with permission from *J. Chem. Theory Comput.* 2019, 15, 1242–1254. Copyright 2019 American Chemical Society.

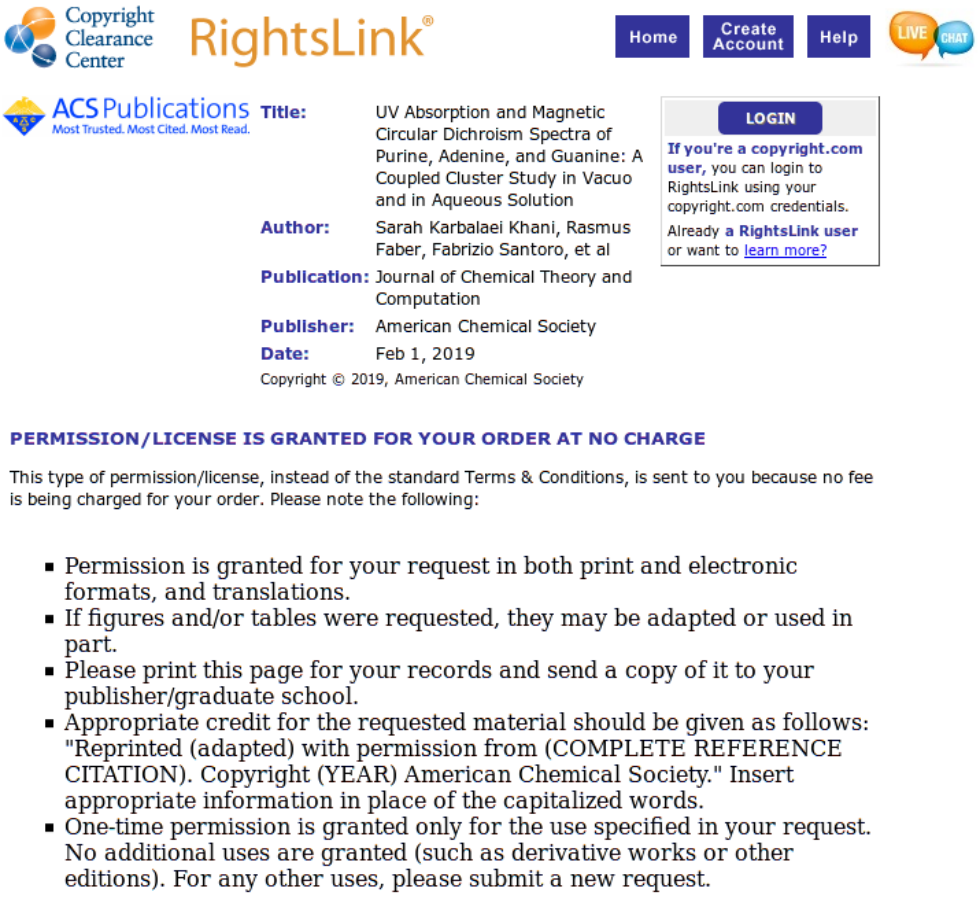
This paper reports the results of a project that I carried out during my international internship in the group of Prof. Sonia Coriani at the Technical University of Denmark (DTU). This sub-project dealt with the combination of the COSMO and coupled cluster theory at the CC2 level to determine the contribution of the solvent to the electronic excitation energies, oscillator strengths and Faraday $\mathcal{B}$ terms of magnetic circular dichroism (MCD) within the post-SCF reaction field approach. The main motivation for developing COSMO-RI-CC2 theory was to evaluate the photochemistry and particularly the relative positions of the $\pi\pi^*$ and $n\pi^*$ electronic transitions for purine, adenine and guanine DNA nucleobases. The computed excitation energies and UV and MCD absorption spectra for all three molecules reproduce the experimental profiles in aqueous solution. Furthermore, our analysis of the sum-over-states expression for the $\mathcal{B}$ term clarified that the relative stability of $\pi\pi^*$ states of adenine, which has been the subject of many theoretical investigations, can not be determined from the sign of the MCD bands.[4,5]

My contribution to this project was to partially develop the theory for the COSMO-RI-CC2

[4]Article: https://pubs.acs.org/doi/pdf/10.1021/acs.jctc.8b00930

[5]ESI: https://pubs.acs.org/doi/suppl/10.1021/acs.jctc.8b00930/suppl_file/ct8b00930_si_001.pdf

and to implemented the required modifications in the TURBOMOLE program package under the guidance of Christof Hättig. In case of computational results, I have carried out the calculations during my stay at DTU under the supervision of Sonia Coriani. The computational results at the CCSD level was reported by our collaborators, Rasmus Faber and Sonia Coriani at Technical University of Denmark. I have prepared all the figures and tables and also the first draft of the manuscript which later on was further developed together with my co-authors.



Copyright Clearance Center RightsLink®

Home | Create Account | Help | LIVE CHAT

ACS Publications
Most Trusted. Most Cited. Most Read.

Title: UV Absorption and Magnetic Circular Dichroism Spectra of Purine, Adenine, and Guanine: A Coupled Cluster Study in Vacuo and in Aqueous Solution

Author: Sarah Karbalaei Khani, Rasmus Faber, Fabrizio Santoro, et al

Publication: Journal of Chemical Theory and Computation

Publisher: American Chemical Society

Date: Feb 1, 2019

Copyright © 2019, American Chemical Society

LOGIN

If you're a copyright.com user, you can login to RightsLink using your copyright.com credentials.

Already a RightsLink user or want to learn more?

PERMISSION/LICENSE IS GRANTED FOR YOUR ORDER AT NO CHARGE

This type of permission/license, instead of the standard Terms & Conditions, is sent to you because no fee is being charged for your order. Please note the following:

- Permission is granted for your request in both print and electronic formats, and translations.
- If figures and/or tables were requested, they may be adapted or used in part.
- Please print this page for your records and send a copy of it to your publisher/graduate school.
- Appropriate credit for the requested material should be given as follows: "Reprinted (adapted) with permission from (COMPLETE REFERENCE CITATION). Copyright (YEAR) American Chemical Society." Insert appropriate information in place of the capitalized words.
- One-time permission is granted only for the use specified in your request. No additional uses are granted (such as derivative works or other editions). For any other uses, please submit a new request.

JCTC Journal of Chemical Theory and Computation

Article

Cite This: J. Chem. Theory Comput. 2019, 15, 1242−1254

pubs.acs.org/JCTC

UV Absorption and Magnetic Circular Dichroism Spectra of Purine, Adenine, and Guanine: A Coupled Cluster Study in Vacuo and in Aqueous Solution

Sarah Karbalaei Khani,*[,†,‡] Rasmus Faber,[‡] Fabrizio Santoro,[¶] Christof Hättig,*[,†] and Sonia Coriani*[,‡]

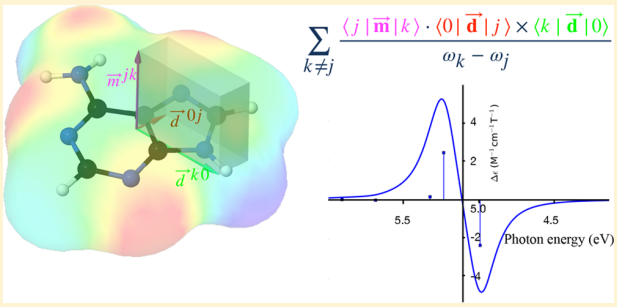
[†]Arbeitsgruppe Quantenchemie, Ruhr-Universität, Bochum D-44780, Germany

[‡]DTU Chemistry, Technical University of Denmark, Kemitorvet Build. 207, DK-2800 Kongens Lyngby, Denmark

[¶]Istituto di Chimica dei Composti Organo-Metallici, Consiglio Nazionale delle Ricerche (ICCOM-CNR), Area della Ricerca, via G. Moruzzi 1, I-56124 Pisa, Italy

Supporting Information

ABSTRACT: The absorption and magnetic circular dichroism (MCD) spectra of purine and of the purine nucleobases adenine and guanine have been calculated in gas phase at the Coupled Cluster Singles and Doubles (CCSD) and Resolution-of-Identity Singles and Approximate Doubles (RI-CC2) levels of theory. Exploiting a new development in the TURBOMOLE program package for computing vertical excitation energies and Faraday $\mathcal{B}$ terms in an implicit solvent approximated by the conductor-like screening model (COSMO) at the CC2 level, we have investigated the solvent effects on the relative positions of the $\pi\pi^*$ and $n\pi^*$ electronic transitions in these three molecules and compared them to the corresponding vacuum results. In the case of adenine, we also included specific solvent effects with a small water cluster. The spectra obtained with the implicit model COSMO are in qualitative agreement with those obtained with explicit water molecules both with and without the inclusion of the bulk solvent effects via the continuum solvent model. This suggests that the inclusion of the electrostatic contributions of the solvent can provide a sufficiently accurate description of the absorption spectra for adenine. The results for purine, adenine, and guanine show that, after the inclusion of bulk solvation, the $\pi\pi^*$ states shift to lower energies while at the same time $n\pi^*$ states show a reversed behavior. The computed MCD spectra show the characteristic bisignate profile found experimentally in all cases, despite, for adenine, remarkable differences in the origin of the individual peaks for different computational methods. Therefore, the ability (or inability) of MCD to determine the relative stability of the L_a and L_b states is critically reassessed. According to our best estimate for adenine in aqueous solution, the L_a state is more stable than L_b.



1. INTRODUCTION

The excited states of DNA bases have in the past years been subject of a plethora of theoretical and experimental studies with the objective of gaining new insights into the photochemistry and dynamics of these systems.[1−4] Purinic (adenine and guanine) nucleobases are one of the key groups of light-absorbing chromophores in the 200−300 nm region, which contain the information in DNA and RNA. Due to the short excited-state lifetimes of purine bases and the ultrafast nonradiative deactivation of excited states, photochemical reactions, and thus the formation of primary photoproducts, are disfavored. This is important for the stability of the DNA against photodamage, which can cause skin cancer, for example.

Because of its biological significance, the photostability of nucleobases against UV-initiated damage and photoactivated processes in purine bases have been and still are intensively studied. In general, providing accurate energetic and spectroscopic data for these nucleobases is essential for understanding the processes in which they are involved. In recent years, the relative stability of the two lowest bright states with $\pi\pi^*$ character of 9H-adenine has been extensively investigated with different methods.[5−10] In the case of purines, these two $\pi\pi^*$ states, which are labeled as L_a and L_b, are characterized as HOMO → LUMO excitation for L_a and a combination of HOMO − 2 → LUMO and HOMO → LUMO + 1 excitations for L_b. In addition to the absorption, also the MCD spectra have been calculated both in vacuo and in aqueous solution[6,10] and compared with existing experimental data[5,11,12] in order to help to discriminate between these two states. A number of TD-DFT (time-dependent

Received: September 14, 2018
Published: November 29, 2018

Downloaded by BOCHUM LIBRARIES at 05:37:19:222 on July 01, 2019
from https://pubs.acs.org/doi/10.1021/acs.jctc.8b00930.

© 2018 American Chemical Society

DOI: 10.1021/acs.jctc.8b00930
J. Chem. Theory Comput. 2019, 15, 1242−1254

density functional theory) investigations have suggested that L_a is energetically more stable than L_b.[6,13] For instance, spectroscopic studies of adenine at the TD-DFT level[6] have predicted a lower energy for the L_a compared to the L_b state by ∼0.1−0.3 eV in vacuum and in aqueous solution (describing solvent effects by cluster models and by the polarizable continuum model (PCM)), where the excitation to L_a carries most of the oscillator strength. Contrary to TD-DFT, most wave function based methods such as EOM-CCSD or EOM-CCSD(T) in vacuo[14−16] and CASSCF/CASPT2 in both vacuum[17,18] and a DNA environment[19] have predicted the L_b state at lower energy than L_a by ∼0.2 eV. An exception is CC2, which gives virtually degenerate results in vacuum for the vertical excitation energies to the L_a and L_b states.[20]

Guanine is a purine nucleobase that exists in several tautomeric forms of which the most stable ones are very close in energy in the gas phase. Quantum mechanical studies at the EOMEE-CCSD(T) level on the biologically most relevant tautomer of guanine, keto-N9H, have predicted that the lowest excitation is a $\pi\pi^*$ transition, while at the EOMEE-CCSD level, the first and second transitions were found to be virtually degenerate and to have πRyd (where Ryd stands for Rydberg) and $\pi\pi^*$ characters.[14] An assignment based on CC2 (using a triple-ζ basis with diffuse functions) predicted a weak πRyd transition along with a substantial $\pi\pi^*$ character for the lowest excited state and a close-lying πRyd transition for the second excited state, while the third and the fourth excited states with, respectively, $n\pi^*$ and πRyd character appear at significantly higher energies.[20] At the TD-DFT level, the two low-lying states have been assigned as $\pi\pi^*$ transitions with the L_b state lower than L_a at 4.64 eV,[21] whereas at the CASPT2 level L_a has been found lower than L_b by ∼0.74 eV.[22]

However, the energy differences between these states are of about the same order as the remaining errors of the currently available methods and basis sets that can be applied to molecules of the size of purinic nucleobases. Thus, despite numerous previous theoretical studies, there are still unsolved important questions, for example, the exact order of their lowest excited states in solution and biological environments. In a biological setting, molecules are embedded in a complex environment with multiple interactions including electrostatic ones. The energy of electronically excited states, particularly those with large transition dipole moments or significant changes in the charge distribution upon excitation, is sensitive to polar environments and solvents. At the same time, solvents also induce remarkable inhomogeneous broadenings that smear out vibronic progressions and make the identification of different close lying electronic states more difficult. In this regard, it has been suggested to use Magnetic Circular Dichroism (MCD) spectroscopy on the purine bases in the UV−vis region to assist in the interpretation of their electronic spectra,[6] since, due to their signed nature, MCD signals improve the capability of locating and separating transitions that are overlapping or have weak intensity in the one-photon absorption (OPA) spectra.[23,24] It was assumed that the signed nature of MCD spectra could elucidate the energy ordering of excited states especially when, as in the adenine case, for example, the debate evolves around the energy ordering of bright excited states.[6] We will in the following critically reassess this assumption.

To facilitate the study of solvent effects on the relative positions, intensities, and even the nature of different electronic states in MCD and UV−vis absorption spectra, we report in the current contribution for the first time an implementation of the conductor-like screening model (COSMO)[25] to include the solvation effects for oscillator strengths and for the Faraday $\mathcal{B}$ term of MCD at the level of the second-order approximate coupled-cluster singles and doubles model, CC2,[26,27] within the post-SCF reaction field scheme.[28−33] We apply the COSMO-RI-CC2 approach to investigate the UV−vis absorption and MCD spectra of purine and the nucleobases adenine and guanine in aqueous solution. To account for higher-order correlation effects beyond CC2, we also performed calculations of excitation energies, oscillator strengths, and Faraday $\mathcal{B}$ terms in vacuum at the CCSD level of theory for both purine and adenine.

2. THEORY

Within coupled cluster (CC) response theory, excitation energies, ω_j, and left and right excitation vectors, $\bar{E}^j(-\omega_j)$ and $E^j(\omega_j)$, for an excited state j are obtained as solutions of the nonsymmetric eigenvalue equations

$$\mathbf{A}E^j(\omega_j) = \omega_j E^j(\omega_j) \quad \text{and} \quad \bar{E}^j(-\omega_j)\mathbf{A} = \omega_j \bar{E}^j(-\omega_j) \tag{1}$$

for the CC Jacobian matrix, $\mathbf{A}$, which is the derivative of the cluster equations with respect to the cluster amplitudes, t_ν

$$A_{\mu\nu} = \langle \mu | \exp(-\hat{T})[\hat{H}, \tau_\nu] \exp(\hat{T}) | \mathrm{HF} \rangle \tag{2}$$

In the last equation, $\hat{T} = \sum_\mu t_\mu \tau_\mu$ is the cluster operator. The transition strength matrix elements (for electric dipole moment components d_α and d_β) for an excitation out of the ground state 0 are determined from the residues of the linear response function and take the form

$$S^{\alpha\beta}_{0\to j} = \frac{1}{2}\{M^{d_\alpha}_{0\leftarrow j} M^{d_\beta}_{j\leftarrow 0} + (M^{d_\beta}_{0\leftarrow j} M^{d_\alpha}_{j\leftarrow 0})^*\} \tag{3}$$

where the left and right transition moments are given by

$$M^{d_\alpha}_{0\leftarrow j} = \eta^{d_\alpha} E^j(\omega_j) + \bar{M}^j(\omega_j)\xi^{d_\alpha} \quad \text{and}$$
$$M^{d_\alpha}_{j\leftarrow 0} = \bar{E}^j(-\omega_f)\xi^{d_\alpha} \tag{4}$$

In the last equation, ξ^{d_α} and η^{d_α} are, respectively, the second derivatives of the Lagrange function with respect to the field strength and Lagrange multipliers and the field strength and cluster amplitudes. $\bar{M}^j(\omega_j)$ is a vector containing auxiliary (zero-order) Lagrange multipliers obtained as solution of the linear equation

$$\bar{M}^j(\mathbf{A} + \omega_j 1) = -\mathbf{F}E^j(\omega_j) \tag{5}$$

where $\mathbf{F}$ is the second derivative of the CC Lagrangian with respect to the cluster amplitudes. The oscillator strengths, $f(0 \to j)$, that determine the intensity of the UV−vis absorption bands, are obtained directly from the diagonal elements of the electric dipole transition strength matrix

$$f(0 \to j) = \frac{2}{3}\omega_j(S^{xx}_{0\to j} + S^{yy}_{0\to j} + S^{zz}_{0\to j}) \tag{6}$$

A derivation of the above equations can be found for instance in ref 34. For details on the implementation of the above equations at the CC2 and CCSD levels in gas phase we refer to refs 35−37 and to refs 38 and 39 for the details on their implementation at the RI-CC2 level in vacuo. In the following,

DOI: 10.1021/acs.jctc.8b00930
J. Chem. Theory Comput. 2019, 15, 1242−1254

we briefly discuss the modifications needed to include solvent effects in the CC2 or RI-CC2 calculations with the conductor-like screening model (COSMO)[25] as continuum solvation model.[40]

The Lagrange function for the approximate coupled cluster singles and doubles model CC2 including the environment contribution within the framework of COSMO can be written as

$$\begin{aligned} L = {} & \mathcal{G}_{\mathrm{HF}} + \langle \mathrm{HF}|\hat{\tilde{F}}_N^{\mathrm{pol}} + \hat{\tilde{W}}_N^{\mathrm{QM}} + [\hat{\tilde{W}}_N^{\mathrm{QM}}, \hat{T}_2]|\mathrm{HF}\rangle \\ & + \langle \bar{t}_1|\hat{\tilde{F}}_N^{\mathrm{pol}} + \hat{\tilde{W}}_N^{\mathrm{QM}} + [\hat{F}_N^{\mathrm{pol}} + \hat{\tilde{W}}_N^{\mathrm{QM}}, \hat{T}_2]|\mathrm{HF}\rangle \\ & + \langle \bar{t}_2|[\hat{F}_N^{\mathrm{pol}}, \hat{T}_2] + \hat{\tilde{W}}_N^{\mathrm{QM}}|\mathrm{HF}\rangle \\ & + \frac{1}{2}\sum_{\kappa} \langle \mathrm{HF} + \bar{t}_1|\hat{\tilde{Q}}_{N,\kappa}|\mathrm{HF}\rangle\langle \mathrm{HF} + \bar{t}_1|\hat{\tilde{V}}_{N,\kappa}|\mathrm{HF}\rangle \end{aligned} \tag{7}$$

In the above equation, $\bar{t}_i$ are the Lagrange multipliers and the tilde accent on the operators indicates a similarity transformation according to $\hat{\tilde{O}} = \exp(-\hat{T}_1)\hat{O}\exp(\hat{T}_1)$ and a lower index N normal ordering. $\mathcal{G}_{\mathrm{HF}}$ is the COSMO Hartree−Fock free energy. The Fock operator for the polarized system $\hat{\tilde{F}}^{\mathrm{pol}}$ and the fluctuation potential $\hat{\tilde{W}}^{\mathrm{QM}}$, along with the density-dependent surface charge and potential operators, $\hat{\tilde{Q}}_{N,\kappa}$ and $\hat{\tilde{V}}_{N,\kappa}$, respectively, for the cavity segments κ are explained in detail in refs 40 and 41. Inclusion of solvent contributions in the calculation of excitation energies and oscillator strengths at the CC2 level within the framework of COSMO and the post-SCF reaction field scheme introduced in ref 42 keeps the expressions for η^{d_α} and ξ^{d_α} in eq 4 the same as in the vacuum case, while it adds some explicit terms to the Jacobian $\mathbf{A}$

$$A^{\mathrm{pol}}_{\mu_1\nu_1} = \langle \mu_1|[\hat{G}^{\mathrm{pol,HF}} + \hat{\tilde{G}}^{\Delta}(\mathbf{D}^{\Delta}), \tau_{\nu_1}] + \hat{\tilde{G}}^{\nu_1}(\mathbf{D}^{\Delta})|\mathrm{HF}\rangle \tag{8}$$

$$A^{\mathrm{pol}}_{\mu_2\nu_2} = \langle \mu_2|[\hat{G}^{\mathrm{pol,HF}}, \tau_{\nu_2}]|\mathrm{HF}\rangle \tag{9}$$

where $\hat{G}^{\mathrm{pol,HF}}$ is the Hartree−Fock reaction field potential. The operators $\hat{\tilde{G}}^{\Delta}(\mathbf{D}^{\Delta})$ and $\hat{\tilde{G}}^{\nu_1}(\mathbf{D}^{\Delta})$ in the singles block $A_{\mu_1\nu_1}$ can be rewritten as

$$\hat{\tilde{G}}^{\Delta}(\mathbf{D}^{\Delta}) = \sum_{\kappa} \hat{\tilde{Q}}_{\kappa}(\mathbf{D}^{\Delta})\langle \mathrm{HF} + \bar{t}_1|\hat{\tilde{V}}_{\kappa,N}|\mathrm{HF}\rangle \tag{10}$$

and

$$\hat{\tilde{G}}^{\nu_1}(\mathbf{D}^{\Delta}) = \sum_{\kappa} \hat{\tilde{Q}}_{\kappa}(\mathbf{D}^{\Delta})\langle \mathrm{HF} + \bar{t}_1|[\hat{V}_{\kappa}, \tau_{\nu_1}]|\mathrm{HF}\rangle \tag{11}$$

where the index κ runs over all cavity segments. The density $\mathbf{D}^{\Delta}$ is defined as

$$\mathbf{D}^{\Delta}_{pq} = \langle \mathrm{HF} + \bar{t}_1|\exp(-\hat{T}_1)\hat{E}_{pq}\exp(\hat{T}_1)|\mathrm{HF}\rangle - \langle \mathrm{HF}|\hat{E}_{pq}|\mathrm{HF}\rangle \tag{12}$$

and $\hat{E}_{pq}$ are spin-free one particle operators.[43] The matrix $\mathbf{F}$ in eq 5 contains the following solvent contributions in the singles block $\mathbf{F}_{\mu_1\nu_1}$

$$\begin{aligned} F^{\mathrm{pol}}_{\mu_1\nu_1} = {} & \langle \bar{t}_1|[[\hat{\tilde{G}}^{\Delta}(\mathbf{D}^{\Delta}), \tau_{\mu_1}], \tau_{\nu_1}]|\mathrm{HF}\rangle \\ & + \sum_{\kappa} \langle \mathrm{HF} + \bar{t}_1|[\hat{\tilde{Q}}_{\kappa}, \tau_{\mu_1}]|\mathrm{HF}\rangle \\ & \times \langle \mathrm{HF} + \bar{t}_1|[\hat{\tilde{V}}_{\kappa}, \tau_{\nu_1}]|\mathrm{HF}\rangle \end{aligned} \tag{13}$$

while the other blocks have the same form as in the vacuum case.

The $\mathcal{B}(0 \rightarrow j)$ terms of MCD can be computed from the derivatives of the one-photon transition strength matrix with respect to the strength of a magnetic field[44,45]

$$\mathcal{B}(0 \rightarrow j) = \frac{1}{2}\sum_{\alpha\beta\gamma} \epsilon_{\alpha\beta\gamma}\Im\left\{\frac{\mathrm{d}S^{\alpha\beta}_{0\rightarrow j}}{\mathrm{d}B_{\gamma}}\right\} \tag{14}$$

where α, β and γ distinguish the three Cartesian components x, y, and z, $\epsilon_{\alpha\beta\gamma}$ is the Levi−Civita tensor, and B_{γ} is the Cartesian component of the magnetic field strength. For a magnetic-field independent basis set, the derivatives of the left and right transition moments are, in terms of the CC building blocks, formulated as[44]

$$\begin{aligned} \frac{\mathrm{d}M^{d_\alpha}_{0\leftarrow j}}{\mathrm{d}B_{\gamma}} = {} & [\mathbf{G}t^{m_\gamma}(0)t^{d_\alpha}(-\omega_j) + \mathbf{F}^{m_\gamma}t^{d_\alpha}(-\omega_j) + \mathbf{F}^{d_\alpha}t^{m_\gamma}(0)] \\ & \times E^{j}(\omega_j) + \bar{M}^{j}(\omega_j)[\mathbf{A}^{d_\alpha}t^{m_\gamma}(0) + \mathbf{A}^{m_\gamma}t^{d_\alpha}(-\omega_j) \\ & + \mathbf{B}t^{m_\gamma}(0)t^{d_\alpha}(-\omega_j)] + \bar{\xi}^{d_\alpha}(-\omega_j)^{\perp}E^{jm_\gamma}(\omega_j, 0) \\ & + \bar{\xi}^{m_\gamma}(0)E^{jd_\alpha}(\omega_j, -\omega_j) \end{aligned} \tag{15}$$

and

$$\frac{\mathrm{d}M^{d_\alpha}_{j\leftarrow 0}}{\mathrm{d}B_{\gamma}} = {}^{\perp}\bar{E}^{jm_\gamma}(-\omega_j, 0)\xi^{d_\alpha} + \bar{E}^{j}(-\omega_j)\mathbf{A}^{d_\alpha}t^{m_\gamma}(0) \tag{16}$$

with $t^{m_\gamma}(0)$ as the amplitude's first-order response to the static magnetic field, $t^{d_\alpha}(\omega)$ as the amplitude's first-order response to the electric field with frequency ω, and similarly for the excited state vectors $E^{jm_\gamma}(\omega_j,0)$ and $E^{jd_\alpha}(\omega_j,-\omega_j)$ for state j with excitation energy ω_j. $\mathbf{G}$ is the third derivative of the CC Lagrangian with respect to the cluster amplitudes, and $\mathbf{B}$ a mixed third derivative where L has been differentiated once with respect to the Lagrange multipliers and twice with respect to the cluster amplitudes.[34] The left vectors $\bar{\xi}^{Y}(\omega_Y)$ (for a generic operator $\hat{Y}$) are defined as $\eta^{Y} + \mathbf{F}t^{Y}(\omega_Y)$ and the amplitude responses $t^{Y}(\omega_Y)$ are determined by the equation

$$[\mathbf{A} - \omega_Y 1]t^{Y}(\omega_Y) = -\xi^{Y} \tag{17}$$

where ω_Y is the frequency associated with the operator $\hat{Y}$, which can be a component of the magnetic or the electric field. The first-order responses $E^{jY}(\omega_j, \omega_Y)$ and $\bar{E}^{jY}(-\omega_j, \omega_Y)$ of the eigenvectors $E^{j}(\omega_j)$ and $\bar{E}^{j}(-\omega_j)$ with respect to the operator Y are obtained solving the linear equations

$$[\mathbf{A} - (\omega_j + \omega_Y)1]E^{jY}(\omega_j, \omega_Y) = -[\mathbf{B}t^{Y}(\omega_Y) + \mathbf{A}^{Y}]E^{j}(\omega_j) \tag{18}$$

$$\bar{E}^{jY}(-\omega_j, \omega_Y)[\mathbf{A} + (\omega_Y - \omega_j)1] = -\bar{E}^{j}(-\omega_j)[\mathbf{B}t^{Y}(\omega_Y) + \mathbf{A}^{Y}] \tag{19}$$

The superscript $\perp$ on the derivatives of the eigenvectors indicates a projection onto the orthogonal complement of the undifferentiated eigenvectors to avoid unphysical divergen-

DOI: 10.1021/acs.jctc.8b00930
J. Chem. Theory Comput. 2019, 15, 1242−1254

ces[44,46,47] for the static magnetic field. See ref 44 for further details and the working equations for CCSD. The implementation of perturbation-induced, that is, first derivatives of one-photon transition moments for CC2 in the TURBOMOLE package has been presented in ref 48 as part of the implementation of spin−orbit induced oscillator strengths, which for the current work has been extended to account for solvent effects within the COSMO model.

We will here only discuss the additional reaction field contributions for the interaction with the solvent. They are for the magnetic-field induced transition moments structurally similar to those for two-photon transition moments, which have been discussed in ref 49 for the atomistic QM/MM-like polarizable embedded PERI-CC2 approach.

In addition to the solvent contributions to the Jacobian **A** and the matrix **F** that have been discussed above, explicit solvent contributions arise for CC2 in the singles/singles/singles blocks of **B** and **G**. For the **B** matrix transformations in eqs 18 and 19, the solvent contributions to the singles/singles/singles block are

$$\begin{aligned} B^{\mathrm{pol}}_{\kappa_1\mu_1\nu_1} t^Y_{\mu_1} E^j_{\nu_1} = {} & \langle \kappa_1 | [[\hat{\tilde{G}}^{\Delta}(\mathbf{D}^{\Delta}), \hat{T}_1^Y], \hat{E}_1^j] | \mathrm{HF} \rangle \\ & + \langle \kappa_1 | \hat{\tilde{G}}^{\Delta}(\mathbf{D}^F(t^Y, E^j)) | \mathrm{HF} \rangle \\ & + \langle \kappa_1 | [\hat{\tilde{G}}^{\Delta}(\mathbf{D}^{\eta}(t^Y)), \hat{E}_1^j] | \mathrm{HF} \rangle \\ & + \langle \kappa_1 | [\hat{\tilde{G}}^{\Delta}(\mathbf{D}^{\eta}(E^j)), \hat{T}_1^Y] | \mathrm{HF} \rangle \end{aligned} \tag{20}$$

and

$$\begin{aligned} \bar{E}^j_{\kappa_1} B^{\mathrm{pol}}_{\kappa_1\mu_1\nu_1} t^Y_{\nu_1} = {} & \langle \bar{E}^j | [[\hat{\tilde{G}}^{\Delta}(\mathbf{D}^{\Delta}), \hat{T}_1^Y], \tau_{\nu_1}] | \mathrm{HF} \rangle \\ & + \langle \mathrm{HF} + \bar{t}_1 | [[\hat{\tilde{G}}^{\Delta}(\mathbf{D}^{\xi}(\bar{E}^j)), \hat{T}_1^Y], \tau_{\mu_1}] | \mathrm{HF} \rangle \\ & + \langle \bar{E}^j | [\hat{\tilde{G}}^{\Delta}(\mathbf{D}^{\eta}(t^Y)), \tau_{\mu_1}] | \mathrm{HF} \rangle \\ & + \langle \mathrm{HF} + \bar{t}_1 | [\hat{\tilde{G}}^{\Delta}(\mathbf{D}^{A}(\bar{E}^j, t^Y)), \tau_{\mu_1}] | \mathrm{HF} \rangle \end{aligned} \tag{21}$$

The contributions arising from the interaction with the solvent in the **G** matrix in eq 15 are obtained as

$$\begin{aligned} G^{\mathrm{pol}}_{\mu_1\nu_1\kappa_1} t^X_{\mu_1} t^Y_{\nu_1} E^j_{\kappa_1} = {} & \langle \bar{t}_1 | [[\hat{\tilde{G}}^{\Delta}(\mathbf{D}^{\eta}(E^j)), \hat{T}_1^X], \hat{T}_1^Y] | \mathrm{HF} \rangle \\ & + \langle \bar{t}_1 | [[\hat{\tilde{G}}^{\Delta}(\mathbf{D}^{\eta}(t^Y)), \hat{T}_1^X], \hat{E}_1^j] | \mathrm{HF} \rangle \\ & + \langle \bar{t}_1 | [[\hat{\tilde{G}}^{\Delta}(\mathbf{D}^{\eta}(t^X)), \hat{T}_1^Y], \hat{E}_1^j] | \mathrm{HF} \rangle \end{aligned} \tag{22}$$

Detailed expressions for the auxiliary reaction field operators and densities can be found in refs 49 and 40.

3. COMPUTATIONAL DETAILS

For all investigated compounds, the ground state structures have been optimized at the MP2[50] level of theory in vacuum and in solution with the cc-pVTZ[51] basis set combined with the corresponding optimized auxiliary basis set.[52] In addition, the B3LYP[53]/cc-pVTZ optimized geometries in vacuum of refs 6 and 10 were considered. The geometry optimizations in solution for both calculations with and without explicit water molecules were carried out at PTE-COSMO-MP2 level employing the ricc2 module of the TURBOMOLE program package version 7.2.[54,55] The frozen core approximation was applied with the $1s^2$ electrons kept frozen for all C, O, and N atoms. The excitation energies, oscillator strengths, and Faraday $\mathcal{B}$ terms were computed at the CC2[27] level of theory using a local development version of the TURBOMOLE program package. Two basis sets were used for CC2 calculations of the spectra: aug-cc-pVDZ and aug-cc-pVTZ[56] combined with their auxiliary basis sets.[52] The post-SCF scheme was applied for the CC2 calculations in solution at the COSMO level.[40,42] For the cavity construction,[25] for a set of atom positions with corresponding atom radii R_α, we used the union of spheres of R_α and the solvent-accessible surface R_{SOLV}. In all COSMO calculations, water has been chosen as the solvent with the dielectric constant of $\varepsilon = 80.4$ and optical dielectric constant of $n^2 = 1.78$ (where n is the index of refraction). These values are taken from ref 57.

In addition, frozen-core CCSD calculations using the aug-cc-pVDZ[56] basis set in vacuo were carried out with the Dalton code[58] for the same vacuum structures mentioned above.

Since all three compounds studied here (see Figure 1) are closed-shell molecules without degenerate excited states, of the three Faraday parameters $\mathcal{A}$, $\mathcal{B}$, and $\mathcal{C}$ used to rationalize the MCD spectral shapes only the $\mathcal{B}$ term is of relevance.[23,45] For the calculation of the $\mathcal{B}$ term, the origin of the coordinate system was placed in the center of mass of the investigated system.



Figure 1. Schematic structures of purine and the nucleobases adenine and guanine.

The absorption spectra reported below display the decadic molar extinction coefficient[59]

$$\begin{aligned} \epsilon(\omega) &= \frac{2e^2\pi^2 N_{\mathrm{A}}}{1000\ln(10)(4\pi\epsilon_0) n m_{\mathrm{e}} c_0} \sum_j a_j(\omega) \frac{3}{2} \frac{f(0 \to j)}{\omega_j} \\ &= 7.03301 \times 10^2 \omega \sum_j a_j(\omega) \frac{3}{2} \frac{f(0 \to j)}{\omega_j} \end{aligned} \tag{23}$$

in units of $\mathrm{M}^{-1}\ \mathrm{cm}^{-1}$. Similarly, the MCD spectra display the anisotropy of the extinction coefficient (per unit of external magnetic field)

$$\begin{aligned} \frac{\Delta\epsilon(\omega)}{B_{\mathrm{ext}}} &= \frac{-8\pi^2 N_{\mathrm{A}} \omega}{3 \times 1000\ln(10)(4\pi\epsilon_0)\hbar c_0} \sum_j a_j(\omega) \mathcal{B}(0 \to j) \\ &= -5.98442 \times 10^{-3} \omega \sum_j a_j(\omega) \mathcal{B}(0 \to j) \end{aligned} \tag{24}$$

in units of $\mathrm{M}^{-1}\ \mathrm{cm}^{-1}\ \mathrm{T}^{-1}$. In the above formulas, ω is the circular frequency of the radiation, N_{A} is the Avogardo number, c_0 is the speed of light in vacuo, ϵ_0 is the dielectric constant, n is the refractive index, $\hbar$ is Planck's constant, m_{e} is the electron mass, $\hbar\omega_j = (E_j - E_0)$ is the excitation energy and $a_j(\omega)$ is a Lorentzian function used to simulate the spectral broadening

$$a_j(\omega) = \frac{1}{\pi} \frac{\gamma}{(\omega_j - \omega)^2 + \gamma^2} \tag{25}$$

The value $\gamma = 1000\ \mathrm{cm}^{-1}$ was adopted to facilitate the comparison with previous investigations.[6,10]

DOI: 10.1021/acs.jctc.8b00930
J. Chem. Theory Comput. 2019, 15, 1242−1254

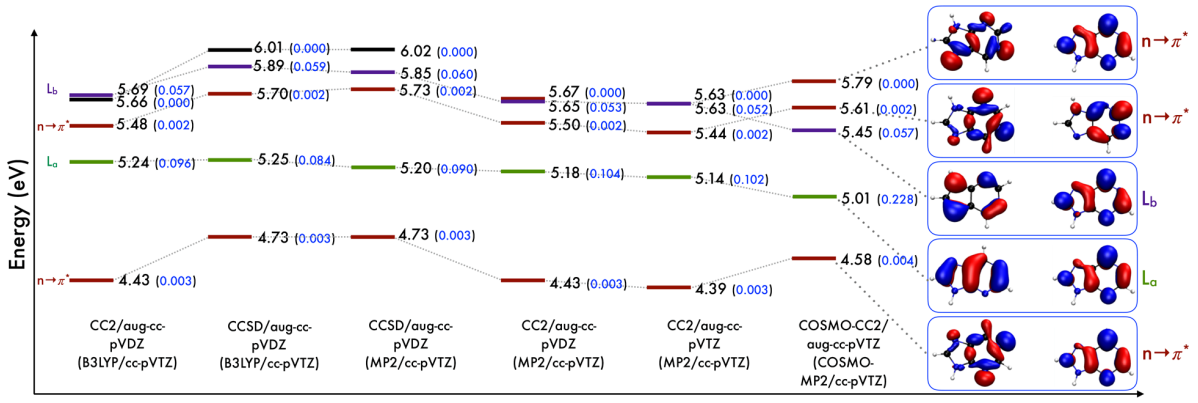


Figure 2. Purine CCSD/aug-cc-pVDZ vertical singlet excitation energies in vacuum and CC2 vertical singlet excitation energies with the aug-cc-pVDZ and aug-cc-pVTZ basis sets in vacuum and in solution using the COSMO solvent model. Oscillator strengths of the transitions are given in blue; the levels of theory used for the (ground state) geometry optimizations are indicated in parentheses.

4. PURINE

In the present study, we include 9H-purine, which is the simplest member of the purine family. For purine, we have investigated independently the effects of using DFT with the B3LYP functional for ground state geometry optimizations for the following CC2 and CCSD calculations and also the basis set size for vertical excitation calculations. Figure 2 presents the calculated excitation energies and oscillator strengths, along with natural transition orbitals (NTOs) and the corresponding assignment of the transitions. Comparison of adjacent columns in Figure 2 shows that the excitation energies of the first and second nπ^* transitions at the CC2/aug-cc-pVDZ level at 4.43 and 5.48 eV are lower by 0.30 and 0.22 eV than the corresponding CCSD results for the same ground state geometry (optimized at the B3LYP level). This is not unexpected since CC2 excitation energies are usually lower than the corresponding CCSD values. The second $\pi\pi^*$ (L_b) transition from CC2 (at 5.69 eV for the B3LYP geometry and at 5.65 eV for the MP2 geometry) appears lower than the CCSD one by 0.20 eV, while for the first $\pi\pi^*$ (L_a) state at ~5.25 eV, the agreement between the two methods is good. The main differences between the two CCSD columns, which differ in the level for the ground state geometry optimization, is that the two $\pi\pi^*$ (L_a and L_b) states are lower by 0.05 and 0.04 eV for MP2-optimized ground state geometry, whereas the second nπ^* state is blued shifted by 0.03 to 5.73 eV.

For the same ground state geometry (optimized with MP2), the largest divergence between CCSD and CC2 can be observed for the first and second nπ^* and also the second $\pi\pi^*$ (L_b) state for which CC2 gives energies which are, respectively, 0.30, 0.23, and 0.2 eV lower. For the larger triple-ζ basis set, the excitation energies for the lowest five states decrease by 0.02−0.06 eV, and thereupon, the highest two states (L_b and nπ^*) become degenerate at 5.63 eV.

Inclusion of solvent effects in the framework of COSMO both for the geometry optimizations and in the excitation energy calculations lowers the excitation energies for the $\pi\pi^*$ (L_a and L_b) transitions by 0.13 and 0.18 eV, while those of the nπ^* transitions rise from 4.39, 5.44, and 5.63 eV to 4.58, 5.61, and 5.79 eV. As a consequence, the order of the second nπ^* and the second $\pi\pi^*$ states becomes reversed.

According to the results shown in Figure 2, as both B3LYP and MP2 predict similar planar geometries for the ground state, changing the level of geometry optimization from DFT to MP2 changes the excitation energies at the CCSD level only very slightly and the order of states remains unchanged. Including the electrostatic contribution of the environment via COSMO stabilizes the $\pi\pi^*$ states from 5.14 to 5.01 eV for L_a and from 5.63 to 5.45 eV for L_b due to the larger transition dipole moments and the increase of the static dipole moments upon excitation by 2.13 D for L_a and 4.88 D for L_b. The interaction with the solvent also increases the intensity of L_a by a factor of ~2. At variance with the $\pi\pi^*$ excitations, the nπ^* states are, as usual, destabilized (blue-shifted) in aqueous solution because of the stabilization of the lone pairs. Given the experimental analysis of the absorption and MCD spectra of purine, the absorption band maximum in aqueous solution is located at 4.71 eV (263 nm) along with a shoulder at 5.17 eV (240 nm).[5] Our calculations are in agreement with this and associate the maximum band to the L_a state and the weak shoulder to L_b. The COSMO−CC2 results for the vertical excitation energies agree with the experimental band maxima within 0.3 eV, which is roughly the intrinsic accuracy of the CC2 method. The deviation of the COSMO−CC2 results from the experimental values has also the expected sign: usually CC2 gives vertical excitation energies that are slightly blue-shifted, and for purine in aqueous solution, the COSMO model probably underestimates the solvent effects on the $\pi\pi^*$ states L_a and L_b by about 0.1 eV compared to calculations that include explicit water molecules.

The MCD spectra obtained for the gas phase at the CCSD and CC2 levels, and in aqueous solution at the COSMO-RI-CC2 level, from the Faraday $\mathcal{B}$ terms along with the OPA spectra of purine are depicted in Figure 3. The $\mathcal{B}$ values used to simulate the spectra are collected in Table 1. The computed MCD spectra predict opposite signs for L_a and L_b and yield bisignate spectra with a positive band on the red and a negative band on the blue side in agreement with the experimental spectrum and also those obtained with the B3LYP and CAM−B3LYP functionals in ref 10.

5. ADENINE

On the basis of the CCSD/aug-cc-pVDZ results for adenine at two different geometries (a planar one optimized at the B3LYP level and a nonplanar one optimized at the RI-MP2 level), the three lowest excited states, two of $\pi\pi^*$ and one of nπ^* character, are rather close in energy, see Table 2.

DOI: 10.1021/acs.jctc.8b00930
J. Chem. Theory Comput. 2019, 15, 1242−1254

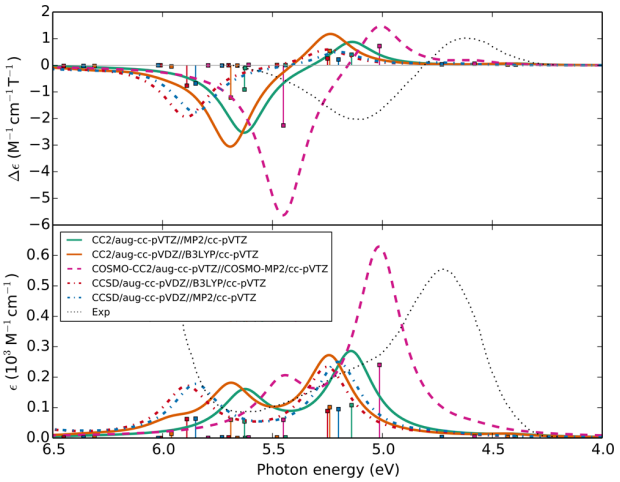


Figure 3. Purine OPA (lower panel) and MCD (upper panel) spectra computed in vacuum at the CCSD and CC2 levels and in water solution as approximated at the COSMO-RI-CC2/aug-cc-pVTZ level for the corresponding optimized structures (at B3LYP, MP2 and COSMO-MP2). All geometry optimizations were done in the cc-pVTZ basis set. Experimental spectra were measured in water at pH = 7 and digitized from ref 5.

To identify the character of these three excitations in CCSD, we have computed the NTOs for each geometry at this level, which are reported in Tables S3 and S4 of the Supporting Information. The most significant geometrical difference between adenine optimized at B3LYP and MP2 arises from the amino group; B3LYP predicts a planar geometry, while MP2 gives some degrees of pyramidalization on NH_2. The level of theory employed for the geometry optimization has a remarkably large effect on the relative ordering of the second $\pi\pi^*$ and $n\pi^*$ states found by CCSD: at the planar B3LYP geometry, the CCSD calculations predict the two close-lying $\pi\pi^*$ and $n\pi^*$ transitions at 5.49 and 5.50 eV, while at the nonplanar MP2 geometry the latter states appear in reversed ordering at 5.46 and 5.55 eV, with an increase in their energy gap. At both geometries, the lowest excitation has $\pi\pi^*$ character and, based on the NTOs, is assigned to L_b, while the second $\pi\pi^*$ state, which carries most of the oscillator strength, is attributed to L_a. Remarkably, at the MP2 geometry, the CCSD excitation characterized as $n\pi^*$ has a relatively large oscillator strength, larger than for the L_b state. This indicates a mixing of the $n\pi^*$ with the L_a state induced by the nonplanarity of the geometry.[60]

Of particular significance is to see how well the CCSD and CC2 results agree for the valence $\pi\pi^*$ and $n\pi^*$ transitions. From the theoretical point of view, CC2 is an approximation to CCSD where the coupling between doubly excited determinants through the fluctuation potential is neglected. It gives usually excitation energies that are lower than for CCSD. Since higher-order correlation effects beyond CCSD often red-shift excitation energies, CC2 profits sometimes from a fortunate partial compensation of these two errors. Comparing the second and third columns of Table 2, the CC2 excitation energy for the $n\pi^*$ state at 5.14 eV is considerably lower than the CCSD result obtained with the same basis set and ground state geometry. The pair of close-lying $\pi\pi^*$ transitions in adenine's spectrum (first and third excitations with CCSD at the MP2-optimized geometry) causes CC2 to fail in resolving them in the aug-cc-pVDZ basis: it gives a pair of complex eigenvalues, as also observed in an earlier study.[20]

In the larger aug-cc-pVTZ basis, CC2 predicts, in agreement to what is obtained in the double-ζ basis, the lowest excitation at 5.10 eV to have $n\pi^*$ character while the two $\pi\pi^*$ transitions are resolved but close in energy at 5.24 and 5.27 eV and carry large values for the Faraday $\mathcal{B}$ terms. Note that the order of these $\pi\pi^*$ transitions is reversed with respect to the CCSD results, but at the same time also the sign of the respective $\mathcal{B}$ terms is inversed. For CC2/aug-cc-pVTZ, in the absorption spectrum the brighter transition (L_a) is lower in energy. A comparison of the results obtained for CC2 in the triple-ζ basis with those at the EOM-CCSD(T) level[14] in the same basis shows that CC2 underestimates the excitation energy for the first $n\pi^*$ transition compared to EOM-CCSD(T) by ~0.18 eV and shifts it down below the first two $\pi\pi^*$ states, while at the EOM-CCSD(T) level, the ordering is flipped. Experimental results for the vertical excitation energies are not available. Molecular beam experiments showed that the band origin (0–0 transition) for the $n\pi^*$ state is slightly below that of a bright $\pi\pi^*$ state.[61]

To investigate the magnitude of solvent effects for aqueous solution and, in particular, how important they are to get the correct ordering of the lowest states, we applied again the COSMO continuum model in both the geometry optimization and the excitation energy and transition strength calculations. In the case of adenine, since we have observed large solvation effects, we have independently examined the effects of COSMO contributions on the ground state geometry and also on vertical transition energies. The results are summarized,

Table 1. Computed Values for Purine of the Excitation Energies ω_j (eV) and Faraday $\mathcal{B}(0 \rightarrow j)$ Terms (au) for the Different Methods Discussed in the Text[a]

		CCSD/aug-cc-pVDZ							
CC2/aug-cc-pVDZ @B3LYP geom		@B3LYP geom		@MP2 geom		CC2/aug-cc-pVTZ @MP2 geom		COSMO-RI-CC2/aug-cc-pVTZ @COSMO-MP2 geom	
ω_j(type)	$\mathcal{B}(0 \rightarrow j)$	ω_j	$\mathcal{B}(0 \rightarrow j)$	ω_j	$\mathcal{B}(0 \rightarrow j)$	ω_j	$\mathcal{B}(0 \rightarrow j)$	ω_j	$\mathcal{B}(0 \rightarrow j)$
4.43 ($n\pi^*$)	−0.933	4.73	−1.19	4.73	−1.31	4.39	−0.93	4.58	−2.23
5.24 ($\pi\pi^*$ (L_a))	−17.1	5.25	−8.05	5.29	−6.96	5.14	−12.9	5.01	−24.0
5.48 ($n\pi^*$)	−0.25	5.70	−0.006	5.73	0.29	5.44	−0.13	5.61	−0.52
5.69 ($\pi\pi^*$ (L_b))	35.7	5.89	21.7	5.85	19.6	5.63	27.0	5.45	69.3
5.66 ($n\pi^*$)	0.31	6.01	0.003	6.02	−0.005	5.63	3.09	5.79	0.11

[a]Note that the sign of the $\mathcal{B}$ term is opposite to the sign of the corresponding MCD peak (compare eq 24)[24].

DOI: 10.1021/acs.jctc.8b00930
J. Chem. Theory Comput. 2019, 15, 1242–1254

Table 2. Adenine Vertical Excitation Energies, ω_j (eV), Oscillator Strengths, $f(0 \rightarrow j)$, and Faraday $\mathcal{B}(0 \rightarrow j)$ Terms (au) in Vacuum Calculated by Different Methods[a]

CCSD aug-cc-pVDZ						CC2			
@B3LYP geom			@MP2 geom			aug-cc-pVDZ @MP2 geom	aug-cc-pVTZ @MP2 geom		
ω_j(type)	f	$\mathcal{B}(0 \rightarrow j)$	ω_j(type)	f	$\mathcal{B}(0 \rightarrow j)$	ω_j	ω_j(type)	f	$\mathcal{B}(0 \rightarrow j)$
5.36 (L_b)	0.008	40.72	5.34 (L_b)	0.030	24.48	5.14	5.10 ($n\pi^*$)	0.009	0.78
5.49 (L_a)	0.280	−11.95	5.46 ($n\pi^*$)	0.064	−3.12	5.29	5.24 (L_a)	0.155	313.14
5.50 ($n\pi^*$)	0.002	−11.68	5.55 (L_a)	0.174	−13.35	5.29	5.27 (L_b)	0.126	−310.06
5.54	0.009	−16.31	5.61	0.023	−5.52	5.39	5.56	0.011	−0.75
5.89	0.001	−0.41	5.95	0.005	−0.35	5.71	5.73	0.003	−0.71

[a]Note that the sign of the $\mathcal{B}$ term is opposite to the sign of the corresponding MCD peak (compare eq 24).[24] The geometry optimizations in all cases were done in the cc-pVTZ basis.

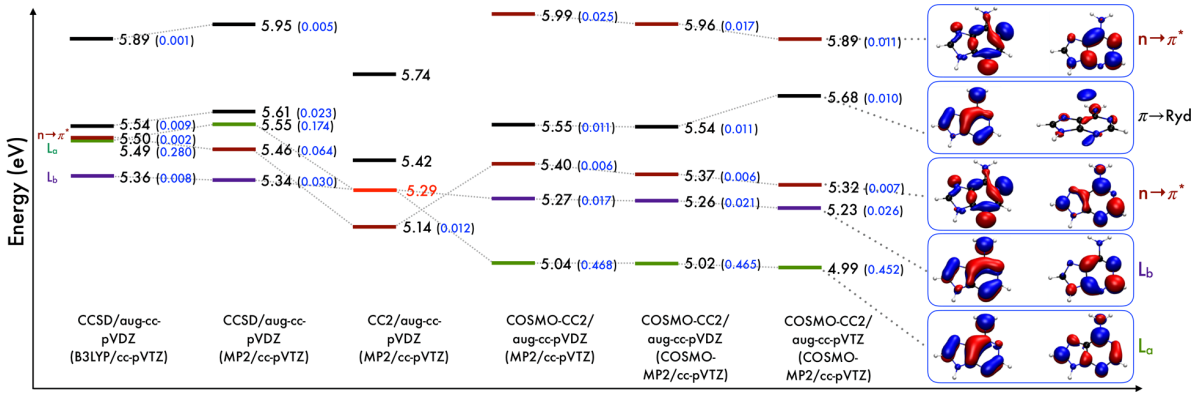


Figure 4. Adenine CCSD/aug-cc-pVDZ singlet vertical excitation energies in vacuum and CC2 singlet vertical excitation energies with the double-ζ and triple-ζ basis sets in vacuum and in solution using the COSMO solvent model at the corresponding ground state optimized geometries. Oscillator strengths of the transitions are given in blue. For CC2/aug-cc-pVDZ, the two lowest $\pi\pi^*$ states are obtained as a conjugated pair of degenerate roots with complex eigenvalues.

Table 3. Adenine Vertical Excitation Energies, ω_j (eV), Oscillator Strengths, $f(0 \rightarrow j)$, and Faraday $\mathcal{B}(0 \rightarrow j)$ Terms (au) Calculated in Vacuo and in Solution at the CC2/aug-cc-pVTZ Level of Theory[a]

vacuum			COSMO			vacuum+5H_2O			COSMO+5H_2O		
ω_j (type)	f	$\mathcal{B}(0 \rightarrow j)$	ω_j	f	$\mathcal{B}(0 \rightarrow j)$	ω_j	f		ω_j	f	$\mathcal{B}(0 \rightarrow j)$
5.24 ($\pi\pi^*$ (L_a))	0.155	313.14	4.99	0.452	77.13	5.02	0.303	117.42	4.87	0.504	101.77
5.27 ($\pi\pi^*$ (L_b))	0.126	−310.06	5.23	0.026	−75.76	5.16	0.063	−121.56	5.14	0.041	−112.00
5.10 ($n\pi^*$)	0.009	0.78	5.32	0.007	−4.55	5.59	0.000	−0.02	5.61	0.002	−1.69
5.56 (πRyd)	0.011	−0.75	5.68	0.010	0.71	5.57	0.005	−1.12	5.64	0.005	0.72
5.73 ($n\pi^*$[b])	0.003	−0.71	5.89	0.011	−0.11	6.10	0.006	0.95	6.06	0.645	103.39

[a]Geometries are optimized at MP2/cc-pVTZ level in the specified environment (vacuo, COSMO, vacuo + 5H_2O, COSMO + 5H_2O). [b]The fifth state has an $n\pi^*$ character for the vacuum and COSMO calculations, while it is a πRyd and $\pi\pi^*$ state for adenine in water cluster without and with COSMO contribution, respectively.

along with the vacuum values, in Figure 4. Once again, the assignment of the excited states is based on NTOs.

In the COSMO-RI-CC2/aug-cc-pVDZ calculations, the lowest two $\pi\pi^*$ excitations are, in contrast to the vacuum case, resolved with one state at 5.04 eV and the second at 5.27 eV for the vacuum geometry. Note that the inclusion of solvent effects causes red shifts of both $\pi\pi^*$ states while, in contrast, the $n\pi^*$ excitation is blue-shifted from 5.14 to 5.40 eV and became the third excited state. These solvent shifts are typical for $n\pi^*$ and bright $\pi\pi^*$ states (e.g., compare ref 41) and have the same direction as those observed in ref 6 at the TD-DFT level.

Furthermore, when the structure is optimized with COSMO for bulk water (the fifth column from left), the energies do not change significantly (on the order of 0.01−0.03 eV) with respect to the same calculations at the vacuum geometry (the fourth column from left). The ordering of the states remains unchanged. As expected, the excitation energies are slightly lower with the aug-cc-pVTZ basis (the last column from left) except for the πRyd state, which is blue-shifted by 0.14 to 5.68 eV. Besides the three valence states, there is a πRyd state around 5.56 eV in vacuum at the CC2/aug-cc-pVTZ level and around 5.68 eV in aqueous solution at the same level of theory. For the ordering of the first five transitions found at the COSMO-RI-CC2 level with both double-ζ and triple-ζ basis sets, using optimized structures in vacuum and solution, there is a definite analogy: $\pi\pi^*$ (L_a) < $\pi\pi^*$ (L_b) < $n\pi^*$ < πRyd < $n\pi^*$. At the higher energy end of the studied region, CC2/aug-

DOI: 10.1021/acs.jctc.8b00930
J. Chem. Theory Comput. 2019, 15, 1242−1254

cc-pVTZ in vacuum predicts another nπ* state at 5.73 eV, which is blue-shifted in solution to 5.89 eV.

For adenine, we decided to study in more detail the effect of hydrogen bonds on the lowest excited states. To this end, we performed additional calculations on a cluster with five explicit water molecules to model part of adenine's first solvation shell, both with and without the COSMO continuum solvation model to include bulk solvent effects. Such a cluster was already adopted in ref 6, and the number of water molecules had been chosen to saturate the hydrogen bond ability of adenine in the molecular plane, where solute−solvent interactions are expected to be stronger. It is known that, in DNA nucleobases, the nπ* states are destabilized in water by an extent not fully captured by continuum models.[4] Note that a single cluster cannot be considered fully representative of all the possible solute/solvent arrangements that should be studied with a proper Molecular Dynamics simulation, but such treatment goes beyond the scope of the present article.

Due to its computational cost, the study on the cluster model was performed only for adenine. This nucleobase was selected because, in gas phase, some of the methods we applied predict a remarkable role of nπ* states in its MCD response, see Table 3. Moreover, the assignment of the relative position of the L_a and L_b states in adenine is controversial and important in the context of studying DNA photodamage.

As far as the excitation energies are concerned, just the inclusion of the explicit water molecules (without COSMO) results in an excitation energy for the first ππ* (L_a) state of 5.02 eV, which is lower than the value in vacuum (by ∼0.22 eV) and only slightly higher (by ∼0.03 eV, compare Table 3) than the result obtained with COSMO without explicit water. For the second ππ* (L_b) transition, the explicit water molecules lower the excitation energy to 5.16 eV, that is ∼0.11 and 0.07 eV lower than those in vacuum and with the continuum solvation model, respectively. The combination of explicit and implicit water models lowers the excitation energies for the ππ* states further and at the same time increases the energy gap between them by a factor of 2 compared to the case where only the explicit water molecules are included.

The nπ* states, however, are significantly blue-shifted, by ∼0.49 to 5.59 eV for the first nπ* state, when explicit water molecules are added to the vacuum calculation. With the continuum solvation included, the addition of explicit water molecules still leads for the first nπ* (1 nπ*) transition to an additional blue shift of 0.29 to 5.61 eV, confirming that a relevant part of the nπ* destabilization in water can only be captured with an explicit description of the solute−solvent H-bonds.

The fifth excited state in vacuum and in the COSMO calculation is the second nπ* state, but when explicit water molecules are added this state is shifted upward and a πRyd transition at 6.10 eV without COSMO and a ππ* transition at 6.06 eV when also the COSMO model is included becomes the fifth excited state.

For the vertical excitation energies in the gas phase, EOM-CCSD(T)/aug-cc-pVTZ results computed at a CCSD/cc-pVDZ geometry are available from ref 14. They are 5.04 eV for the L_b, 5.23 eV for the L_a, and 5.28 eV for the 1 nπ* state, and 0.26, 0.24, and 0.26 eV lower than the respective CCSD results for the same basis set and structure. CCSD/cc-pVDZ structures are inferior to MP2/cc-pVTZ structures for organic closed-shell molecules. Therefore, we prefer to add the CCSD → EOM-CCSD(T) shifts from ref 14 and the aug-cc-pVDZ → aug-cc-pVTZ shifts from the CC2 calculations (0.05, 0.02, and 0.04 eV for L_a, L_b, and 1 nπ*, respectively) to the current CCSD/aug-cc-pVDZ results for the MP2/cc-pVTZ geometry to obtain best estimates for gas phase vertical excitation energies. This gives 5.06 eV for the L_b, 5.26 eV for the L_a, and 5.16 eV for the 1 nπ* state. Compared to these best estimates, the gas-phase CC2/aug-cc-pVDZ results overestimate the excitation energies for the L_b and L_a states by 0.23 and 0.03 eV, respectively, and underestimate that for the 1 nπ* state by 0.02 eV. If we add these shifts to the COSMO−CC2 results for adenine with five explicit water molecules, we arrive at best estimates for the excitation energies in aqueous solution of 4.84 eV for L_a, 4.91 eV for L_b, and 5.63 eV for 1 nπ*.

From the above discussion and the results displayed in Figure 4, one can draw the following conclusions: due to remaining correlation errors on the order of 0.2 eV, which have different trends for different types of states, CC2 cannot reproduce the ordering of states obtained in EOM-CCSD(T) for the gas phase. The position of the 1 nπ* is, however, also sensitive to the structure: at the CCSD/cc-pVDZ structure, this excitation appears at 0.07 and 0.05 eV above the L_a state for EOM-CCSD and EOM-CCSD(T), respectively; for the B3LYP/cc-pVTZ structure, it is almost degenerate with L_a at the CCSD level and for the MP2/cc-pVTZ structure, it is found at 0.09 and 0.15 eV below L_a for CCSD and CC2, respectively. Experimentally the band origin of the nπ* state is slightly below that of the lowest ππ* excitation.[61] However, these uncertainties are small compared to the solvent shifts for aqueous solution, which are −0.37 eV for the L_a, −0.13 eV for the L_b, and +0.51 eV for the 1 nπ* state. As also found in a previous TD-DFT study,[6] continuum solvation models underestimate in this case the solvent effects because of hydrogen bond interactions, although they already shift the 1 nπ* above the L_a and L_b states and bring the brighter L_a state below L_b. The inclusion of explicit water molecules is necessary to obtain quantitative results and further boosts the energy gap between the L_b and the 1 nπ* state by 0.38 eV. In summary, both the CC2 results and our "best estimates" predict that for adenine in aqueous solution L_a is more stable than L_b, confirming previous TD-DFT results.[6] This result is partially at variance with a CASPT2/MM study,[62] which adopting a nonpolarizable molecular mechanics (MM) force field, predicted L_b slightly more stable than L_a by 0.02 eV.

Experimentally, the absorption band maximum of adenine in aqueous solution is located at 4.77 eV (260 nm) compared with 4.92 eV (252 nm) in the gas phase, which corresponds to a red shift of 0.15 eV (8 nm).[63,64] In the same way as the experimental results, the L_a state, which carries most of the oscillator strength, is red-shifted by ∼0.37 eV (18 nm) in our COSMO-RI-CC2 calculations including the water cluster with respect to the results in the gas phase. The best estimate of 4.84 eV obtained by including higher-order correlation effects agrees very well with the experimental band maximum in aqueous solution.

The computed absorption and MCD spectra of adenine in vacuum and aqueous solution including the water cluster at the CCSD and CC2 levels are shown in Figure 5. They were obtained from the values of the excitation energies, oscillator strengths, and Faraday $\mathcal{B}$ terms provided by our calculations in Table 2 and Table 3. In the vacuum CC2/aug-cc-pVTZ case, even though the two ππ* states have large oppositely signed $\mathcal{B}$ terms, the energy gap between them is so small that the

DOI: 10.1021/acs.jctc.8b00930
J. Chem. Theory Comput. 2019, 15, 1242−1254

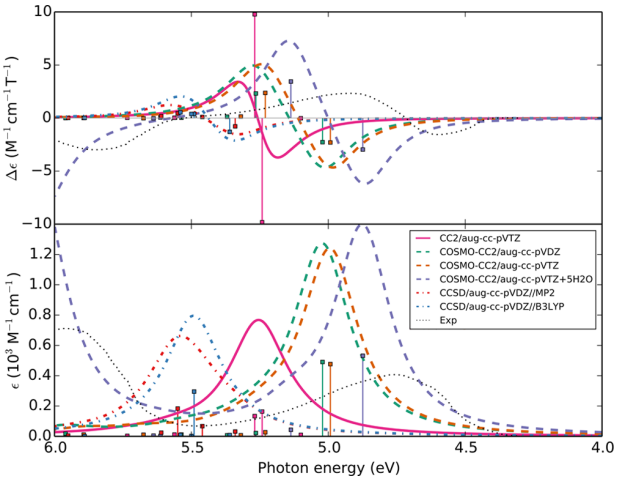


Figure 5. Adenine MCD and OPA spectra computed for a single optimized structure (at MP2/cc-pVTZ level) in vacuum and in water solution, as approximated at COSMO, at CCSD and CC2 levels using double-ζ and triple-ζ basis sets. Experimental spectra were measured in water at pH = 7 digitized from ref 11.

broadening will result in an inconspicuous signal. In all CC2 calculations, L_a is at lower energy than L_b and has a positive $\mathcal{B}$ term (i.e., a negative MCD peak), whereas L_b is at higher energy with a negative $\mathcal{B}$ term (positive MCD peak). The CCSD calculations, on the other hand, predict L_b in the gas phase energetically lower than L_a, and it is in this case L_b that carries the positive $\mathcal{B}$ term (negative MCD peak) and L_a the negative one. Moreover, the intensity of the positive MCD peak originates, in the gas phase CCSD calculation, not only from the $\pi\pi^*$ state but also from the $n\pi^*$ states (compare Table 2). As a consequence, the spectral profile of the computed MCD spectra is, for CCSD in the gas phase and CC2 in the gas phase and in solution, compatible with that from experiment[5,11,12] and the TD-DFT calculations,[6] showing the characteristic pair of negative and positive bands in the region of 4.87−5.27 eV, despite the different relative positions of the L_a and L_b states and the different composition of the second band yielded by CCSD.

The above observation has led us to reconsider whether MCD can indeed give direct evidence on the relative position of the L_a and L_b states, as proposed in ref 6. In this regard, it is useful to inspect the sum-over-state (SOS) expression of the $\mathcal{B}(0 \rightarrow j)$ term[65] and look in particular at the following term:

$$\sum_{k\neq j} \frac{\langle j|\mathbf{m}|k\rangle\cdot\langle 0|\mathbf{d}|j\rangle \times \langle k|\mathbf{d}|0\rangle}{\omega_k - \omega_j} \equiv \epsilon_{\alpha\beta\gamma} \sum_{k\neq j} \frac{m_\alpha^{jk} d_\beta^{0j} d_\gamma^{k0}}{\omega_k - \omega_j} \tag{26}$$

where 0 is the ground state, j is the final excited state, and k runs on all states except j; $d_\alpha^{jk} = \langle j|d_\alpha|k\rangle$ and similarly for the other terms.

If, for two close lying excited states, the $\mathcal{B}$ terms are dominated by this contribution, they fulfill the relation

$$\mathcal{B}(0 \rightarrow 1) \approx \epsilon_{\alpha\beta\gamma} \frac{m_\alpha^{12} d_\beta^{01} d_\gamma^{20}}{\omega_2 - \omega_1} \tag{27}$$

$$\mathcal{B}(0 \rightarrow 2) \approx \epsilon_{\alpha\beta\gamma} \frac{m_\alpha^{21} d_\beta^{02} d_\gamma^{10}}{\omega_1 - \omega_2} = \epsilon_{\alpha\beta\gamma} \frac{-m_\alpha^{12} d_\beta^{20} d_\gamma^{01}}{\omega_1 - \omega_2} = \epsilon_{\alpha\gamma\beta} \frac{-m_\alpha^{12} d_\gamma^{20} d_\beta^{01}}{\omega_1 - \omega_2} = +\epsilon_{\alpha\beta\gamma} \frac{m_\alpha^{12} d_\beta^{01} d_\gamma^{20}}{\omega_1 - \omega_2} \tag{28}$$

Thus, the two $\mathcal{B}$ terms only differ in sign because of their energy difference in the denominator and a bisignate spectral profile with a positive and a negative band of equal magnitude will be obtained. The characters of the two states determine through the transition moments the magnitude and the sign of the numerator. Since the MCD spectra computed at the CC2 level exhibit such an antisymmetric relation between the $\mathcal{B}$ terms for the L_a and L_b states, it is reasonable to assume that this contribution is the dominant one.

To test this hypothesis, we evaluated the SOS expression for a three state (S_0, L_a, and L_b) model with transition moments evaluated at the COSMO−CC2/aug-cc-pVTZ level for the COSMO structure. Including all SOS terms gave for this model 74.1 and −73.4 au compared to 77.13 and −75.76 au from the CC2 response calculation. The contribution from the magnetic dipole moment between the L_a and L_b states to this SOS model is 72.9 and −72.9 au. These results support the above assumption that the Faraday $\mathcal{B}$ term of the L_a and L_b states in adenine are in fact dominated by the contribution given in eq 26. The SOS procedure for nonvariational CC methods is outlined in the Supporting Information.

As a consequence, and contrary to what was assumed in ref 6, the positive or negative sign of the two red peaks in the MCD spectrum of adenine is not related to whether the underlying electronic states are L_a or L_b, and MCD cannot be used to ascertain the relative position of these two states. In other words, even if different methods predict opposite relative positions of L_a and L_b, the MCD profiles are still correctly reproduced for all of them.

The wall time for the calculations of vertical excitation energies plus transition moments and magnetic Faraday $\mathcal{B}$ terms in solution at COSMO-RI-CC2 is very close to that of corresponding calculations for vacuum case. In the case of adenine, the calculations of these quantities for five states in solution using the aug-cc-pVDZ basis set with no explicit water clusters took 5 h and 17 min with OpenMP parallelization on 8 CPUs of an Intel Xeon X5670 CPU with 8 GiB core memory.

6. GUANINE

The structure of 9H-guanine has been optimized in vacuo and in aqueous solution via COSMO at the MP2/cc-pVTZ level. The geometries are basically planar, except for a slight pyramidalization at the amino group (coordinates are available in the Supporting Information). Excitation energies of the first five transitions have been obtained in vacuum and also in aqueous solution in the framework of the COSMO solvent model at the CC2 level using the aug-cc-pVTZ basis set. Figure 6 shows the results of these calculations along with the corresponding NTOs and the assignments.

As shown in Figure 6, the lowest-energy transition in vacuum is a $\pi\pi^*$ (L_a) transition at 5.02 eV, in agreement with previous calculations on guanine with EOM-CCSD(T),[14] CC2,[20] and CASPT2,[22] while the assignments based on EOM-CCSD[14] and TD-DFT are given as πRyd and $\pi\pi^*$ (L_b), respectively.

DOI: 10.1021/acs.jctc.8b00930
J. Chem. Theory Comput. 2019, 15, 1242−1254

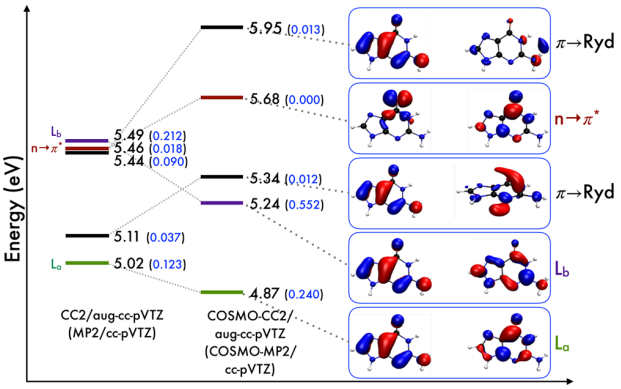


Figure 6. Guanine CC2/aug-cc-pVTZ vertical singlet excitation energies in vacuum and solution using COSMO solvent model at the corresponding ground state optimized geometries. Oscillator strengths of the transitions are given in blue.

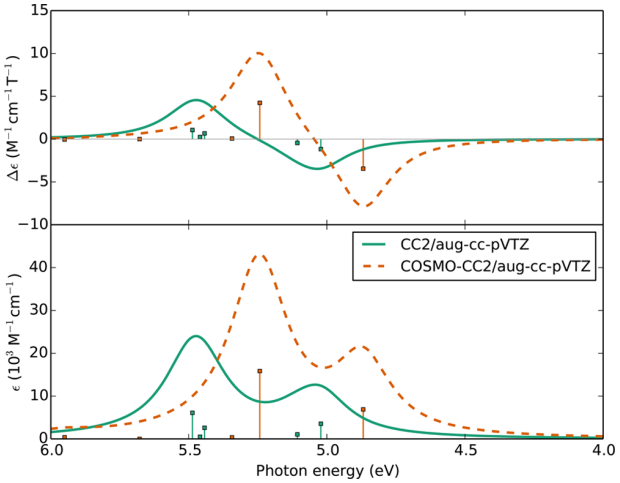


Figure 7. Guanine absorption and MCD spectra computed for a single structure (optimized at MP2/cc-pVTZ level) in vacuo and in water solution as approximated by COSMO at CC2/aug-cc-pVTZ level.

The CC2 results in Figure 6 predict πRyd character for the two transitions above the L_a state located at 5.11 and 5.44 eV, with nonzero intensities. It is interesting to note that CCSD(T) and the current CC2 calculations in vacuum agree well on the order of the three lowest excited states, although CC2 predicts higher energies for those states. The nπ^* state, which involves a lone pair of the oxygen atom, lies at 5.46 eV, just below the second $\pi\pi^*$ (L_b) state at 5.49 eV. The energy of this nπ^* transition is obtained slightly higher than with EOM-CCSD(T) (by ∼0.03 eV) and, due to near-degeneracy in vacuum at the CC2 level (compare Figure 6), the oscillator strength of the $\pi\pi^*$ (L_b) transition is partially distributed to the nπ^* and πRyd transitions. Although the nπ^* and $\pi\pi^*$ (L_b) transitions are very close in energy (their gap is ∼0.03 eV), underestimation of the nπ^* excitation energy at the CC2 level yields the nπ^* transition below L_b, contrary to CCSD and CCSD(T) where the reversed ordering is predicted.[14]

In aqueous solution, the lowest transitions are energetically more separated than those in vacuum (compare Figure 6). Inclusion of the electrostatic effects of an isotropic environment lowers the energies of the most intense $\pi\pi^*$ type transitions to 4.87 and 5.24 eV, which can be attributed to the large transition dipole moments. The intensities are also doubled with respect to vacuum. Similar to purine and adenine, the different behavior of the $\pi\pi^*$ and nπ^* transitions in aqueous solution affects the relative ordering of the states by blue shifting the nπ^* transition to 5.68 eV, that is, above the $\pi\pi^*$ states, while its intensity decreases to zero. Finally, the πRyd transitions show similar trends as nπ^*: in aqueous solution they appear at higher energies (5.34 and 5.95 eV) and have lower intensities. For guanine, given that the assignments of the transitions are clear, no further calculations have been done.

Figure 7 shows a simulation of the absorption and MCD spectra obtained from the computed excitation energies, oscillator strengths, and MCD $\mathcal{B}$ terms summarized in Table 4. The CC2/aug-cc-pVTZ results in vacuum and in solution for 9H-guanine lead again to a bisignate spectrum (Figure 7), analogous to the one obtained at the TD-DFT level (B3LYP and CAM−B3LYP functionals) in ref 6 and in agreement with both the experimental spectrum of the guanine derivative guanosine[11] and the experimental peak maxima of guanine at pH = 2 reported in ref 12.

Table 4. Guanine Vertical Excitation Energies, ω_j (eV), Oscillator Strengths, $f(0 \rightarrow j)$, and Faraday $\mathcal{B}(0 \rightarrow j)$ Terms (au) Calculated in Vacuo and in Aqueous Solution (COSMO) at Two Different Geometries

CC2/aug-cc-pVTZ			COSMO−CC2/aug-cc-pVTZ		
ω_j (type)	f	$\mathcal{B}(0 \rightarrow j)$	ω_j	f	$\mathcal{B}(0 \rightarrow j)$
5.02 ($\pi\pi^*$ (L_a))	0.123	39.0	4.87	0.240	118
5.11 (πRyd)	0.037	14.6	5.34	0.012	−2.15
5.44 (πRyd)	0.090	−20.5	5.95	0.013	1.41
5.46 (nπ^*)	0.018	−7.39	5.68	0.000	−0.09
5.49 ($\pi\pi^*$)	0.212	−32.2	5.24	0.552	−135

In the COSMO−CC2 calculation the signal originates exclusively from the oppositely signed $\mathcal{B}$ terms of the L_a and L_b states, whereas in the vacuum case, the MCD intensity is distributed on $\pi\pi^*$, πRyd, and nπ^* states. In aqueous solution, $\pi\pi^*$ states, L_a and L_b, are red-shifted where L_a is ∼0.37 eV more stable than L_b.

7. CONCLUSIONS

The vertical transition energies, oscillator strengths, and Faraday $\mathcal{B}$ terms of purine and of the two primary nucleobases adenine and guanine have been investigated by the ab initio methods CCSD and CC2 in gas phase. The electrostatic effects of an isotropic environment on the absorption and MCD spectra were taken into account using the implicit continuum solvation model COSMO at the CC2 level of theory. The main aim of this study was to evaluate the performance of CCSD and CC2 in vacuum along with the solvent effects on the ordering of the transitions and on the MCD spectra. In the case of purine, in gas phase, the latter methods agree well on the order of the two lowest $\pi\pi^*$ transitions, where L_a is lower than L_b. Although in some calculations for purine at the CC2 level the nπ^* excitation energies are underestimated compared to CCSD (sometimes by as much as 0.35 eV), there is a reasonable agreement between these two methods even for the nπ^* transitions, and connected triple excitations are expected to red shift the CCSD results by ∼0.2 eV. Our COSMO-RI-CC2 calculations for purine in aqueous solution show that the

DOI: 10.1021/acs.jctc.8b00930
J. Chem. Theory Comput. 2019, 15, 1242−1254

energy ordering between the $\pi\pi^*$ and $n\pi^*$ transitions is affected by the solvent as the $\pi\pi^*$ states are red-shifted and the $n\pi^*$ states are blue-shifted.

Our results for adenine reproduce the discrepancy in the energy order of the $\pi\pi^*$ transitions in gas phase between CCSD and CC2: the former method predicts the L_b state below L_a, while this order is flipped at the CC2 level. Inclusion of bulk solvent effects as described by the COSMO model has significant effects. It enlarges the energy gap between the two $\pi\pi^*$ transitions and destabilizes the $n\pi^*$ transitions. Concerning specific solvent effects from hydrogen bonding to the solute, we observed a qualitative agreement for the transition energies and the energy order of the L_a and L_b states in adenine between the COSMO calculations with and without explicit water molecules and calculations with explicit water molecules without COSMO. We can thus conclude that for the nucleobase adenine including the bulk effect of the environment can be sufficient for a qualitative description of the vertical excitation energies, but for quantitative results, explicit water molecules are necessary. For guanine, the absolute values of the CC2 excitation energies in vacuum agree well with those from CCSD(T);[14] however, there is a discrepancy in the ordering of the transitions: CC2 gives an $n\pi^*$ below L_b,[20] while CCSD(T) predicts a reversed order for the latter transitions. On the other hand, the inclusion of solvent effects for aqueous solution in the CC2 calculations for guanine changes the arrangement of the transitions by lowering the $\pi\pi^*$ and upshifting the $n\pi^*$ transitions.

The spectral profiles of the computed MCD spectra with all methods used (vacuum CCSD, vacuum CC2, and COSMO-RI-CC2) are found to match the (bisignate) experimental profiles, apart from some shifts on the energy scale and variations in intensity.

For adenine in water, CC2 with any of the solvent models predicts the lower energy $\pi\pi^*$ state to be of L_a type and to bear a positive $\mathcal{B}$ term (negative MCD peak) in agreement with what was previously found by two of us at the TD-DFT level.[6] In vacuo, at variance with CC2, CCSD predicts the MCD negative band to be due to the L_b state and the positive one to be a sum of contributions from L_a, $n\pi^*$, and πRyd states. Stimulated by these conflicting predictions, we performed an analysis of the sum-over-states expression of the $\mathcal{B}$ term, finding strong arguments that indicate that the sign of the MCD bands cannot be used to ascertain the relative stability of the L_a and L_b states of adenine.[66]

■ ASSOCIATED CONTENT

Supporting Information

The Supporting Information is available free of charge on the ACS Publications website at DOI: 10.1021/acs.jctc.8b00930.

Values for Faraday $\mathcal{B}$ terms at RI-CC2 and CCSD in vacuum and solution, NTOs for adenine at CCSD, NTOs for adenine with water cluster including COSMO at RI-CC2, and Cartesian coordinates of the nucleobases (PDF)

■ AUTHOR INFORMATION

Corresponding Authors

*E-mail: Sarah.Karbalaeikhani@rub.de.
*E-mail: Christof.Haettig@rub.de.
*E-mail: soco@kemi.dtu.dk.

ORCID

Sarah Karbalaei Khani: 0000-0002-7366-2916
Rasmus Faber: 0000-0001-8524-0684
Fabrizio Santoro: 0000-0003-4402-2685
Christof Hättig: 0000-0002-5752-2710
Sonia Coriani: 0000-0002-4487-897X

Notes

The authors declare no competing financial interest.

■ ACKNOWLEDGMENTS

S.C. thanks J. Michl for discussions. R.F. and S.C. acknowledge financial support from DTU Chemistry (start-up postdoctoral grant) and from the Independent Research Fund Denmark through the DFF-Forskningsprojekt2 Grant No. 7014-00258B. S.K. and C.H. acknowledge financial support from the Cluster of Excellence RESOLV (EXC 1069) and project Ha 2588/8-1 funded by the Deutsche Forschungsgemeinschaft.

■ REFERENCES

(1) Kohler, B. Nonradiative Decay Mechanisms in DNA Model Systems. *J. Phys. Chem. Lett.* **2010**, *1*, 2047−2053.
(2) Crespo-Hernandez, C. E.; Cohen, B.; Hare, P. M.; Kohler, B. Ultrafast Excited-State Dynamics in Nucleic Acids. *Chem. Rev.* **2004**, *104*, 1977−2020.
(3) Middleton, C. T.; de La Harpe, K.; Su, C.; Law, Y. K.; Crespo-Hernandez, C. E.; Kohler, B. DNA Excited-State Dynamics: From Single Bases to the Double Helix. *Annu. Rev. Phys. Chem.* **2009**, *60*, 217.
(4) Improta, R.; Santoro, F.; Blancafort, L. Quantum Mechanical Studies on the Photophysics and the Photochemistry of Nucleic Acids and Nucleobases. *Chem. Rev.* **2016**, *116*, 3540−3593.
(5) Djerassi, C.; Bunnenberg, E.; Elder, D. L. Organic Chemical Applications of Magnetic Circular Dichroism. *Pure Appl. Chem.* **1971**, *25*, 57−90.
(6) Santoro, F.; Improta, R.; Fahleson, T.; Kauczor, J.; Norman, P.; Coriani, S. Relative Stability of the L_a and L_b Excited States in Adenine and Guanine: Direct Evidence from TD-DFT Calculations of MCD Spectra. *J. Phys. Chem. Lett.* **2014**, *5*, 1806−1811.
(7) Fülscher, M. P.; Serrano-Andrés, L.; Roos, B. O. A Theoretical Study of the Electronic Spectra of Adenine and Guanine. *J. Am. Chem. Soc.* **1997**, *119*, 6168−6176.
(8) Lan, Z.; Lu, Y.; Fabiano, E.; Thiel, W. QM/MM nonadiabatic decay dynamics of 9H-adenine in aqueous solution. *ChemPhysChem* **2011**, *12*, 1989−1998.
(9) Mondal, S.; Puranik, M. Ultrafast structural dynamics of photoexcited adenine. *Phys. Chem. Chem. Phys.* **2017**, *19*, 20224−20240.
(10) Fahleson, T.; Kauczor, J.; Norman, P.; Santoro, F.; Improta, R.; Coriani, S. TD-DFT Investigation of the Magnetic Circular Dichroism Spectra of Some Purine and Pyrimidine Bases of Nucleic Acids. *J. Phys. Chem. A* **2015**, *119*, 5476−5489.
(11) Sutherland, J. C.; Griffin, K. Magnetic Circular Dichroism of Adenine, Hypoxanthine, and Guanosine 5′-Diphosphate to 180 nm. *Biopolymers* **1984**, *23*, 2715−2724.
(12) Voelter, W.; Records, R.; Bunnenberg, E.; Djerassi, C. Magnetic Circular Dichroism Studies. VI. Investigation of Some Purines, Pyrimidines, and Nucleosides. *J. Am. Chem. Soc.* **1968**, *90*, 6163.
(13) Gustavsson, T.; Improta, R.; Markovitsi, D. DNA/RNA: Building Blocks of Life under UV Irradiation. *J. Phys. Chem. Lett.* **2010**, *1*, 2025−2030.
(14) Szalay, P. G.; Watson, T.; Perera, A.; Lotrich, V. F.; Bartlett, R. J. Benchmark Studies on the Building Blocks of DNA. 1. Superiority of Coupled Cluster Methods in Describing the Excited States of Nucleobases in the Franck-Condon Region. *J. Phys. Chem. A* **2012**, *116*, 6702−6710.

DOI: 10.1021/acs.jctc.8b00930
J. Chem. Theory Comput. 2019, 15, 1242−1254

(15) Szalay, P. G.; Watson, T.; Perera, A.; Lotrich, V. F.; Fogarasi, G.; Bartlett, R. J. Benchmark Studies on the Building Blocks of DNA. 2.Effect of Biological Environment on the Electronic Excitation Spectrum of Nucleobases. *J. Phys. Chem. A* **2012**, *116*, 8851−8860.
(16) Szalay, P. G.; Watson, T.; Perera, A.; Lotrich, V. F.; Bartlett, R. J. Benchmark Studies on the Building Blocks of DNA. 3. *J. Phys. Chem. A* **2013**, *117*, 3149−3157.
(17) Silva-Junior, M. R.; Schreiber, M.; Sauer, S. P. A.; Thiel, W. Benchmarks for Electronically Excited States: Time-Dependent Density Functional Theory and Density Functional Theory Based Multireference Configuration Interaction. *J. Chem. Phys.* **2008**, *129*, 104103.
(18) Serrano-Andrés, L.; Merchán, M.; Borin, A. Adenine and 2-Aminopurine: Paradigms of Modern Theoretical Photochemistry. *Proc. Natl. Acad. Sci. U. S. A.* **2006**, *103*, 8691−8696.
(19) Conti, I.; Altoé, P.; Stenta, M.; Garavelli, M.; Orlandi, G. Adenine Deactivation in DNA Resolved at the CASPT2//CASSCF/AMBER Level. *Phys. Chem. Chem. Phys.* **2010**, *12*, 5016−5023.
(20) Fleig, T.; Knecht, S.; Hättig, C. Quantum-Chemical Investigation of the Structures and Electronic Spectra of the Nucleic Acid Bases at the Coupled Cluster CC2 Level. *J. Phys. Chem. A* **2007**, *111*, 5482−5491.
(21) Shukla, M. K.; Leszczynski, J. TDDFT Investigation on Nucleic Acid Bases: Comparison with Experiments and Standard Approach. *J. Comput. Chem.* **2004**, *25*, 768−778.
(22) Yamazaki, S.; Domcke, W.; Sobolewski, A. L. Nonradiative Decay Mechanisms of the Biologically Relevant Tautomer of Guanine. *J. Phys. Chem. A* **2008**, *112*, 11965−11968.
(23) Mason, W. R. *A Practical Guide to Magnetic Circular Dichroism Spectroscopy*; Wiley: New York, 2007.
(24) Michl, J. Magnetic Circular Dichroism of Aromatic Molecules. *Tetrahedron* **1984**, *40*, 3845−3934.
(25) Klamt, A.; Schüürmann, G. COSMO: A new approach to dielectric screening in solvents with explicit expressions. *J. Chem. Soc., Perkin Trans. 2* **1993**, 799−805.
(26) Christiansen, O.; Koch, H.; Jørgensen, P. The second-order approximate coupled cluster singles and doubles model CC2. *Chem. Phys. Lett.* **1995**, *243*, 409−418.
(27) Hättig, C.; Weigend, F. CC2 excitation energy calculations on large molecules using the resolution of the identity approximation. *J. Chem. Phys.* **2000**, *113*, 5154−5161.
(28) Cammi, R. Quantum cluster theory for the polarizable continuum model.I. The CCSD level with analytical first and second derivatives. *J. Chem. Phys.* **2009**, *131*, 164104.
(29) Cammi, R. Coupled-Cluster theories for the polarizable continuum model.II. Analytical gradients for excited states of molecular solutes by the equation of motion coupled-cluster method. *Int. J. Quantum Chem.* **2010**, *110*, 3040−3052.
(30) Cammi, R. Coupled-Cluster theory for the polarizable continuum model. III. A response theory for molecules in solution. *Int. J. Quantum Chem.* **2012**, *112*, 2547−2560.
(31) Caricato, M. Exploring potential energy surfaces of electronic excited states in solution with the EOM-CCSD-PCM method. *J. Chem. Theory Comput.* **2012**, *8*, 5081−5091.
(32) Caricato, M. A corrected-linear response formalism for the calculation of electronic excitation energies for solvated molecules with the CCSD-PCM method. *Comput. Theor. Chem.* **2014**, *1040*, 99−105.
(33) Caricato, M. Linear response coupled cluster theory with the polarizable continuum model within the singles approximation for the solvent response. *J. Chem. Phys.* **2018**, *148*, 134113.
(34) Christiansen, O.; Jørgensen, P.; Hättig, C. Response functions from Fourier component variational perturbation theory applied to a time-averaged quasienergy. *Int. J. Quantum Chem.* **1998**, *68*, 1.
(35) Christiansen, O.; Koch, H.; Jørgensen, P. The second-order approximate coupled cluster singles and doubles model CC2. *Chem. Phys. Lett.* **1995**, *243*, 409−418.
(36) Christiansen, O.; Halkier, A.; Koch, H.; Jørgensen, P.; Helgaker, T. Integral-direct coupled cluster calculations of frequency-dependent polarizabilities, transition probabilities and excited-state properties. *J. Chem. Phys.* **1998**, *108*, 2801−2816.
(37) Hättig, C.; Christiansen, O.; Jørgensen, P. Multiphoton transition moments and absorption cross sections in coupled cluster response theory employing variational transition moment functionals. *J. Chem. Phys.* **1998**, *108*, 8331−8354.
(38) Hättig, C.; Weigend, F. CC2 excitation energy calculations on large molecules using the resolution of the identity approximation. *J. Chem. Phys.* **2000**, *113*, 5154−5161.
(39) Friese, D. H.; Hättig, C.; Ruud, K. Calculation of two-photon absorption strengths with the approximate coupled cluster singles and doubles model CC2 using the resolution-of-identity approximation. *Phys. Chem. Chem. Phys.* **2012**, *14*, 1175−1184.
(40) Karbalaei Khani, S.; Marefat Khah, A.; Hättig, C. COSMO-RI-ADC(2) Excitation Energies And Excited State Gradients. *Phys. Chem. Chem. Phys.* **2018**, *20*, 16354−16363.
(41) Lunkenheimer, B.; Köhn, A. Solvent Effects on Electronically Excited States Using the Conductor-Like Screening Model and the Second-Order Correlated Method ADC(2). *J. Chem. Theory Comput.* **2013**, *9*, 977−994.
(42) Schwabe, T.; Sneskov, K.; Haugaard Olsen, J. M.; Kongsted, J.; Christiansen, O.; Hättig, C. PERI-CC2: A Polarizable Embedded RI-CC2 Method. *J. Chem. Theory Comput.* **2012**, *8*, 3274−3283.
(43) Helgaker, T.; Jørgensen, P.; Olsen, J. *Molecular Electronic-Structure Theory*; John Wiley & Sons: Chichester, 2000.
(44) Coriani, S.; Hättig, C.; Jørgensen, P.; Helgaker, T. Gauge-origin independent magneto-optical activity within coupled cluster response theory. *J. Chem. Phys.* **2000**, *113*, 3561.
(45) Kjærgaard, T.; Coriani, S.; Ruud, K. Ab initio calculation of magnetic circular dichroism. *WIREs Comput. Mol. Sci.* **2012**, *2*, 443−455.
(46) Hättig, C.; Jørgensen, P. Derivation of coupled cluster excited states response functions and multiphoton transition moments between two excited states as derivatives of variational functionals. *J. Chem. Phys.* **1998**, *109*, 9219.
(47) Hättig, C.; Christiansen, O.; Coriani, S.; Jørgensen, P. Static and frequency-dependent polarizabilities of excited singlet states using coupled cluster response theory. *J. Chem. Phys.* **1998**, *109*, 9237.
(48) Helmich-Paris, B.; Hättig, C.; Van Wüllen, C. A CC2 Implementation of Induced Transitions between Singlet Ground and Triplet Excited States. *J. Chem. Theory Comput.* **2016**, *12*, 1892−1904.
(49) Hrsak, D.; Marefat Khah, A.; Christiansen, O.; Hättig, C. Polarizable Embedded RI-CC2 Method for Two-Photon Absorption Calculations. *J. Chem. Theory Comput.* **2015**, *11*, 3669−3678.
(50) Head-Gordon, M.; Pople, J. A.; Frisch, M. J. MP2 energy evaluation by direct methods. *Chem. Phys. Lett.* **1988**, *153*, 503−506.
(51) Feller, D. Application of systematic sequences of wave functions to the water dimer. *J. Chem. Phys.* **1992**, *96*, 6104−6114.
(52) Weigend, F.; Köhn, A.; Hättig, C. Efficient use of the correlation consistent basis sets in resolution of the identity MP2 calculations. *J. Chem. Phys.* **2002**, *116*, 3175−3183.
(53) Becke, A. D. Density-Functional exchange-energy approximation with correct asymptotic behavior. *Phys. Rev. A: At., Mol., Opt. Phys.* **1988**, *38*, 3098−3100.
(54) *TURBOMOLE* V7.2 2017, a development of University of Karlsruhe and Forschungszentrum Karlsruhe GmbH, 1989−2007, TURBOMOLE GmbH, since 2007; available from http://www.turbomole.com.
(55) Furche, F.; Ahlrichs, R.; Hättig, C.; Klopper, W.; Sierka, M.; Weigend, F. *WIREs Computational Molecular Science* **2014**, *4*, 91−100.
(56) Dunning, T. H., Jr. Gaussian basis sets for use in correlated molecular calculations. I. The atoms boron through neon and hydrogen. *J. Chem. Phys.* **1989**, *90*, 1007−1023.
(57) Mewes, J.-M.; You, Z.-Q.; Wormit, M.; Kriesche, T.; Herbert, J. M.; Dreuw, A. Experimental benchmark data and systematic evaluation of two *a posteriori*, polarizable-continuum corrections for vertical excitation energies in solution. *J. Phys. Chem. A* **2015**, *119*, 5446−5464.

DOI: 10.1021/acs.jctc.8b00930
J. Chem. Theory Comput. 2019, 15, 1242−1254

(58) Aidas, K.; Angeli, C.; Bak, K. L.; Bakken, V.; Bast, R.; Boman, L.; Christiansen, O.; Cimiraglia, R.; Coriani, S.; Dahle, P.; Dalskov, E. K.; Ekström, U.; Enevoldsen, T.; Eriksen, J. J.; Ettenhuber, P.; Fernández, B.; Ferrighi, L.; Fliegl, H.; Frediani, L.; Hald, K.; Halkier, A.; Hättig, C.; Heiberg, H.; Helgaker, T.; Hennum, A. C.; Hettema, H.; Hjertenæs, E.; Høst, S.; Høyvik, I.-M.; Iozzi, M. F.; Jansik, B.; Jensen, H. J. A.; Jonsson, D.; Jørgensen, P.; Kauczor, J.; Kirpekar, S.; Kjærgaard, T.; Klopper, W.; Knecht, S.; Kobayashi, R.; Koch, H.; Kongsted, J.; Krapp, A.; Kristensen, K.; Ligabue, A.; Lutnæs, O. B.; Melo, J. I.; Mikkelsen, K. V.; Myhre, R. H.; Neiss, C.; Nielsen, C. B.; Norman, P.; Olsen, J.; Olsen, J. M. H.; Osted, A.; Packer, M. J.; Pawlowski, F.; Pedersen, T. B.; Provasi, P. F.; Reine, S.; Rinkevicius, Z.; Ruden, T. A.; Ruud, K.; Rybkin, V. V.; Salek, P.; Samson, C. C. M.; de Merás, A. S.; Saue, T.; Sauer, S. P. A.; Schimmelpfennig, B.; Sneskov, K.; Steindal, A. H.; Sylvester-Hvid, K. O.; Taylor, P. R.; Teale, A. M.; Tellgren, E. I.; Tew, D. P.; Thorvaldsen, A. J.; Thøgersen, L.; Vahtras, O.; Watson, M. A.; Wilson, D. J. D.; Ziolkowski, M.; Ågren, H. The Dalton Quantum Chemistry Program System. *WIREs Comput. Mol. Sci.* **2014**, *4*, 269.

(59) Rizzo, A.; Coriani, S.; Ruud, K. In *Computational Strategies for Spectroscopy. From Small Molecules to Nano Systems*; Barone, V., Ed.; John Wiley and Sons, 2012; Chapter 2, pp 77−135.

(60) Picconi, D.; Avila Ferrer, F. J.; Improta, R.; Lami, A.; Santoro, F. Quantum-classical effective-modes dynamics of the $\pi\pi^* \rightarrow n\pi^*$decay in 9H-adenine. A quadratic vibronic coupling model. *Faraday Discuss.* **2013**, *163*, 223−242.

(61) Kim, N. J.; Kang, H.; Park, Y. D.; Kim, S. K. Dispersed fluorescence spectroscopy of jet-cooled adenine. *Phys. Chem. Chem. Phys.* **2004**, *6*, 2802−2805.

(62) Ludwig, V.; da Costa, Z. M.; do Amaral, M. S.; Borin, A. C.; Canuto, S.; Serrano-Andrés, L. Photophysics and photostability of adenine in aqueous solution: A theoretical study. *Chem. Phys. Lett.* **2010**, *492*, 164−169.

(63) Clark, L. B.; Peschel, G. G.; Tinoco, I., Jr Vapor Spectra and Heats of Vaporization of Some Purine and Pyrimidine Bases. *J. Phys. Chem.* **1965**, *69*, 3615−3618.

(64) Voet, D.; Gratzer, W. B.; Cox, R. A.; Doty, P. Absorption spectra of nucleotides, polynucleotides, and nucleic acids in the far ultraviolet. *Biopolymers* **1963**, *1*, 193−208.

(65) Buckingham, A.; Stephens, P. Magnetic Optical Activity. *Annu. Rev. Phys. Chem.* **1966**, *17*, 399.

(66) Michl, J. Private Communication, 2018.

DOI: 10.1021/acs.jctc.8b00930
J. Chem. Theory Comput. 2019, 15, 1242−1254

4 Solvent effects on the absorption and fluorescence of halogen-bonded ion pairs

The major goal of this sub-project was to better understand solvent effects on the photochemistry of halogen-bonded Iodoimidazolium compounds and scan the role of halogen-centered noncovalent interactions between iodine and halogen-bond donors in the distribution of electron density through photoexcitation and relaxation mechanisms. For the calculation of electronic excited state energies, transition moments and also the relaxation mechanisms to investigate the possible fluorescence emission we used the COSMO-RI-ADC(2) method (cmp. Chapter 2) along with the post-SCF reaction field scheme.

My contribution to this project comprises all the calculations and visualizations under the supervision of Christof Hättig. I have prepared the first draft which was later on further improved together with my co-author.

Solvent Effects on the Absorption and Fluorescence of Halogen-bonded Ion Pairs

Sarah Karbalaei Khani* and Christof Hättig

Arbeitsgruppe Quantenchemie, Ruhr-Universität, Bochum 44780, Germany

E-mail: Sarah.Karbalaeikhani@ruhr-uni-bochum.de

Abstract

We report a theoretical investigation of solvation effects on the absorption and fluorescence of iodo-imidazolium halogen-bond acceptors. For this study the correlated wavefunction methods MP2 (the second-order Møller-Plesset perturbation theory) and ADC(2) (the algebraic diagrammatic construction through second order) are combined with the conductor-like screening model (COSMO) to account for continuum solvation effects. The impacts of halogen-bond interaction and of solvation are analyzed for the structure of the ground state and the absorption and fluorescence emission of the lowest excited singlet states. As model systems we investigate in addition to two monodentate halogen bond complexes of the iodo-imidazolium and iodo-benzimidazolium cations with triflate counterions also a bidentate complex of the bis(iodo-benzimidazolium) dication with Cl^- as counterion in acetonitrile solution. The results indicate that the two monodentate complexes relax after photoexcitation towards a minimum on the S_1 potential energy surface where the C–I bond and the I–O halogen bond are partially broken. For the bidentate complex with the smaller Cl^- counterion, however, the halogen-bond interaction stays intact in the S_1 minimum that is reached after relaxation from the Franck-Condon point. The halogen-bond interaction

leads in this complex to an enlarged Stokes shift for the fluorescence emission.

Introduction

Halogen bonding (XB) is a non-covalent interaction between the σ-hole (an electron charge depletion region) in the anisotropic charge distribution of covalently bound halogen atoms and a Lewis base. The effects of halogen bonding have been extensively studied *e.g.* in the field of crystal engineering[1] and there are also several theoretical studies of XB complexes in vacuum.[2–4] However, several aspects of this interaction in solution are not yet fully understood[5,6] despite its importance for many applications *e.g.* in organocatalysis and molecular recognition.[7–10]

Many theory groups have studied XB complexes with different *ab initio* methods and different energy decomposition schemes to clarify the relative importance of contributions from electrostatic, dispersion, polarization and charge transfer interactions.[4,11,12] In 2008, Riley *et al.* explored the interaction energies for XB halomethane-formaldehyde complexes with Hartree-Fock (HF), second-order Møller-Plesset perturbation theory (MP2), and coupled-cluster singles and doubles with a perturbative triples correction, CCSD(T).[2] Results from their study with symmetry-adapted perturbation theory (SAPT) showed that halogen bonds are dominated by electrostatic and dispersion forces. For example, for systems containing iodine as XB acceptor the electrostatic interaction accounts for more than half of the attractive contributions. An extensive survey of the wavefunction methods MP2, MP3, CCSD and their spin-component scaled (SCS) counterparts along with CCSD(T) and density functional theory (DFT) for geometries and dissociation energies of XB complexes was carried out in 2013 by Kozuch *et al.*[3] Their benchmark results revealed that for dissociation energies of halogen bonds the wavefunction methods SCS-MP2 and CCSD(T) by using complete basis set extrapolation technique are on average more accurate than DFT due to the fact that the latter has a hard time covering different halogen bonding components (electrostatic,

dispersion, polarization, and charge transfer). Furthermore, they argued that, because of the overestimation of dynamic electron correlation, MP2 overbinds while SCS-MP2 provides more accurate results for dissociation energies and predicts the range of dissociation energies to be between 1.4 kcal·mol^{-1} for weak and 10.1 kcal·mol^{-1} for strong halogen bonds.

A challenge for the theoretical description of XB complexes in solution are the large solvent effects for ions which weaken the halogen bonding.[13–15] This can change significantly the relative stability of different minima (*vide infra*).

Among the XB complexes used in organocatalysis are *e.g.* aromatic iodo(benz)imidazolium-based XB acceptors to activate hetero Diels-Alder reactions and dicationic bis(iodoimidazolium) compounds[16] to activate classical Diels-Alder reactions of enones with cyclopentadiene.[17–19] Due to the positive charge on the imidazolium moieties of iodo(benz)imidazolium compounds the halogen bond competes with an anion-π interaction between the anion (halogen bond donor) and the face side of the haloimidazolium ring. For instance, in a recent study by Huber *et al.* on the binding mode of 2-iodoimidazolium-based ion pairs in acetonitrile solution, the authors investigated the relative importance of XB and anion-π interactions for various imidazolium salts with bromide as counterion by sterically shielding potential bonding sites against hydrogen bonding and anion-π interactions as competitors for halogen bonding.[20] In general, stronger halogen bonds are obtained with bidentate XB receptors. As an example for bidentate XB receptors, in 2012 Zapata *et al.* reported a family of fluorescent bidentate chloro-, bromo-, and iodo-imidazoliophane receptors. They showed that bromo-imidazoliophane and syn iodo-imidazoliophane exhibit strong and selective XB recognition of iodide and bromide anions, respectively.[21]

The aim of the current work is to gain insight into the effects of halogen bonding on electronic excitation. As model compounds we study the complexes of 2-iodoimidazolium and 2-iodobenzimidazolium with the triflate (OTf) anion and of the complex of a bis(2-iodobenzimidazolium) dication with a chloride anion and compute for them the absorption spectra and the Stokes shifts for emitted fluorescent light in acetonitrile solution. The latter

requires not only for the ground but also for the excited state potential energy surface a balanced account of the electrostatic and London dispersion interactions as it is usually not obtained with time-dependent density functional theory (TDDFT). We employ for this reason MP2 for the ground state in combination with the algebraic diagrammatic construction through second order, ADC(2), for the excitation energies and include the solvent effects via the conductor-like screening model (COSMO).[22] Further investigations on the deexcitation mechanism were carried out by the calculation of the associated excited state equilibrium structures in acetonitrile solution. For this we use a recently developed implementation of analytic excited state gradients at the COSMO-ADC(2) level of theory.[23] To study the influence of halogen bonding on the excitation energies and the characters of excited states we have carried out the same calculations for these iodoimidazolium cations in acetonitrile solution without counterion as XB donors.

Computational Methods

For all three investigated systems the ground state structures in vacuum have been optimized at the MP2[24] level of theory using the doubly polarized triple-zeta basis def2-TZVPP[25] as orbital basis set combined with the corresponding optimized auxiliary basis sets for the resolution-of-the-identity (RI) approximation.[26] For iodine we used the Stuttgart-Cologne 28 electron effective core potential (ECP).[27] The frozen core approximation was applied to all non-hydrogen atoms: for C, O and N atoms the $1s^2$ electrons were kept frozen and for sulfur and chlorine in addition all electrons in the $2s^22p^6$ shell. For iodine we excluded (in addition to the electrons modeled by the ECP) also the electrons in the $4s^24p^6$ shell from the correlation treatment.

For the calculations in acetonitrile as solvent the ground state structures have been optimized at the COSMO-MP2(PTE) level (PTE stands for the perturbation to energy scheme) with the same basis sets as in vacuum.[22,28] Vertical excitation energies, oscillator

strengths and the excited state structures in vacuum were obtained at the RI-ADC(2)/def2-TZVPP level[29,30] and in acetonitrile with the COSMO-RI-ADC(2)/def2-TZVPP within the post-SCF reaction field scheme using the implementation reported in Ref. 23.

All the Hartree-Fock, RI-MP2 and RI-ADC(2) calculations in vacuum were done with version V7.2 of the TURBOMOLE program package.[31] For the COSMO-RI-ADC(2) calculations we used a development version of the `ricc2` module of the TURBOMOLE program package.[23,32] For the calculations in solution, acetonitrile has been chosen as the solvent with a dielectric constant of $\varepsilon = 36.7$ and a refractive index of $n^2 = 1.81$.

2-Iodo-imidazolium·OTf

An initial search for the ground state equilibrium structures of the complex formed by a 2-iodoimidazolium cation with a triflate anion in vacuum and in acetonitrile solution revealed two minima: the XB structure (S_0-eq), Fig 1 **a**, and a structure with an anion-π interaction between the positively charged imidazolium ring and the OTf counterion (S_0'-eq), Fig 1 **c**. MP2/def2-TZVPP predicts the anion-π structure to be in vacuum 12.6 kcal·mol^{-1} and in acetonitrile still 1.6 kcal·mol^{-1} below the XB structure, due to the stronger dispersion interaction in the former geometry. However, the COSMO solvation model does not account for the dispersion interaction between the QM solute and the solvent which should in solution further weaken the stability of the anion-π structure (with a larger dispersion contribution to its binding energy) relative to the XB complex, so that MP2 probably overestimates the stability of the anion-π complex. To avoid this imbalance we did a second set of geometry optimizations at the B3-LYP/def2-TZVPP level[33] (without a dispersion correction[34]). This changes the energy difference in favor of the XB complex and makes it more stable than the anion-π complex by ≈ 2.77 kcal·mol^{-1} in acetonitrile solution while in vacuum the anion-π complex is still lower in energy by ≈ 7.08 kcal·mol^{-1} which means that in solution the XB structure should be dominant.[35] COSMO-B3-LYP/def2-TZVPP with-

out dispersion correction gives a ground state equilibrium structure, where, relative to the COSMO-MP2/def2-TZVPP(PTE) results, the I–O distance of the XB complex in solution stays essentially unchanged at 2.08 Å while the C–I bond length becomes longer by 0.04 Å.

Since our aim is to investigate the effect of the halogen-bond interaction on electronic spectra and excited states, we targeted the XB structure as the ground state geometry for the subsequent calculations. The vertical excitation energies and oscillator strengths for the five lowest excited states at the S_0-eq structures in vacuum and in acetonitrile solution were computed with ADC(2). The results for the XB complex in acetonitrile are summarized in Fig. 2 along with the corresponding natural transition orbitals (NTOs) for the excited states. Additional results for the complex in vacuum and the 2-iodoimidazolium cation in solution without counterion are given in Tables S4 and S5 of the supporting information (SI).

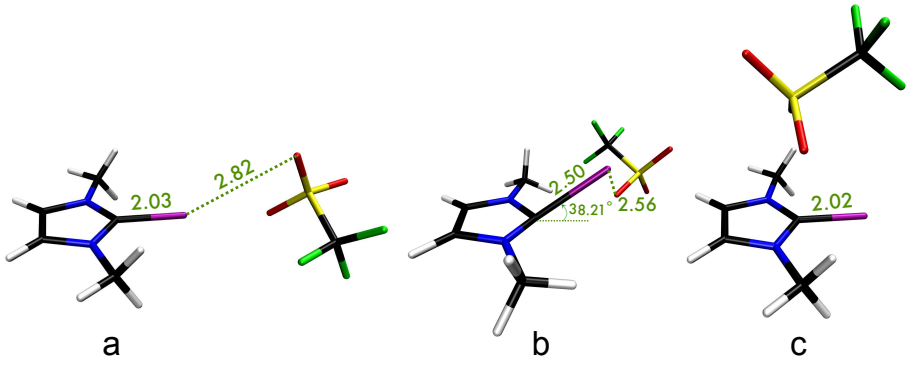


Figure 1: Optimized geometries of 2-iodo-imidazolium·OTf in (**a**) the ground state S_0-eq with XB interaction, (**b**) the first excited state S_1-eq and (**c**) the ground state S_0'-eq with an anion-π interaction. All structures have been computed for solution in acetonitrile with the COSMO-MP2/def2-TZVPP(PTE) for the ground state and the COSMO-RI-ADC(2)/def2-TZVPP(post-SCF) for the excited state.

In contrast to vacuum, the polar solvent acetonitrile screens the Coulomb attraction between the ions and weakens their interaction. The stabilization of the charges by the polar solvent blue shifts the charge transfer (CT) excitations from the lone pairs of iodine and OTf^- which decreases the polarity of the ion pair. The contributions from transitions out of the lone pairs of OTf^- to the lowest excitations become insignificant (cmp. Fig. 2).

Instead, the lowest excitations in solution are dominated by local transitions within the iodoimidazolium cation. As shown in Fig. 2, in acetonitrile solution from the two close-lying lowest excited states S_1 and S_2 only the S_1 state at 5.59 eV has a significant oscillator strength. It is a $\pi\pi^*$ transition mostly localized on the iodoimidazolium ring with a partial charge transfer from iodine to the ring. S_2 at 5.62 eV is a $\pi\sigma^*$ transition mainly from iodine non-bonding electrons into the σ^* orbital of the C–I bond. The third lowest excited state at 6.34 eV with $n\sigma^*$ character from a lone pair of iodine to the σ^* orbital of the C–I bond and the S_4 and S_5 with $n\pi^*$ and $\pi\pi^*$ character have very small oscillator strengths and do not contribute to the UV absorption spectrum.

To evaluate the impacts of XB interaction on the absorption spectrum, we compared the results for the excitation energies and oscillator strengths of the XB complex and the cation without OTf^- counterion in Table 1.

Table 1: Vertical excitation energies ω and oscillator strengths f of 2-iodoimidazolium · OTf complex and 2-iodoimidazolium cation in acetonitrile at COSMO-ADC(2)/def2-TZVPP(post-SCF) level.

	XB Complex			Cation		
State	type	ω	f	type	ω	f
1	$\pi\pi^*$	5.59	0.437	$\pi\sigma^*$	5.06	0.000
2	$\pi\sigma^*$	5.62	0.005	$\pi\pi^*$	5.59	0.388
3	$n\sigma^*$	6.34	0.004	$n\sigma^*$	5.83	0.001
4	$n\pi^*$	6.59	0.000	$n\pi^*$	6.72	0.000
5	$\pi\pi^*$	6.84	0.000	$\pi\sigma^*$	6.95	0.000

Compared to the spectrum of the 2-iodoimidazolium cation (cmp. SI Table S5), the $\pi\sigma^*$ and $n\sigma^*$ transitions into the antibonding orbital of the C–I bond are by the XB interaction blue shifted by $\approx$ 0.56 and 0.51 eV. These transitions are, however, dark. The bright excitation of the cation into the lowest $\pi\pi^*$ state (S_2) appears at the same energy as in the XB complex *i.e.* at 5.59 eV. On the other hand, the S_4 state, which shows an $n\pi^*$ character for both XB complex and the cation, is red shifted by $\approx$ 0.13 eV in the presence of the XB interaction.

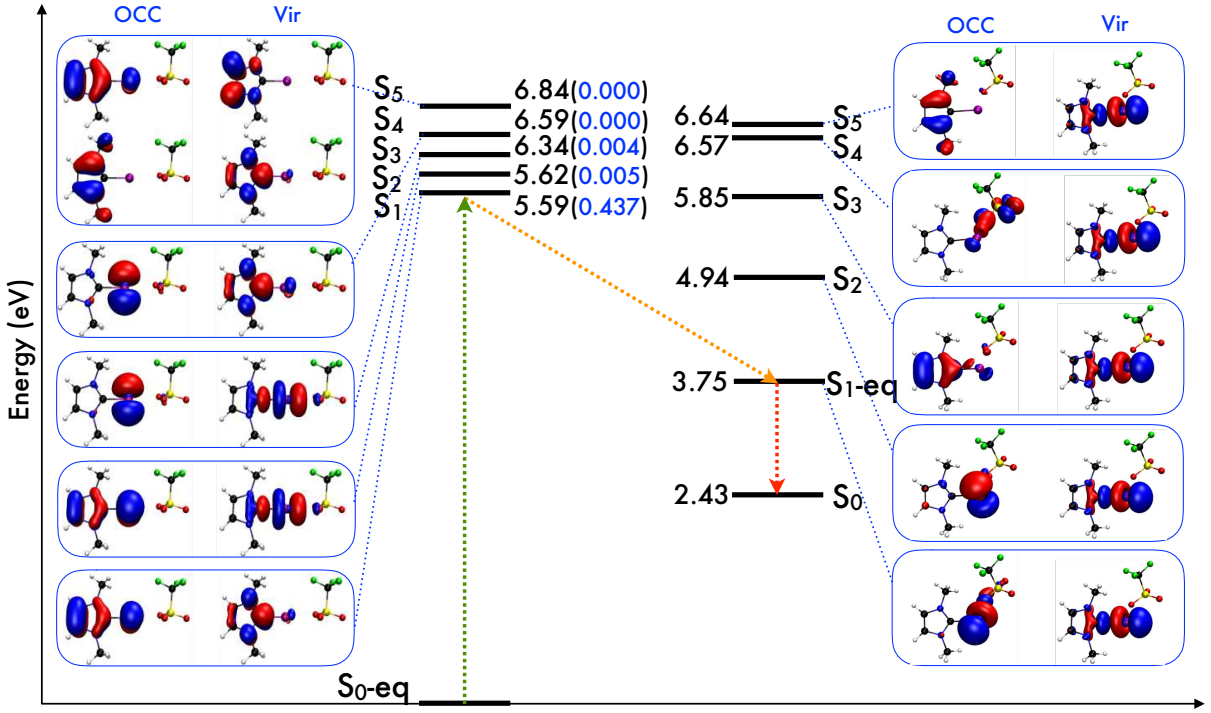


Figure 2: 2-Iodo-imidazolium · OTf: Natural transition orbitals, vertical excitation energies (eV) (green arrow) and oscillator strengths (in blue) at the Franck-Condon geometry of the XB complex. A geometry optimization on the S_1 potential energy surface leads to S_1-eq (orange arrow). The emission energy (eV) at S_1-eq structure to S_0 is indicated by a red arrow. All excited state results are at the COSMO-RI-ADC(2)/def2-TZVPP(post-SCF) level in acetonitrile solution. The ground state geometry for S_0-eq was optimized at the COSMO-MP2/def2-TZVPP(PTE) level in acetonitrile.

In the gas phase, the unscreened Coulomb attraction between the 2-iodoimidazolium cation and OTF^- leads to a strong XB interaction and large effects on the electronic transitions in the cation. The two lowest vertical transitions of the XB iodoimidazolium·OTf complex in vacuum appear at 5.22 and 5.33 eV. These transition states are bright with a mixture of $n\pi^*$ and $\pi\pi^*$ characters (cmp. SI Table S4).

After photoexcitation of the 2-iodoimidazolium·OTf complex in acetonitrile solution and relaxation of S_1 state from the Franck-Condon point to the S_1-eq structure, where S_1 has a $\pi\sigma^*$ character, the C–I bond is elongated by about 0.47 Å to 2.50 Å and tilted out of the plane of the imidazole ring by $\approx 38°$. The elongation of the C–I bond in the S_1-eq structure is accompanied by a reorientation of the triflate anion and, to some extent, a stronger XB

interaction between iodine and an oxygen atom of OTf^- which causes a shortening of the I–O distance by 0.26 Å to 2.56 Å (cmp. Fig. 2). The reorientation of the halogen bond is triggered by the change of the character of S_1 into an $n\sigma^*$ transition from a lone pair of iodine into the C–I antibonding orbital which shifts the σ-hole away from the C–I bond axes.

The NTOs of the five lowest transitions at the S_1-eq structure show that these excitations are all either $n\sigma^*$ or $\pi\sigma^*$ transitions, mostly from iodine non-bonding orbitals into the σ^* orbital of the C–I bond, Fig. 2. The electronic deexcitation of the XB complex from S_1 into S_0 at the S_1-eq geometry emits $\approx$ 1.32 eV energy which can lead to a fast decay of the excitation without observable fluorescence. This emission energy is $\approx$ 1.26 eV lower than for the cation without XB counterion for which the deexcitation energy is 2.58 eV. After the deexcitation to S_0, the relaxation of the complex on the ground state surface in solution does not lead back to the XB S_0-eq structure but rather to the S_0'-eq structure with an anion-π interaction between the positively charged imidazole ring and OTf^- which is energetically lower at the MP2 level.

The structural changes of the iodoimidazolum moiety along the relaxation on the S_1 surface are slightly larger for the XB complex than for the 2-iodoimidazolium cation without counterion. In case of the cation, the C–I bond length at the S_1-eq structure is 2.45 Å, which is longer than the S_0-eq by 0.43 Å, and is tilted out of the plane of the imidazole ring by $\approx 31°$.

The binding energy of OTf^- to iodoimidazolium cation is in the ground state 6.9 kcal·mol^{-1} which in the excited state at the S_1-eq structure increases to 10.9 kcal·mol^{-1}. One can thus conclude that the interaction becomes stronger in the excited state at the S_1-eq structure due to the $n\sigma^*$ character of the transition.

2-Iodo-benzimidazolium·OTf

Also for the 2-iodobenzimidazolium·OTf complex we found on the (COSMO-)MP2 ground state potential energy surface in vacuum and in acetonitrile solution two different minima, shown in Fig. 3 **a** and **c**. As for 2-iodoimidazolium·OTf, due to the London dispersion interaction, the equilibrium structure with the anion-π interaction, Fig. 3 **c**, is energetically more favorable than the XB minimum, in vacuum by ≈ 18.6 kcal·mol^{-1} and in acetonitrile solution at the COSMO-MP2 level still by ≈ 3.7 kcal·mol^{-1}. Again, to avoid the unbalanced treatment of dispersion interactions within the complex and between the complex and the solvent, we did in addition COSMO-B3-LYP/def-TZVPP calculations without dispersion correction in acetonitrile solution. This calculation predicts the anion-π complex by 1.2 kcal·mol^{-1} below the XB complex. Compared to the respective MP2 results, the I–O distance and the C–I bond length increased with DFT by 0.01 Å and 0.04 Å, respectively. Since we are interested into the effects of the halogen bond on the spectrum we continued again with the XB structure. The results for the vertical excitation energies at the XB minimum and at the minimum on the S_1 surface reached from the Franck-Condon point in acetonitrile are summarized in Fig. 4. The results of similar calculations for the XB complex in vacuum and the 2-iodobenzimidazolium cation in solution without close interaction with OTf^- are given in Table 2 and Tables S7, S8 and S9 of the SI.

The extension of the π-system by a benzene ring decreases the energies of the unoccupied π-orbitals so that for the 2-iodobenzimidazolium cation and its XB complex with OTf^- the lowest singlet excitations, located at, respectively , 4.73 and 4.74 eV, are bright $\pi\pi^*$ transitions with a partial intra-molecular charge transfer from the iodine atom into the benzimidazole ring without direct contributions from orbitals of the counterion.

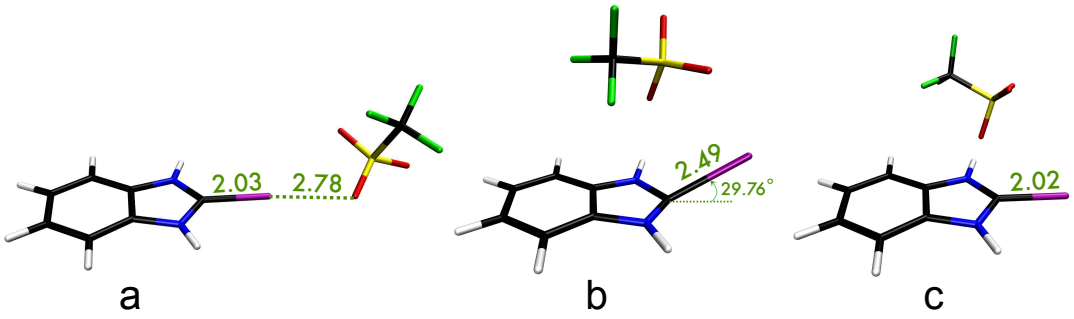


Figure 3: Optimized geometries of 2-iodobenzimidazolium·OTf in (**a**) the ground state S_0-eq with XB interaction, (**b**) the first excited state S_1-eq and (**c**) the ground state S_0'-eq with an anion-π interaction. All structures have been computed for acetonitrile solution with COSMO-MP2/def2-TZVPP(PTE) for the ground state and COSMO-RI-ADC(2)/def2-TZVPP(post-SCF) for the excited state.

As shown in Fig. 4, the next two lowest $\pi\pi^*$ states (S_2 and S_4) of the XB complex in solution are located at 5.22 and 5.80 eV, respectively, with S_4 having significantly more intensity than S_2. Both are local transitions within the benzimidazolium moiety. Located between them is S_3, a dark $\pi\sigma^*$ transition into the σ^* orbital of the C–I bond. Also S_5 at 6.11 eV has no significant oscillator strength. This is an $n\pi^*$ transition from a non-bonding orbital of iodine into a π^* orbital localized mostly on the imidazolium moiety.

Table 2: Vertical excitation energies ω and oscillator strengths f of the 2-iodobenzimidazolium·OTf (XB) complex and the 2-iodobenzimidazolium cation in acetonitrile at COSMO-ADC(2)/def2-TZVPP(post-SCF) level.

	XB			Cation		
State	type	ω	f	type	ω	f
1	$\pi\pi^*$	4.74	0.482	$\pi\pi^*$	4.73	0.445
2	$\pi\pi^*$	5.22	0.096	$\pi\sigma^*$	5.10	0.000
3	$\pi\sigma^*$	5.67	0.001	$\pi\pi^*$	5.14	0.093
4	$\pi\pi^*$	5.80	0.474	$n\sigma^*$	5.71	0.001
5	$n\pi^*$	6.11	0.000	$\pi\pi^*$	5.82	0.429

The interaction with OTf^- in the XB complex increases the excitation energies for the lowest five transitions with the exception of S_1 which has in the XB complex almost the same excitation energy as in the cation without counterion. The second $\pi\pi^*$ transition for the XB complex at 5.22 eV corresponds to the S_3 state of the iodobenzimidazolium cation at 5.14

eV. But even more blue shifted in the XB complex is the $\pi\sigma^*$ transition into the antibonding σ^* orbital of the C–I bond, where the XB interaction increases the excitation energy from 5.10 eV to 5.67 eV.

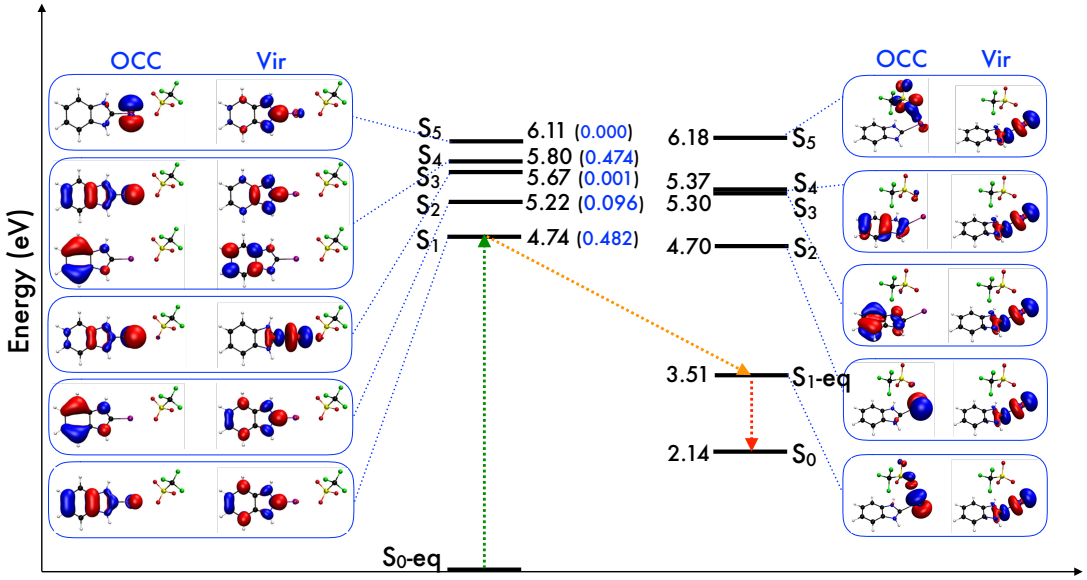


Figure 4: 2-Iodo-benzimidazolium · OTf: Natural transition orbitals, vertical excitation energies (eV) (green arrow) and oscillator strengths (in blue) at the Franck-Condon geometry of the XB complex. A geometry optimization on the S_1 potential energy surface leads to S_1-eq (orange arrow). The emission energy (eV) at the S_1-eq structure to S_0 is indicated by a red arrow. All excited state calculations are at COSMO-RI-ADC(2)/def2-TZVPP(post-SCF) level in acetonitrile solution. The ground state geometry of S_0-eq was optimized at the COSMO-MP2/def2-TZVPP(PTE) level in acetonitrile.

For the XB complex in the gas phase, S_1 is a $\pi\pi^*$ transition that is mainly localized on the iodobenzimidazolium moiety with partial CT out of the lone pairs of the iodine and the oxygen atoms of OTf^- to a π^* orbital of benzimidazolium. This transition at 4.55 eV is a bright state with an oscillator strength of 0.4. The S_2 state is a CT transition from oxygen lone pairs of OTf^- to the iodobenzimidazolium moiety at 4.67 eV.

To obtain the Stokes shift for the fluorescence emission, we optimized the geometry of the bright S_1 state in acetonirile solution and determined the minimum reached from the Franck-Condon point of the XB complex (S_1-eq) at the COSMO-RI-ADC(2)/def2-TZVPP level. The structure is shown in Fig. 3 **b** and reveals that similar as in 2-iodoimidazolium·OTf, several

internal coordinates change during the relaxation to the S_1-eq: the CF_3 group of the OTf anion turns to the face side of the organic ring system which leads to an anion-π interaction similar as for the S_1-eq structure of 2-iodoimidazolium·OTf, the C–I bond lengthens by $\approx$ 0.46 Å and bends out of the molecular plane by $\approx$ 30°. The lengthening of the C–I bond in the XB complex with OTf^- is larger than for the 2-iodobenzimidazolium cation without interaction with OTf^- by $\approx$ 0.09 Å, where at the S_1-eq minimum of the cation this bond bends out of the molecular plane by $\approx$ 36°. Along the relaxation on the S_1 surface, the character of this state changes for both the XB complex and the iodobenzimidazolium cation, similar as for 2-iodoimidazolium·OTf, to an nσ^* excitation from iodine non-bonding electrons into the antibonding σ^* orbital of the C–I bond.

The emission energy at the optimized S_1-eq geometry from S_1 to S_0 is for the XB complex with 1.37 eV approximately 1.2 eV lower than for the 2-iodobenzimidazolium cation without XB interaction. Also similar as for 2-iodoimidazolium·OTf, the relaxation on the ground state potential energy surface starting from S_1-eq geometry leads to the S_0'-eq ground state structure, shown in Fig. 3 **c**, with an anion-π interaction.

In summary, the calculations indicate that the formation of a halogen bond with OTF^- in acetonitrile solution does not change the energy of the bright $\pi\pi^*$ transition significantly. Furthermore, the extension of the π-system may increase the excited state lifetime of the XB complex relative to the 2-iodoimidazolium·OTf and enhance the fluorescence emission. The calculations predict that the XB interaction red shifts the fluorescence signal, if the emission happens close to the S_1-eq geometry. In the ground state, the binding energy of OTf^- to the 2-iodobenzimidazolium cation is 7.4 kcal·mol^{-1}. This energy increases in the excited state to 14.4 kcal·mol^{-1} due to the $n\sigma^*$ character of the excited state at the S_1-eq geometry which is stabilized by the presence of the counterion. One can altogether conclude that monodentate 2-iodoimidazolium cations might be too weak XB acceptors in order to exhibit in acetonitrile solution any significant changes in their absorption or fluorescence spectra that can be attributed to the XB interaction.

Bis(2-Iodo-benzimidazolium)·Cl

The bis(2-iodobenzimidazolium) dication can potentially act as a bidentate Lewis acid. The rotation of the halobenzimidazolium moieties around the C-N axis which connects these groups to the benzene core are sterically inhibited by the trifluoromethyl group in the 2-position of the 1,3-disubstituted benzene ring.[16] The bidentate structure of the bis(iodo-benzimidazolium) cation prompted us to study this compound as a halogen-bond acceptor in an XB complex with a chloride counterion, Fig. 5**a**. The binding energy of Cl^- to the bis(2-iodobenzimidazolium) dication in acetonitrile solution is $\approx$ 18.6 kcal·mol^{-1} in the ground state and increases in S_1 at the S_1-eq structure to 28.7 kcal·mol^{-1}. These binding energies are much higher than the corresponding values for the monodentate 2-iodoimidazolium and 2-iodobenzimidazolium cations with the OTf^- counterion.

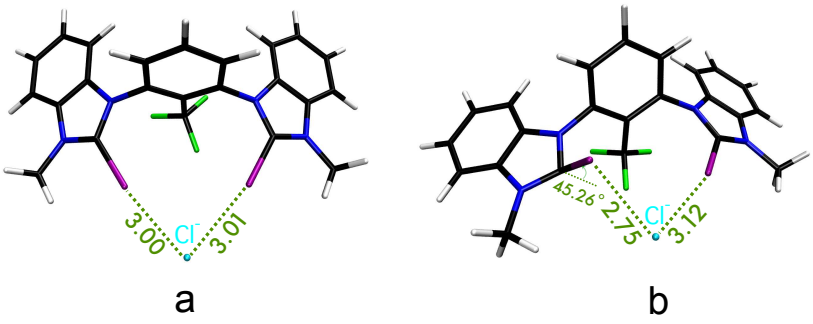


Figure 5: Optimized geometries of bis(2-iodobenzimidazolium)·Cl in (**a**) the ground state S_0-eq with XB interaction at the COSMO-MP2/def2-TZVPP(PTE) level and (**b**) the first excited state S_1-eq at the COSMO-RI-ADC(2)/def2-TZVPP(post-SCF) level in acetonitrile solution.

The UV-vis absorption spectra for the XB complex were calculated in acetonitrile solution and in vacuum and the results for the excitation energies and oscillator strengths for the lowest five electronic excited states are shown in Fig. 6 and Table S10 of the SI. In solution the excitation energies, intensities and also the characters of the excited states change relative to the vacuum. As shown in Fig. 6, in solution the S_1 and S_2 states are nearly degenerate at excitation energies of 4.53 eV and 4.59 eV with S_2 as the brightest state. These two

excitations are comprised of plus and minus combinations of $\pi\pi^*$ transitions mainly localized on the 2-iodobenzimidazolium moieties with a partial CT from iodine to the π^* orbitals of the π-conjugated benzimidazolium rings. The NTOs given for the excited states of the XB complex in Fig. 6 clearly show that the negative charge on the Cl^- is stabilized by the polar solvent which results in negligible contributions from the orbitals at the Cl^- counterion to the NTOs for the lowest five states. The third and forth states (S_3 and S_4) are located at, respectively, 4.90 eV and 4.93 eV of the spectrum with S_3 carrying a significant oscillator strength of 0.35. Similar as for S_1 and S_2, these two states are comprised of symmetric and antisymmetric linear combinations of local $\pi\pi^*$ transitions on the two iodobenzimidazolium moieties. The first transition localized on the central benzene linker appears as S_5 at 4.95 eV. Because of its small oscillator strength this state does not contribute to the UV absorption spectrum of the XB complex.

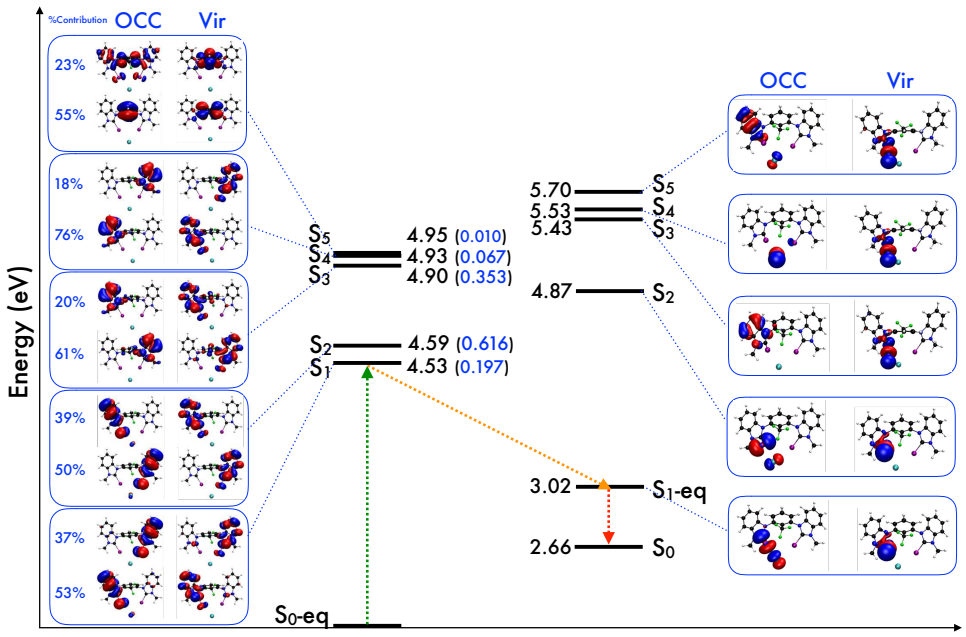


Figure 6: Bis(2-Iodo-benzimidazolium) · Cl: Natural transition orbitals, vertical excitation energies (eV) (green arrow) and oscillator strengths (in blue) at the Franck-Condon geometry of the XB complex. A geometry optimization on the S_1 potential energy surface leads to S_1-eq (orange arrow). The emission energy (eV) at the S_1-eq structure to S_0 is indicated by a red arrow. All excited state calculations are at the COSMO-RI-ADC(2)/def2-TZVPP(post-SCF) level in acetonitrile solution. The ground state geometry of S_0-eq was optimized at the COSMO-MP2/def2-TZVPP(PTE) level in acetonitrile.

The four lowest electronic transitions of the dication without counterion have similar characters and oscillator strengths as of the XB complex (cmp. Table 3 and Table S11 of the SI). The XB interaction does not effect the energies of the S_1 and S_2 states compared to the dication, while it blue shifts the energies of S_3 and S_4 by ≈ 0.1 eV. The S_5 state of diaction is a $\pi\sigma^*$ transition from the π orbitals of the iodoimidazolium moieties to the σ^* orbital of the C–I bonds and is a dark state.

Table 3: Vertical excitation energies ω and oscillator strengths f of the bis(2-iodobenzimidazolium) · Cl (XB) complex and bis(2-iodobenzimidazolium) dication in acetonitrile at the COSMO-ADC(2)/def2-TZVPP(post-SCF) level.

	XB			Dication		
State	type	ω	f	type	ω	f
1	$1\pi\pi^*$	4.53	0.197	$1\pi\pi^*$	4.54	0.120
2	$2\pi\pi^*$	4.59	0.616	$2\pi\pi^*$	4.58	0.605
3	$3\pi\pi^*$	4.90	0.353	$3\pi\pi^*$	4.81	0.302
4	$4\pi\pi^*$	4.93	0.067	$4\pi\pi^*$	4.83	0.059
5	$5\pi\pi^*$	4.95	0.010	$\pi\sigma^*$	5.00	0.004

The results for the vertical excitation of the XB complex in vacuum reveal that the lowest five electronic states have CT character. They are transitions mainly from non-bonding orbitals of Cl^- to the imidazolium moieties and the phenyl ring. The two close-lying S_1 and S_2 states in vacuum appear at ≈ 4.30 eV and carry oscillator strengths of ≈ 0.2. The S_3 state at 4.45 eV is a CT transition from non-bonding orbitals at chloride and iodine into the central benzene linker. The S_4 and S_5 states at 4.48 and 4.54 eV are, respectively, symmetric and antisymmetric combinations of $n\pi^*$ CT transitions from Cl^- to the imidazolium moieties.

Going back to the results in solution, as pointed out above, S_1 and S_2 are at the almost C_S-symmetric ground state structure nearly degenerate mixtures of the lowest local excitations in the benzimidazolium groups. The relaxation after photoexcitation from the Franck-Condon point towards the minima on the excited state potential energy surface breaks the near C_S symmetry and leads to a localization of S_1 on one and of S_2 on the other benzimidazolium group and should end in two symmetry-equivalent minima on the excited state potential. The result for the equilibrium structure reached after relaxation from the Franck-Condon

point in the S_1 state, S_1-eq, in acetonitrile solution is given in Fig. 3 **b**. The relaxation slightly twists the complex and leads after localization of the excitation on one side of the complex to similar structural changes in the corresponding iodoimidazolium group as observed in the previous sections with an out-of-plane bending angle of the C–I bond by $\approx 45°$ and a lengthening of the C–I bond by 0.36 Å. The NTOs for the S_1 transition at the S_1-eq geometry shown in Fig. 6 indicate that an electron is excited from an anti-bonding orbital between iodine and chloride to the σ^* orbital of the C–I bond. This explains the elongation of the C–I bond length compared to the ground state geometry, Fig. 5 **a**, from 2.05 to 2.41 Å, while the other C–I bond length remains almost unchanged, and at the some time, the shortening of the I–Cl distance by ≈ 0.25 Å.

For the bis(iodobenzimidazolium) dication without the XB partner, the relaxation from the Franck-Condon point to the associated S_1-eq geometry is accompanied with an out-of-plane bending by $\approx 43°$ and an elongation of the C–I bond for one of the imidazolium groups. However, in this case the C–I bond elongation is with 0.18 Å significantly smaller than in the XB complex. The NTOs of the S_1 state at the S_1-eq structure of the dication in Fig. 7 show a CT from π^* orbitals of one of the iodoimidazolium fragments to the σ^* orbital of the C–I bond. The emission energy at this structure from S_1 to S_0 is with 2.30 eV almost 2 eV larger than for the XB complex in Fig. 6, where the S_1-eq is stabilized by the formation of a partial covalent I–Cl bond. For both the XB complex and the dication, after deexcitation from S_1-eq to S_0 the structures relax back to the original ground state minimum S_0-eq.

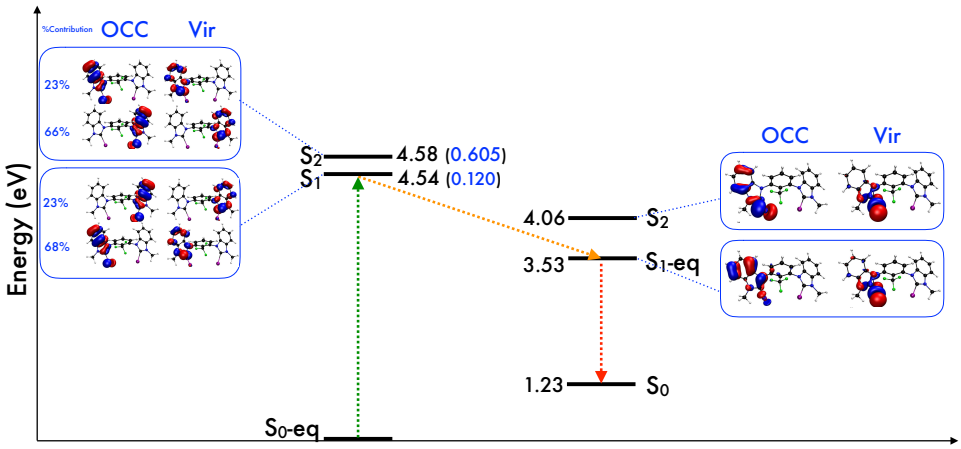


Figure 7: Bis(2-Iodo-benzimidazolium) dication: Natural transition orbitals, vertical excitation energies (eV) (green arrow) and oscillator strengths (in blue) at the Franck-Condon geometry. A geometry optimization on the S_1 potential energy surface leads to S_1-eq (orange arrow). The emission energy (eV) at S_1-eq to S_0 is indicated by a red arrow. All excited state calculations are at the COSMO-RI-ADC(2)/def2-TZVPP(post-SCF) level in acetonitrile solution. The ground state geometry of S_0-eq was optimized at the COSMO-MP2/def2-TZVPP(PTE) level in acetonitrile.

Thus, for the bis(iodobenzimidazolium) · Cl complex, after excitation into S_1 the XB interaction stays intact and is even strengthened during the relaxation to the S_1-eq structure. The strong stabilization of S_1-eq should have a large influence on the fluorescence spectrum. At the same time, for the dication without XB partner our calculations predict a larger fluorescence emission energy.

Conclusion

In this study we have used the correlated wavefunction-based method ADC(2) in combination with the COSMO solvation model to investigate the effects of the halogen-bond interaction on the excited states of iodimidazolium compounds. We investigated in particular the excited state minima reached by relaxation on the S_1 potential energy surfaces and the emission energies which is relevant to understand the influence of the halogen-bond interaction on the fluorescence properties of these compounds. To this end, we studied the five lowest

excited states of the XB complexes 2-iodoimidazolium · OTf, 2-iodobenzimidazolium · OTf and bis(2-iodobenzimidazolium) · Cl in acetonitrile solution and analyzed the corresponding NTOs. The calculations show that for these compounds the inclusion of a solvent model is essential because the results in vacuum predict completely different spectra due to the much stronger interaction between the ions without screening dielectric environment.

For the iodoimidazolium · OTf and iodobenzimidazolium · OTf on the S_1 potential energy surface the calculations predict relaxation pathways which after deexcitation lead to other minima on the ground state potential energy surface with anion-π interactions between the counterion and the face side of the imidazolium ring where the halogen bond is broken up. In contrast to this, for the bidentate XB complex bis(2-iodobenzimidazolium) · Cl the relaxation on the S_0 potential after deexcitation at the excited state equilibrium structure, S_1-eq, brings the molecule back to the original ground state XB structure, S_0-eq.

Examination of the influence of the halogen bonding on the excited state properties in solution by excluding the counterion from the calculations for the 2-iodoimidazolium, 2-iodobenzimidazolium and bis(2-iodobenzimidazolium) cations gave excited states that are mostly similar to those for the corresponding XB complexes.

Our calculations indicate that in contrast to the monodendate complexes, the bidendate bis(2-iodobenzimidazolium) · Cl will not only have a fluorescence that is red shifted relative to the dication without counterion, but also stay intact after photoexcitation.

Acknowledgement

We acknowledge financial support from the Cluster of Excellence RESOLV (EXC 2033) and project Ha 2588/8-1 funded by the Deutsche Forschungsgemeinschaft.

References

(1) Gajda, R.; Katrusiak, A.; Crassous, J. Pressure-controlled aggregation in carboxylic acids. A case study on the polymorphism of bromochlorofluoroacetic acid. *Cryst. Eng. Comm.* **2009**, *11*, 2668–26776.

(2) Riley, K. E.; Hobza, P. Investigations into the nature of halogen bonding including symmetry adopted perturbation theory analysis. *J. Chem. Theory Comput.* **2008**, *4*, 232–242.

(3) Kozuch, S.; Martin, J. M. L. Halogen bonds: benchmarks and theoretical analysis. *J. Chem. Theory Comput.* **2013**, *9*, 1918–1931.

(4) Wolters, L. P.; Schyman, P.; Paven, M. J.; Jorgensen, W. L.; Bickelhaupt, T. M.; Kozuch, S. The many faces of halogen bonding: a review of theoretical models and methods. *WIREs Comput. Mol. Sci.* **2014**, *4*, 523–540.

(5) Lindblad, S.; Mehmeti, K.; Veiga, A. X.; Nekoueishahraki, B.; Gräfenstein, J.; Erdélyi, M. Halogen bond asymmetry in solution. *J. Am. Chem. Soc.* **2018**, *140*, 13503–13513.

(6) Lu, Y.; Li, H.; Zhu, X.; Liu, H.; Zhu, W. Effects of solvent on weak halogen bonds: density functional theory calculations. *Int. J. Quantum Chem.* **2012**, *112*, 1421–1430.

(7) Jungbauer, S. H.; Schindler, S.; Kniep, F.; Walter, S. M.; Rout, L.; Huber, S. M. Multidentate halogen-bond donors as Lewis acidic activators or catalysts in halides abstraction reactions. *Synlett.* **2013**, *24*, 2624–2628.

(8) Kniep, F.; Rout, L.; Walter, S. M.; Bensch, H. K. V.; Jungbauer, S. H.; Hertweck, E.; Huber, S. M. 5-Iodo-1,2,3-triazolium-based multidentate halogen-bond donors as activating reagents. *Chem. Commun.* **2012**, *48*, 9299–9301.

(9) Tepper, R.; Schulze, B.; Jäger, M.; Friebe, C.; Scharf, D. H.; Görls, H.; Schubert, U. S. Anion receptors based on halogen bonding with halo-1,2,3-triazolium. *J. Org. Chem.* **2015**, *80*, 3139–3150.

(10) Cavallo, G.; Metrangolo, P.; Milani, R.; Pilati, T.; Priimagi, A.; Resnati, G.; Terraneo, G. The halogen bond. *Chem. Rev.* **2016**, *116*, 2478–2601.

(11) Siiskonen, A.; Priimagi, A. Benchmarking DFT methods with small basis sets for the calculation of halogen-bond strengths. *J. Mol. Model* **2017**, *23*, 50.

(12) Anderson, L. N.; Aquino, F. W.; Raeber, A. E.; Chen, X.; Wong, B. M. Halogen bonding interactions: revised benchmarks and a new assesment of exchange vs. dispersion. *J. Chem. Theory Comput.* **2018**, *14*, 180–190.

(13) Beale, T. M.; Chudzinski, M. G.; Sarwar, M. G.; Taylor, M. S. Halogen bonding in solution: thermodynamics and applications. *Chem. Soc. Rev.* **2013**, *42*, 1667–1680.

(14) Gilday, L. C.; Robinson, S. W.; Barendt, T. A.; Langton, M. J.; Mullaney, B. R.; Beer, P. D. Halogen bonding in supramolecular chemistry. *Chem. Rev.* **2015**, *115*, 7118–7195.

(15) Lu, Y.; Li, H.; Zhu, X.; Zhu, W.; Liu, H. How does halogen bonding behave in solution? A theoretical study using implicit solvation model. *J. Phys. Chem. A* **2011**, *115*, 4467–4475.

(16) Jungbauer, S. H.; Huber, S. M. Cationic multidentate halogen-bond donors in halide abstraction organocatalysis: catalyst optimization by preorganization. *J. Am. Chem. Soc.* **2015**, *137*, 12110–12120.

(17) Jungbauer, S. H.; Walter, S. M.; Schindler, S.; Rout, L.; Kniep, F.; Huber, S. M. Activation of carbonyl compound by halogen bonding. *Chem. Commun.* **2014**, *50*, 6281–6284.

(18) Takeda, Y.; Hisakuni, D.; Lin, C.-H.; Minakata, S. 2-halogenimidazolium salt catalyzed aza-diels-alder reaction through halogen-bond formation. *Org. Lett.* **2015**, *17*, 318–321.

(19) Walter, S. M.; Kniep, F.; Herdtweck, E.; Huber, S. M. Halogen-bond-induced activation of a carbon-heteroatom bond. *Angew. Chem. Int. Ed.* **2011**, *50*, 7187–7191.

(20) Schulz, N.; Sokkar, P.; Engelage, E.; Schindler, S.; Erdelyi, M.; Sanchez-Garcia, E.; Huber, S. M. The interaction modes of haloimidazolium salts in solution. *Chem. Eur. J.* **2018**, *24*, 3464–3473.

(21) Zapata, F.; Caballero, A.; White, N. G.; Claridge, T. D. W.; Costa, P. J.; Félix, V.; Beer, P. D. Fluorescent charge-assisted halogen-bonding macrocyclic halo-imidazolium receptors for anion recognition and sensing in aqueous media. *J. Am. Chem. Soc.* **2012**, *134*, 11533–11541.

(22) Klamt, A.; Schüürmann, G. COSMO: A new approach to dielectric screening in solvents with explicit expressions. *J. Chem. Soc. Perkin Trans. 2* **1993**, 799–805.

(23) Khani, S. K.; Khah, A. M.; Hättig, C. COSMO-RI-ADC(2) excitation energies and excited state gradients. *Phys. Chem. Chem. Phys.* **2018**, *20*, 16354–16363.

(24) Head-Gordon, M.; Pople, J. A.; Frisch, M. J. MP2 energy evaluation by direct methods. *Chem. Phys. Lett.* **1988**, *153*, 503–506.

(25) Weigend, F.; Ahlrichs, R. Balanced basis sets of split valence, triple zeta valence and quadruple zeta valence quality for H to Rn: Design and assessment of accuracy. *Phys. Chem. Chem. Phys.* **2005**, *7*, 3297–3305.

(26) Hellweg, A.; Hättig, C.; Höfener, S.; Klopper, W. Optimized accurate auxiliary basis sets for RI-MP2 and RI-CC2 calculations for the atoms Rb to Rn. *Theor. Chem. Acc.* **2007**, *117*, 587–597.

(27) Peterson, K. A.; Figgen, D.; Goll, E.; Stoll, H.; Dolg, M. Systematically convergent basis sets with relativistic pseudopotentials. II. Small-core pseudopotentials and correlation consistent basis sets for the post-d group 16-18 elements. *J. Chem. Phys.* **2003**, *119*, 11113–11123.

(28) Hättig, C.; Weigend, F. CC2 excitation energy calculations on large molecules using the resolution of the identity approximation. *J. Chem. Phys.* **2000**, *113*, 5154–5161.

(29) Schirmer, J. Beyond the random-phase approximation: a new approximation scheme for the polarization propagator. *Phys. Rev. A* **1982**, *26*, 2395–2416.

(30) Hättig, C. Structure optimization for excited states with correlated second-order methods: CC2, CIS(D_∞) and ADC(2). *Adv. Quant. Chem.* **2005**, *50*, 37–60.

(31) TURBOMOLE V7.2 2017, a development of University of Karlsruhe and Forschungszentrum Karlsruhe GmbH, 1989-2007, TURBOMOLE GmbH, since 2007; available from `http://www.turbomole.com`.

(32) Furche, F.; Ahlrichs, R.; Hättig, C.; Klopper, W.; Sierka, M.; Weigend, F. *WIREs Comput. Mol. Sci.* **2014**, *4*, 91–100.

(33) Becke, A. D. Density-Functional exchange-energy approximation with correct asymptotic behavior. *Phys. Rev. A* **1988**, *38*, 3098–3100.

(34) Grimme, S. Density functional theory with London dispersion corrections. *WIREs Comput. Mol. Sci.* **2011**, *1*, 211–228.

(35) Kreienborg, N. M.; Merten, C. How do substrates bind to a bifunctional thiourea catalyst? A vibrational CD study on carboxylic acid binding. *Chem. Eur. J.* **2018**, *24*, 17948–17954.

5 Comparison of reaction field schemes for coupling continuum solvation models with wavefunction methods for excitation energies

In an effort to clarify the significance of post-HF contributions to the solvent reaction field in the calculation of vertical excitation energies, herein, we compare the performance of the PTE, PTED and post-SCF schemes at the COSMO-ADC(2) level of theory. To do so, we compared the computed solvent shifts at the COSMO-ADC(2)/def2-TZVP level with the associated experimental values for two sets of benchmark data. The first data set comprises aromatic molecular structures with $\pi\pi^*$ electronic transitions and the second set includes diverse structures with the mixture of $\pi\pi^*$ and $n\pi^*$ transitions. In addition, in the framework of the post-SCF scheme, the solvent shifts calculated at the COSMO-CC2 level were also compared with the experimental shifts.

My contribution to this study includes designing and collecting the second data set, calculations and statistical analysis and finally preparing the first version of the manuscript which later on was further developed together with my co-author.

Comparison of Reaction Field Schemes for Coupling Continuum Solvation Models with Wavefunction Methods for Excitation Energies

Sarah Karbalaei Khani* and Christof Hättig

Arbeitsgruppe Quantenchemie, Ruhr-Universität, Bochum 44780, Germany

E-mail: Sarah.Karbalaeikhani@ruhr-uni-bochum.de

Abstract

We report an evaluation of the performance of the perturbation to energy (PTE), perturbation to energy and density (PTED) and post-SCF reaction field schemes for vertical excitation energies using the algebraic diagrammatic construction through second order (ADC(2)) method combined with the continuum-like screening model (COSMO) as a solvation model. For this purpose we use two sets of experimental benchmark data in gas- and solution phase with $\pi\pi^*$ and $n\pi^*$ electronic transitions. The experimental solvatochromic shifts are compared to the corresponding calculated values at the COSMO-ADC(2) level within the framework of PTE, PTED and post-SCF schemes and also at the approximate coupled-cluster singles and doubles (CC2) level combined with the COSMO via the post-SCF scheme. As could be expected, PTE scheme at the COSMO-ADC(2) level produces less accurate solvent shifts relative to the PTED and post-SCF approaches. At the same time, the statistically most accurate prediction of solvatochromism is obtained with the post-SCF scheme, while there are some cases that PTED and post-SCF show similar performance.

Introduction

Polarizable continuum models offer an efficient way to include bulk electrostatic effects, usually the principal environment effects for small, polar molecules and in particular for charge-transfer states, with quantum mechanical (QM) descriptions. Avoiding the sampling of the environment, which is included implicitly in the macroscopic parameters, makes the continuum models computationally efficient and clear to setup. The conductor-like screening model (COSMO) is a variant of polarizable dielectric continuum solvation models and is a black box computational tool, that, after the construction of a molecular cavity for the solute, needs only two parameters: the macroscopic dielectric constant ε and the optical dielectric constant $\varepsilon_{opt} = n^2$, where n stands for the index of refraction for a specific solvent.[1]

Different schemes of the coupling between continuum solvent models (CSMs) and QM models have been proposed in the context of post-HF methods including perturbation to energy (PTE), perturbation to density[2] (PTD), PTE(S) and PTES (where "S" stands for singles),[3] perturbation to energy and density[4] (PTED) and post-SCF.[5] The PTE scheme computes the solute-solvent interaction energy self-consistently at the HF level, then uses the resulting polarized molecular orbitals to compute the amplitudes of the post-HF method which can be the second-order Møller-Plesset perturbation theory[6] (MP2) for the ground state or the algebraic diagrammatic construction through second order[7] (ADC(2)) for the excited state. There are two variants for the PTD scheme: one computes SCF orbitals and correlation energy in vacuum and then measures the solvation energy from the correlated gas-phase density,[8] while the other one employs the post-HF density computed for the self-consistently polarized HF molecular orbitals.[2] Both PTE and the first version of the PTD schemes[8] suffer from the lack of coupling between solvation and electronic correlation. As an approximation to the PTE, in PTE(S), coupling between the reaction field (RF) and electron correlation is introduced as an energy correction to the PTE free energy. However, in PTES, the solvation terms contribute explicitly to the CCSD equations.[3] The most expensive PTED scheme, equilibrates the correlated density and the solvent RF such that the solute-solvent

interaction, either for the ground state or excited state, is computed self-consistently.[9] At the post-SCF level, which has been designed for excitation energies and gradients, the polarized SCF molecular orbitals are used to evaluate the RF contribution to the correlated density via the single excitation parts of the amplitudes and multipliers.[4,5]

There are two principal approaches to treat solvent effects for electronically excited molecules: the state-specific approach[10] and the linear-response approach.[11] The state specific approach accounts for the effect of a change in charge distribution of the solute molecule due to an excitation and also the interaction with the reaction field in the surrounding polarizable environment induced by this charge distribution. The linear-response approach accounts for a coupling of the transition density of the solute and the fast response of the environment, associated with the relaxation of electrons. Although these approaches have been considered as alternatives to each other, Lunkenheimer and Köhn[9] claimed that both contributions are equally important, and combined them in an implementation of COSMO-ADC(2) within the PTED scheme. Another implementation of COSMO-ADC(2) for excitation energies within the post-SCF reaction field scheme has been reported by us.[4] This scheme was introduced by Schwabe *et al.* to combine the polarizable embedding (PE) method with the resolution-of-the-identity implementation of the approximate coupled-cluster singles and doubles method CC2.[5] We applied this scheme for the first time with the COSMO solvation model and called it as "post-SCF".

The post-SCF scheme is an intermediate between PTE and PTED as it includes linear-response contributions to the reaction field at the correlated ADC(2) level. The implementation of the post-SCF scheme includes neither perturbative corrections nor, unlike PTED, state specific contributions via self-consistent construction of the reaction field. Besides, excitation energies within the post-SCF are obtained directly from an eigenvalue problem, therefore, the resulted excited states are orthogonal. Accordingly, this is a suitable approach for the description of avoided crossings and conical intersections of the excited states and also for the implementation of excited state analytic gradients. In terms of the computational

cost, out of the two PTED and post-SCF approaches that take the environment effects into account at the correlated level, post-SCF is more affordable.

Up to this point, no systematic evaluation of the PTED and post-SCF reaction field schemes has been reported for a CSM excepting the benchmark study carried out by Mewes *et al.*[2] This benchmark analysis has focused on the coupling of CSMs and wavefunction methods via the PTE and PTD schemes by using a data set mainly limited to nitrobenzene derivatives.

In the present contribution, we analyze the performance of the PTE, PTED and post-SCF reaction field schemes for the calculation of vertical excitation energies at the ADC(2) level within the COSMO framework. For this purpose, we discuss and compare the solvatochromic shifts resulted from ADC(2) to the experimental results for two different data sets. In the same way, the performance of the COSMO-CC2 method within the post-SCF scheme was analyzed for vertical excitation energies by comparing the computed solvatochromic shifts to experiment.[12]

Reaction Field Models

Within the COSMO solvent model, the apparent surface charges Q_κ on the segments κ of the cavity that surrounds the solute are obtained as

$$Q_\kappa = -f(\varepsilon) \sum_\lambda [\mathcal{A}^{-1}]_{\kappa\lambda} V_\lambda \ , \tag{1}$$

where V_λ is the electric potential at the center of the segment λ due to the charge distribution of the QM system. $\mathcal{A}_{\kappa\lambda}$ is the COSMO kernel describing the interaction between surface segments and $f(\varepsilon)$, a scaling factor that depends on the dielectric constant ε, which in principle depends on the frequency.

In the current work we study vertical excitation energies for comparison with experimental absorption band maxima. We thus use ground state equilibrium structures for the solute

and assume that the solvent around the solute is in equilibrium with the ground state charge distribution of the solute. The rapid transition to an electronically excited state in the solute perturbs this equilibrium. During the fast absorption process, however, only the fast electronic component of the solvent polarizability can respond to the change in the solute, while the slow nuclear polarizability can not follow. In reaction field theory, this situation is usually called non-equilibrium solvation. Similar as in other polarizable continuum models, within the COSMO framework, this is accounted for by determining the ground state surface charges with the static dielectric constant and their response to the electronic transition process with the dielectric constant for optical frequencies obtained from the square of the refractive index, n^2.

In the simplest reaction field scheme, PTE, the molecular orbitals (MOs) are obtained from a COSMO-Hartree-Fock calculation where the reaction field or the surface charges are made fully self-consistent with the charge distribution in the QM system at the Hartree-Fock (HF) level. In the subsequent post-HF calculations, i.e. in the correlation treatment and the response calculations, these charges are then kept fix. The solute-solvent interaction appears in the post-HF calculations only as a static potential and modified MOs. Otherwise these calculations are identical to the vacuum case.

At the ADC(2) level, the excitation energies ω_i are obtained as eigenvalues of a secular matrix:[7]

$$\begin{pmatrix} \mathbf{A}_{\mu_1\nu_1} & \mathbf{A}_{\mu_1\nu_2} \\ \mathbf{A}^{\dagger}_{\mu_1\nu_2} & \mathbf{A}_{\mu_2\nu_2} \end{pmatrix} \begin{pmatrix} \mathbf{E}^i_{\nu_1} \\ \mathbf{E}^i_{\nu_2} \end{pmatrix} = \omega_i \begin{pmatrix} \mathbf{E}^i_{\mu_1} \\ \mathbf{E}^i_{\mu_2} \end{pmatrix} \ , \tag{2}$$

where the indices run over singly and doubly excited slater determinants.

The reaction field contributions to the secular matrix in the COSMO-ADC(2)(PTE) are

$$\mathbf{A}^{\mathrm{pol}}_{\mu_1,\nu_1} = \langle \mu_1 | \hat{G}^{\mathrm{pol,HF}} | \mathrm{HF} \rangle \tag{3}$$

$$\mathbf{A}^{\mathrm{pol}}_{\mu_2,\nu_2} = \langle \mu_2 | [\hat{G}^{\mathrm{pol,HF}}, \tau_{\nu_2}] | \mathrm{HF} \rangle \ , \tag{4}$$

where, $\hat{G}^{\mathrm{pol,HF}} = \sum_\kappa \langle \mathrm{HF}|\hat{Q}_\kappa|\mathrm{HF}\rangle \hat{V}_\kappa$ is the Hartree-Fock reaction field potential and usually included in the Fock matrix.

As mentioned in the introduction, in the PTED scheme the reaction field potential and the correlated electron density are equilibrated until full self-consistency (within a given threshold). It is thus the physically most complete reaction field scheme for post Hartree-Fock calculations on a single electronic state. For excitation energies one can either combine it with a state-specific approach and solve the non-linear equations for the PTED scheme for the initial and the final state and determine the excitation energy as the difference of the total energies. The state-specific approach fully accounts for the relaxation of the reaction field to the electronic densities of the initial and the final state, but not for the coupling between the reaction field response and the transition density.[9] It is in particular well-suited to treat long-lived excited states after a lifetime that is longer than the reorientation of the solvent molecules, i.e. when the environment has been fully relaxed with respect to the excited state density.

Alternatively, on can use the PTED scheme only for the initial (or reference) state and determine vertical excitation energies by linear response theory. This scheme is better suited to describe absorption spectra since it includes the coupling between the reaction field and the transition density, which is in particular important for bright states with large transition dipole moments, and is easy to adapt to the non-equilibrium solvation where only the fast electronic polarization of the environment relaxes during the excitation process. The linear response approach does, however, not include the coupling between the excited state density (or the density difference) and the reaction field. For the relaxation of the fast polarization, the corrected linear response (cRL) terms are perturbatively added to the excited state energy.

In general, within the state specific approach, PTED solves a non-linear Schrödinger equation for each state I self-consistently until the surface charges converge within a specific

threshold

$$(\hat{H}^{\mathrm{QM}} + 2\hat{G}^{\mathrm{pol}}_{\Psi^{I*}_{\mathrm{QM}}\Psi^{I}_{\mathrm{QM}}})|\Psi_{\mathrm{QM}}\rangle = E_I|\Psi_{\mathrm{QM}}\rangle \ , \tag{5}$$

and gives the uncorrected excited state energy as

$$\Delta E_{I\to J} = E_J - E_I \ , \tag{6}$$

then, as a state specific perturbative correction, the coupling of the excited state density and the fast response of the environment is added to the uncorrected excited state energy.

The polarization contribution to the secular matrix of the COSMO-ADC(2)(PTED), given by Lunkenheimer and Köhn,[9] comes only in the first and fourth matrix elements as

$$\mathbf{A}^{\mathrm{pol}}_{\mu_1,\nu_1} = \langle\mu_1|[\hat{G}^{\mathrm{pol,MP2}}, \tau_{\nu_1}] + \hat{G}^{\nu_1}|\mathrm{HF}\rangle + \frac{1}{2}\Big(\langle\mu_1|[\hat{G}^{\nu_1}, \hat{T}_2]|\mathrm{HF}\rangle + \langle\nu_1|[\hat{G}^{\mu_1}, \hat{T}_2]|\mathrm{HF}\rangle\Big) \tag{7}$$

$$\mathbf{A}^{\mathrm{pol}}_{\mu_2,\nu_2} = \langle\mu_2|[\hat{G}^{\mathrm{pol,MP2}}, \tau_{\nu_2}]|\mathrm{HF}\rangle \ . \tag{8}$$

We note that $\hat{G}^{\mathrm{pol,MP2}}$ accounts for the polarization contribution for a ground state at the PTED-COSMO-MP2 level and is included via the Fock operator. The operator $\hat{G}^{\nu_1}$ is defined as

$$\hat{G}^{\nu_1} = \sum_{\kappa}\langle\mathrm{HF}|[\hat{Q}_\kappa, \tau_{\nu_1}]|\mathrm{HF}\rangle\hat{V}_\kappa \ . \tag{9}$$

The scaling factor of the screening charge $f(\epsilon)$, given in Eq. 1, in the secular matrix transformation of the COSMO-ADC(2) depends on the frequency associated with vectors transformed with $\mathcal{A}$; in the static case, *e.g.* for the calculation of $\hat{G}^{\mathrm{pol,MP2}}$, it is $f(\varepsilon)$, where ε is the static dielectric constant. In the optical regime, *e.g.* for the calculation of $\hat{G}^{\nu_1}$, it is $f(n^2)$, where n is the refractive index.

In the framework of PTED scheme, the perturbative corrections of the cLR terms of

the state specific approach make this reaction field scheme problematic for excited states with conical intersections and avoided crossings. Furthermore, using macro-iterations to make the reaction field self-consistent with the solute charge density in PTED, makes the implementation of excited state gradients challenging and potentially unstable.

The post-SCF scheme does not include macro-iterations and, therefore, the implementation of the excited state gradients is more straightforward for it. Within the framework of post-SCF, the ground state polarization with the HF density is determined self-consistently which follows by the coupling of the post-HF transition density and the fast response of the environment in a separate self-consistent iteration without back-coupling to the ground state HF. For the second order ADC(2) and CC2 methods, the implementation of the post-SCF scheme neglects the coupling of doubles contribution to the unrelaxed post-HF density while it goes beyond the second order.

Without state specific corrections, the polarization contributions to the secular matrix elements of the COSMO-ADC(2)(post-SCF) reads as

$$\mathbf{A}^{\mathrm{pol}}_{\mu_1,\nu_1} = \langle \mu_1 | [\hat{G}^{\mathrm{pol,HF}}, \tau_{\nu_1}] + \hat{G}^{\nu_1} | \mathrm{HF} \rangle \tag{10}$$

$$\mathbf{A}^{\mathrm{pol}}_{\mu_2,\nu_2} = \langle \mu_2 | [\hat{G}^{\mathrm{pol,HF}}, \tau_{\nu_2}] | \mathrm{HF} \rangle \ , \tag{11}$$

with $\hat{G}^{\mathrm{pol,HF}}$ accounts for the polarization contribution for the ground state COSMO-HF, which is included via the Fock matrix.

Computational Details

The first data set, taken from a benchmark study by Mewes *et al.*,[2] consists the experimental band maxima in gas phase and solution for the *meta*- and *para*-substituted nitroaromatic,[13] methoxy-nitroanilines,[14] nitrobenzene, benzofuran, cumarin and 4-nitroaniline.[2] The second data set includes the experimental band maxima in gas phase and solution for acrolein,[15,16] azobenzene,[17,18] benzaldehyde,[19,20] 4-dimethylaminonitrobenzene (DMABN),[21]

pyridazine,[22,23] anthracene,[24,25] adenine,[26–28] guanine,[28,29] uracile,[20,28] indole,[30–32] xanthone[33] and aceton.[34,35]

Given that the first data set consists of molecules that are structurally very close, we decided to collect a second data set with more diverse molecular structures. Furthermore, to avoid the analysis being biased towards the $\pi\pi^*$ states, we decided to evaluate the two data sets (one with 35 $\pi\pi^*$ transitions and the other one with a mixture of 14 $\pi\pi^*$ and 7 $n\pi^*$ states), separately.

Gas phase as well as solvent relaxed geometries for the ground state were obtained at the MP2/def2-TZVP level of theory[36] in combination with the COSMO solvation model within the PTE scheme as implemented in TURBOMOLE.[37] The optimized auxiliary basis sets for def2-TZVP was used for the resolution-of-the-identity approximation.[38] The frozen core approximation was applied to all non-hydrogen atoms: for all C, O, N atoms the $1s^2$ electrons were kept frozen and for chlorine, in addition, all electrons in the $2s^22p^6$ shell. A comparison of the solvatochromic shifts with COSMO-ADC(2)/def2-TZVP within the PTE and PTED RF schemes for gas phase and solvent relaxed geometries were computed with released version of TURBOMOLE[37] and for the post-SCF scheme a locally modified version of TURBOMOLE was used.[39] In case of COSMO-ADC(2)(PTED) calculations the ground state as the reference state is in equilibrium with the solvent and the final values for excitation energies do not include the out-lying charge corrections. The solvent parameters are given in Table 1. In this work, the COSMO cavity construction is of solvent accessible surface (SAS) type[1] and is controlled by atomic radii and solvent radius which, in our calculations, is kept constant at the value of $r_{solv} = 1.30$ Å for all solvents.

Table 1: Dielectric constants for different solvents used in the calculations.

solvent	static dielectric ε	optical dielectric n^2
hexane (Hex)	1.89	1.88
cyclohexane (cyHex)	2.03	2.02
diethyl ether (Et_2O)	4.32	1.83
ethanol (EtOH)	24.6	1.85
acetonitrile (MeCN)	36.7	1.81
water (H_2O)	80.4	1.78

Results and Discussion

First Data Set

The first data set consists the data points for nitrobenzene and *meta*- and *para*-isomers of nitrotoluene, nitroanisole and nitrochlorobenzene in cyclohexane (cyHex), diethylether (Et_2O) and acetonitrile (MeCN), along with *meta*- and *para*-nitroaniline and methoxynitroanilines in cyHex. The solvatochromic shifts for this selection of molecules are mainly due to the bulk electrostatic interaction, while for the rest of the molecules of this data set, including pyridine, benzofurane and cumarine in hexane (Hex) and MeCN, the electrostatic interaction of solute with the bulk environment is very weak as reflected in their small experimental solvatochromic shifts.[2]

The calculated solvent shifts in above mentioned solvents at COSMO-ADC(2) within the PTE, PTED and post-SCF RF schemes are compared to the respective experimental values in Fig. 1. As noted in Ref. 2, solvent shifts for cumarine, benzofurane, pyridine and nitrobenzene, with weak electrostatic interaction with the solvent, are both computationally and experimentally low, especially for pyridine and the lowest bright state of cumarine and benzofurane, while for their second bright states, we see a larger shift. The weak solute-solvent interactions for these states come with negligible solvent shifts computed in the PTE approach. From non-polar to polar solvents, the deviation of the computed solvent shifts using the PTE scheme from the experiment becomes smaller. It shows that for polar solvent,

in particular for MeCN, PTE overestimate the solvent shift due to the poor description of the solute-solvent polarization in the ground state at the HF level (HF-reaction field).

To compare the PTED and post-SCF RF schemes that include the RF contribution to the correlation energy, it can be remarked that for non-polar and intermediate-polar solvents (cyHex and Et_2O), the energy gap between the solvent shifts computed with these two approaches are larger than for polar solvents. In non-polar solvents, the red shifts for the post-SCF scheme are smaller than the PTED scheme and, at the same time, for most cases closer to the associated experimental value. On the other hand, in MeCN, the solvent red shifts computed with those two approaches become closer.

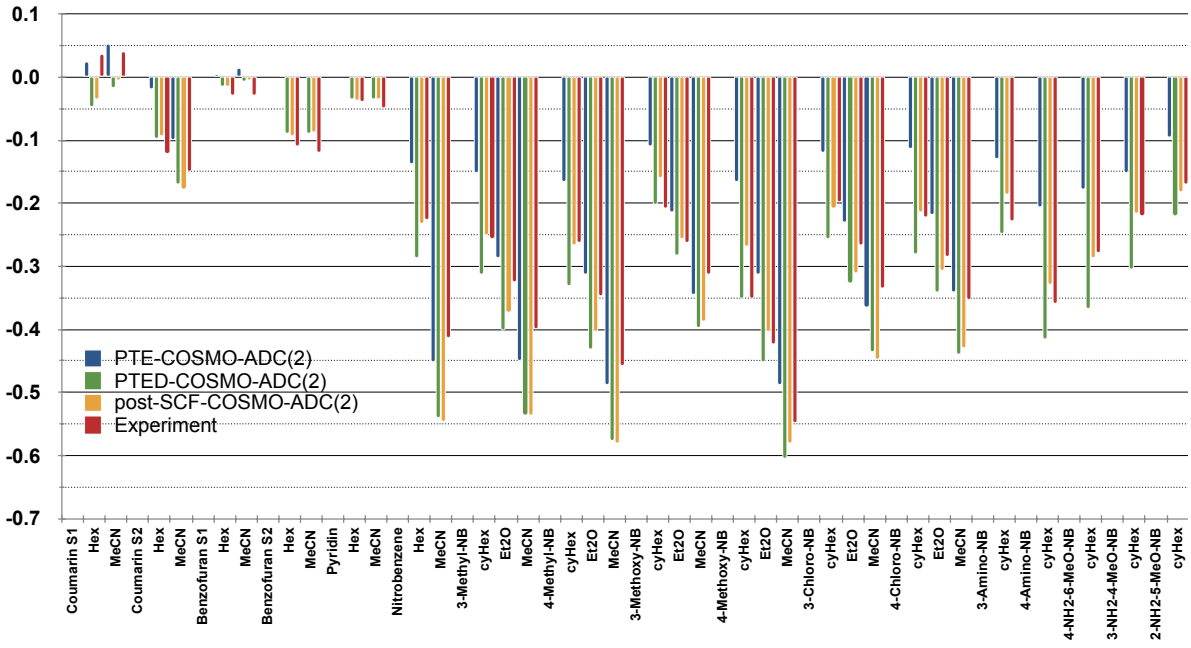


Figure 1: The experimental and computational solvent shifts at the COSMO-ADC(2)/def2-TZVP level within the PTE, PTED and post-SCF reaction field schemes. From left side the name of the molecule follows by solvents.

A statistical analysis of the error for the calculated solvatochromic shifts investigated by the COSMO-ADC(2)(PTE, PTED and post-SCF) and COSMO-RI-CC2(post-SCF) methods are given in Fig. 2. At the COSMO-ADC(2) level, the most accurate RF scheme is clearly post-SCF, while the mean absolute error (MAE) for all three schemes are bellow 110 meV. From the less accurate PTE approach to PTED, the accuracy of the computed shifts

improved in particular for molecules in Hex, cyHex and Et_2O solutions. At the same time, the average deviation in the solvent shifts for these three solvents using the post-SCF scheme is smaller than for PTED with MAE of 23 meV, 23 meV and 33 meV for Hex, cyHex and Et_2O.

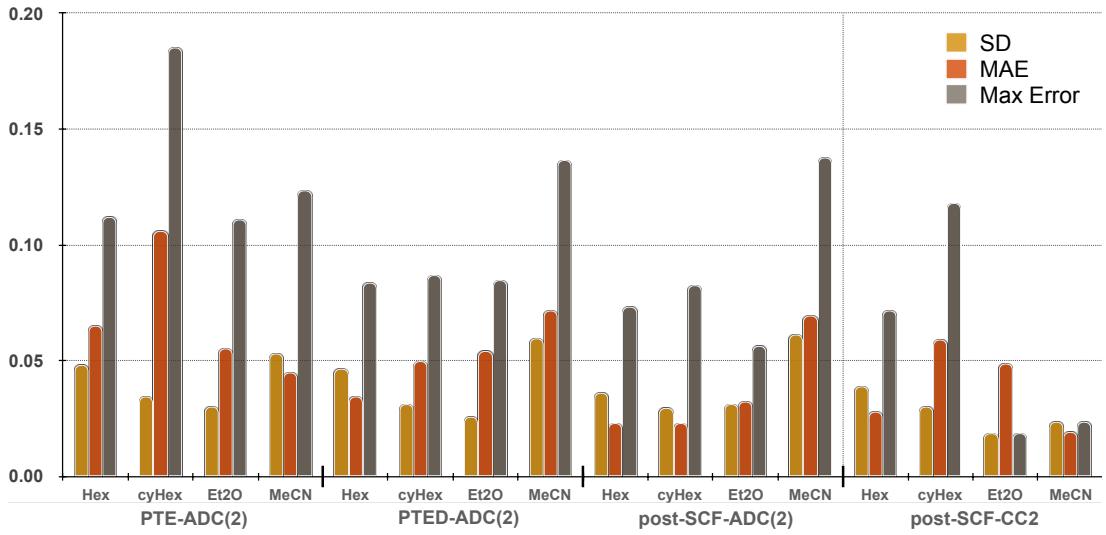


Figure 2: Statistical errors for the difference between calculated and experimental solvatochromic shifts at COSMO-ADC(2)/def2-TZVP level within PTE, PTED and post-SCF reaction field schemes and COSMO-CC2/def2-TZVP(post-SCF) level.

Probably due to error compensation, for molecules in MeCN solution, the shifts with PTE scheme show a better accuracy (MAE = 45 meV and Max Error = 123 meV) compared with the more advanced PTED and post-SCF schemes. It should be noted that for this polar solvent both post-SCF and PTED produce similar accuracy with MAE of 70 meV and 72 meV and Max Error of 138 meV and 137 meV, respectively. Interestingly, within the post-SCF framework, COSMO-RI-CC2 method predicts more accurate solvent shifts for molecules in MeCN solvent.

Generally, for the calculations at the COSMO-ADC(2) level, PTE scheme is not a preferable approach due to the lack of the coupling between the RF and the transition density. However, from the PTED and post-SCF approaches which include the coupling between solvation and electron correlation, post-SCF scheme produce more reliable results for energies

of molecules with $\pi\pi^*$ electronic transitions at a lower computational cost.[40]

In the current section, the study was focused on excited states with only $\pi\pi^*$ character and the data set lacks diversity. In this regard, we collected a second data set including more diverse molecular structures having $\pi\pi^*$ and $n\pi^*$ electronic transitions.

Second Data Set

In this section the computed solvent shifts of 12 different molecules as a mixture of $\pi\pi^*$ and $n\pi^*$ states in the solvents water (H_2O), Hex, MeCN and ethanol (EtOH) at the COSMO-ADC(2)/def2-TZVP level using PTE, PTED and post-SCF schemes are discussed and compared to the corresponding experimental values. An inspection of Fig. 3 for $\pi\pi^*$ transitions reveals that the deviation of the computed shifts from the experiment for the post-SCF scheme (mean error ($ME^{\pi\pi^*}$) = 7.8 meV and $MAE^{\pi\pi^*}$ = 46 meV) is almost similar to the PTED ($ME^{\pi\pi^*}$ = 8.4 meV and $MAE^{\pi\pi^*}$ = 46 meV), while the results from the PTE scheme show a significantly larger divergence with the values of $ME^{\pi\pi^*}$ = 91 meV and MAE = 106 meV.

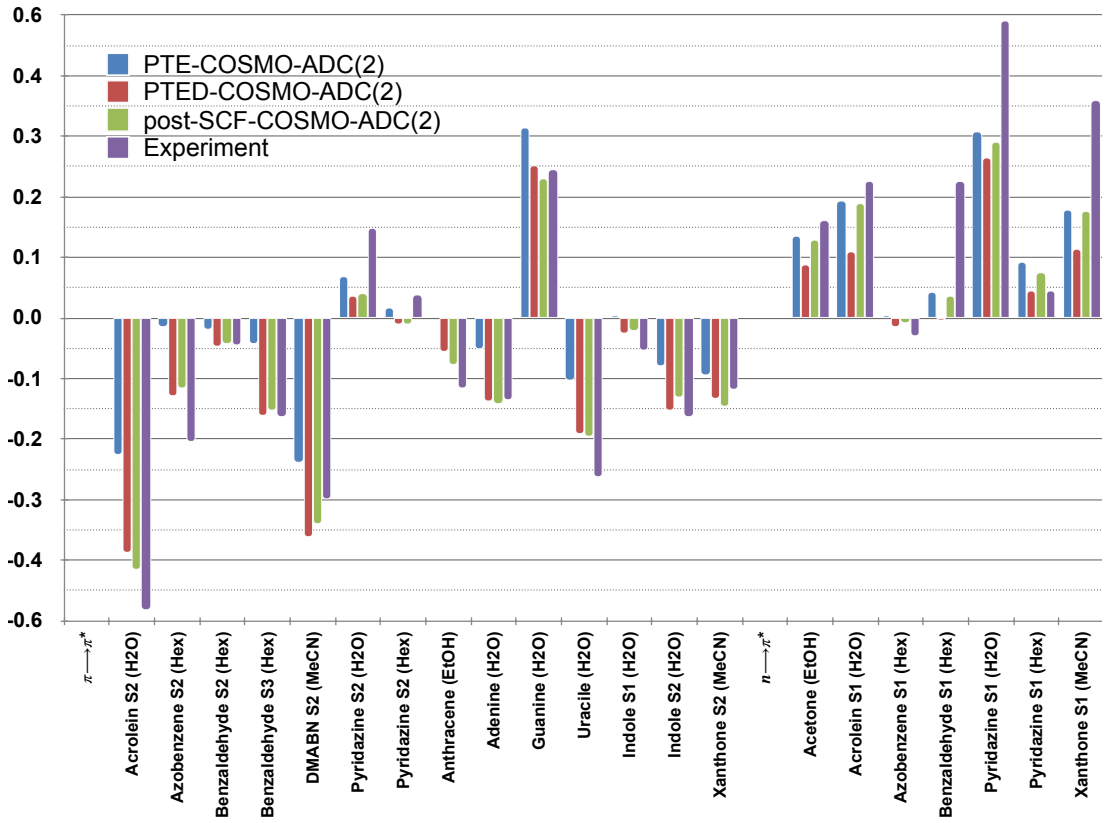


Figure 3: The experimental and computational solvent shifts at the COSMO-ADC(2)/def2-TZVP level within the PTE, PTED and post-SCF reaction field schemes.

The blue solvent shifts observed for $n\pi^*$ transitions in both experiment and theory can be attributed to the specific interaction, *e.g.* hydrogen bridging, of the solvent molecules with electrons in the n orbital of the solute which leads to the stabilization of the ground state with respect to the excited state. Solvent shifts for $n\pi^*$ states predicted by the post-SCF are small with the $\mathrm{ME}^{n\pi^*}$ of -93 meV and $\mathrm{MAE}^{n\pi^*}$ of 109 meV, while the PTED scheme is rather more deviated from the experiment with the $\mathrm{ME}^{n\pi^*} = -138$ meV and $\mathrm{MAE}^{n\pi^*} = 143$ meV. The values of the $\mathrm{ME}^{n\pi^*}$ and $\mathrm{MAE}^{n\pi^*}$ for the PTE scheme for this type of transitions are -82 meV and 109 meV.

For cases with large deviations with respect to the experiment, it is speculated that specific solute-solvent interactions, such as hydrogen bonding, should be included by adding explicit solvent molecules in the QM calculations, although it can significantly increase the

computational cost.

Fig. 4 presents statistical measures for both $\pi\pi^*$ and $n\pi^*$ transitions. Overall, at the COSMO-ADC(2) level, the post-SCF scheme shows a more balanced performance for both $\pi\pi^*$ and $n\pi^*$ transitions with the smallest standard deviation (SD) of 86 meV and MAE of 71 meV comparing to the PTE and PTED and is preferred over both schemes (cmp. Fig. 4). Within the post-SCF scheme, the COSMO-CC2 method shows a slightly less good performance than COSMO-ADC(2). This can be attributed to the underestimation of excitation energies for $n\pi^*$ states at the CC2 level.

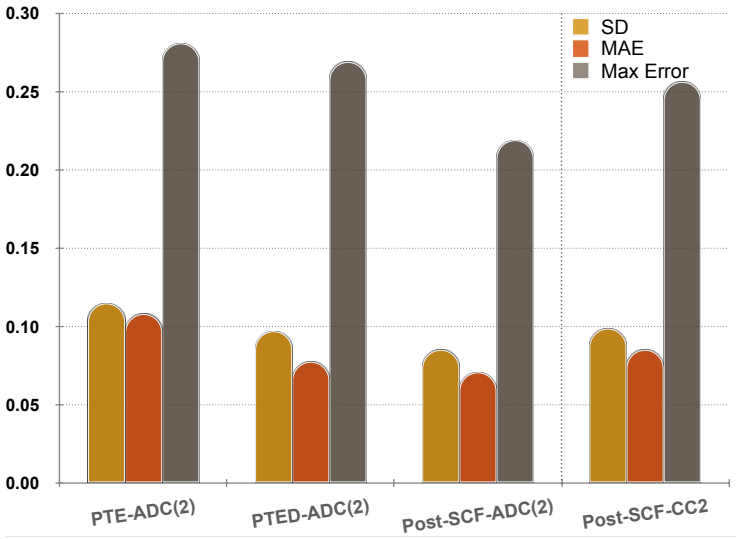


Figure 4: Statistical errors for the difference between calculated and experimental solvatochromic shifts at COSMO-ADC(2)/def2-TZVP level within the PTE, PTED and post-SCF reaction field schemes and COSMO-CC2/def2-TZVP(post-SCF) level.

Conclusion

We have presented the first systematic evaluation of PTE, PTED and post-SCF reaction field schemes for vertical excitation energies at the COSMO-ADC(2) level of theory by comparison to experimental solvent shifts. To this end, we used an experimental benchmark data set composed by Mewes *et al.*[2] for solvatochromism in molecules with $\pi\pi^*$ transitions along with a second data set we composed ourselves which incorporates diverse molecular structures

with $\pi\pi^*$ and $n\pi^*$ transitions. By comparison to the experimental results, we showed that the COSMO-ADC(2) method within the post-SCF scheme provides more accurate solvent shifts than PTED and less computational cost. At the same time, both approaches show a better performance than the PTE scheme. It is also worth mentioning that the post-SCF scheme describes the avoided crossings and conical intersections of the excited states more properly than PTED, because, unlike the latter approach, it does not include perturbative corrections and a self-consistent construction of the reaction field.

Acknowledgement

We acknowledge financial support by the Deutsche Forschungsgemeinschaft through project Ha 2588/8-1 and the Cluster of Excellence RESOLV (EXC 2033).

References

(1) Klamt, A.; Schüürmann, G. COSMO: A new approach to dielectric screening in solvents with explicit expressions. *J. Chem. Soc. Perkin Trans. 2* **1993**, 799–805.

(2) Mewes, J. M.; You, Z. Q.; Wormit, M.; Kriesche, T.; Herbert, J. M.; Dreuw, A. Experimental benchmark data and systematic evaluation of two a posteriori, polarizable-continuum corrections for vertical excitation energies in solution. *J. Phys. Chem. A* **2015**, *119*, 5446–5464.

(3) Caricato, M. CCSD-PCM: Improving upon the reference reaction field approximation at no cost. *J. Chem. Phys.* **2011**, *135*, 074113–1–7.

(4) Khani, S. K.; Khah, A. M.; Hättig, C. COSMO-RI-ADC(2) excitation energies and excited state gradients. *Phys. Chem. Chem. Phys.* **2018**, *20*, 16354–16363.

(5) Schwabe, T.; Sneskov, K.; Olsen, J. M. H.; Kongsted, J.; Christiansen, O.; Hättig, C.

PERI-CC2: A polarizable embedded RI-CC2 method. *J. Chem. Theory Comput.* **2012**, *8*, 3274–3283.

(6) Head-Gordon, M.; Pople, J. A.; Frisch, M. J. MP2 energy evaluation by direct methods. *Chem. Phys. Lett.* **1988**, *153*, 503–506.

(7) Hättig, C. Structure optimization for excited states with correlated second-order methods: CC2, CIS(D_∞) and ADC(2). *Adv. Quant. Chem.* **2005**, *50*, 37–60.

(8) Valle, F. J. O. D.; Tomasi, J. Electron correlation and solvation effects. I. Basic formulation and preliminary attempt to include the electron correlation in the quantum mechanical polarizable continuum model so as to study solvation phenomena. *Chem. Phys.* **1991**, *150*, 139–150.

(9) Lunkenheimer, B.; Köhn, A. Solvent effects on electronically excited states using the conductor-like screening model and the second-order correlated method ADC(2). *J. Chem. Theory Comput.* **2013**, *9*, 977–994.

(10) Mennucci, B.; Cammi, R.; Tomasi, J. Excited states and solvatochromic shifts within a nonequilibrium solvation approach: A new formulation of the integral equation formalism method at the self-consistent field, configuration interaction, and multiconfiguration self-consistent field level. *J. Chem. Phys.* **1998**, *109*, 2798–2807.

(11) Mikkelsen, K. V.; Jørgensen, P.; Jensen, H. J. A. A multiconfiguration self-consistent reaction field response method. *J. Chem. Phys.* **1994**, *100*, 6597–6607.

(12) Khani, S. K.; Faber, R.; Santoro, F.; Coriani, S.; Hättig, C. UV Absorption and Magnetic Circular Dichroism Spectra of Purine, Adenine, and Guanine: A Coupled Cluster Study in Vacuo and in Aqueous Solution. *J. Chem. Theory Comput.* **2019**, *15*, 1242–1254.

(13) Millefiori, S.; Zuccarello, F.; Buemi, G. Excited state dipole moments of nitrobenzene derivatives. *J. Chem. Soc. Perkin Trans. 2* **1978**, 849–852.

(14) Buemi, G.; Millefiori, S.; Zuccarello, F.; Millefiori, A. Excited state properties of nitrobenzene derivatives. *Can. J. Chem.* **1979**, *57*, 2167–2171.

(15) Moskvin, A. F.; Yablonskii, O. P.; Bondar, L. F. An experimental investigation of the effect of alkyl substituents on the position of the K and R absorption bands in acrolein derivatives. *Theor. Exp. Chem.* **1966**, *2*, 636–640.

(16) Aidas, K.; M, A.; Nilsson, E. J. K.; Johson, M. S.; Mikkelsen, K. V.; Söderhjelm, O. C. P.; Kongsted, J. On the performance of quantum chemical methods to predict solvatochromic effects: The case of acrolein in aqueous solution. *J. Chem. Phys.* **2008**, *128*, 194503.

(17) Andersson, J.; Petterson, R.; Tegner, L. Flash photolysis experiments in the vapour phase at elevated temperatures I: Spectra of azobenzene and the kinetics of its thermal cis-trans isomerization. *J. Photochemistry* **1982**, *20*, 17–32.

(18) Lednev, I.; Ye, T.; Matousek, P.; Towrie, M.; Foggi, P.; Neuwahl, F.; Umapathy, S.; Hester, R.; Moore, J. Femtosecond time-resolved UV-visible absorption spectroscopy of trans-azobenzene: dependence on excitation wavelength. *Chem. Phys. Lett.* **1998**, *290*, 68–74.

(19) Abe, H.; Kamei, S.; Mikami, N.; Ito, M. Sensitized phosphorescence excitation spectra of biacetyl, benzaldehyde and benzophenone in supersonic jets. *Chem. Phys. Lett.* **1984**, *109*, 217–220.

(20) Jacquemin, D.; Wathelet, V.; Perpete, E. A.; Adamo, C. Extensive TD-DFT Benchmark: Singlet-Excited States of Organic Molecules. *J. Chem. Theory Comput.* **2009**, *5*, 2420–2435.

(21) Georgieva, I.; Aquino, A. J. A.; Plasser, F.; Trendafilova, N.; Köhn, A.; Lischka, H. Intramolecular charge-transfer excited-state processes in 4(N,NDimethylamino)benzonitrile: The role of twisting and the $\pi\sigma^*$ state. *J. Phys. Chem. A* **2015**, *119*, 6232–6243.

(22) Parkin, J. E.; Innes, K. K. The vacuum ultraviolet spectra of pyrazine, pyrimidine and pyridazine vapors. *J. Mol. Spectrosc.* **1965**, *15*, 407–434.

(23) Halverson, F.; c. Hirt, R. The near ultraviolet absorption spectra of the diazines. *J. Chem. Phys.* **1949**, *17*, 1165–1166.

(24) Lambert, W. R.; Felker, P. M.; Syage, J. A.; Zewail, A. H. Jet spectroscopy of anthracene and deuterated anthracenes. *J. Chem. Phys.* **1984**, *81*, 2197–2208.

(25) Jones, R. N. The ultraviolet absorption spectra of anthracene derivatives. **1947**, 353–371.

(26) Li, L.; Lubman, D. M. Ultraviolet-visible absorption spectra of biological molecules in the gas phase using pulsed laser-induced volatilization enhancement in a diode array spectrophotometer. *Anal. Chem.* **1987**, *15*, 2538–2541.

(27) Barbatti, M.; Aquino, A. J. A.; Lischka, H. The UV absorption of nucleobases: semi-classical ab initio spectra simulations. *Phys. Chem. Chem. Phys.* **2010**, *12*, 4959–4967.

(28) Clark, L. B.; Peschel, G. G.; Tinoco, I. Vapor spectra and heats of vaporization of some purine and pyrimidine bases. *J. Phys. Chem.* **1965**, *69*, 3615–3618.

(29) Middleton, C. T.; de La Harpe, K.; Su, C.; Law, Y. K.; Crespo-Hernández, C. E.; Kohler, B. DNA excited-state dynamics: From single bases to the double Helix. *Annu. Rev. Phys. Chem.* **2009**, *60*, 217–239.

(30) Hollas, J. M. Vapour-phase ultra-violet absorption spectra of indene, indole, coumarone and thionaphthene. *Spectrochim. Acta* **1963**, *19*, 753–767.

(31) Parac, M.; Grimme, S. Comparison of multireference Møller-Plesset Theory and Time-Dependent methods for the calculation of vertical excitation energies of molecules. *J. Phys. Chem. A* **2002**, *106*, 6844–6850.

(32) Eftink, R. M. *Fluorescence techniques for studying protein structure. In Methods of Biochemical Analysis; Suelter, C. H*; John Wiley & Sons: New York, 1991, Vol. 35.

(33) Lalevee, J.; Blanchard, N.; Tehfe, M. A.; Fries, C.; Morlet-Savary, F.; Gigmesc, D.; Fouassier, J. P. New thioxanthone and xanthone photoinitiators based on silyl radical chemistry. *Polym. Chem.* **2011**, *2*, 1077–1084.

(34) Walzl, K. N.; Koerting, C. F.; Kuppermann, A. Higher excited states of polyatomic molecules. *J. Chem. Phys.* **1987**, *87*, 3796–3803.

(35) Bayliss, N. S.; McRae, E. G. Solvent effects in the spectra of acetone, crotonaldehyde, nitromethane and nitrobenzene. *J. Phys. Chem.* **1954**, *58*, 1006–1011.

(36) Weigend, F.; Ahlrichs, R. Balanced basis sets of split valence, triple zeta valence and quadruple zeta valence quality for H to Rn: Design and assessment of accuracy. *Phys. Chem. Chem. Phys* **2005**, *7*, 3297–3305.

(37) TURBOMOLE V7.3 2018, a development of University of Karlsruhe and Forschungszentrum Karlsruhe GmbH, 1989-2007, TURBOMOLE GmbH, since 2007; available from
`http://www.turbomole.com`.

(38) Hellweg, A.; Hättig, C.; Höfener, S.; Klopper, W. Optimized accurate auxiliary basis sets for RI-MP2 and RI-CC2 calculations for the atoms Rb to Rn. *Theor. Chem. Acc.* **2007**, *117*, 587–597.

(39) Furche, F.; Ahlrichs, R.; Hättig, C.; Klopper, W.; Sierka, M.; Weigend, F. *WIREs Comput. Mol. Sci.* **2014**, *4*, 91–100.

(40) Ángyán, J. G. Choosing between alternative MP2 algorithms in the self-consistent reaction field theory of solvent effects. *Chem. Phys. Lett* **1995**, *241*, 51–56.

6 Outlook

In this dissertation[6], I have presented a new implementation of the COSMO-RI-ADC(2) method, and for the first time, an implementation of COSMO-RI-CC2 for the calculation of molecular vertical excitation energies in solution using the post-SCF reaction field scheme. The most important methodological development of the thesis has, however, been the first implementation of excited state analytic gradients at the COSMO-RI-ADC(2)(post-SCF) level, which for the first time allows to study electronic deexcitation mechanisms and fluorescence emission energies of organic molecules with a continuum solvation model beyond the TDDFT. To further improve the applicability of the COSMO-RI-ADC(2) method, particularly for excited states with charge transfer character which come with a significant change of the electron density relative to the ground state, the relaxation of the reaction field with respect to the excited state density of the solute can be added as perturbative state-specific correction not only to the energy but also to the gradient. It needs, however, to be tested in which situations this correction improves the potential energy surface and in which situations the perturbative correction causes sever artefacts, as *e.g.* additional maxima and minima.

Although continuum models have been originally developed to describe the electrostatic interactions between solute and solvent, there are systems for which the non-electrostatic solute-solvent interactions are required to be considered. For instance, during our studies on the excited state properties of the halogen-bonded complexes in solution we figured out that

[6]This chapter shares the references with chapter 1.

neglecting the contribution of dispersion interaction between the solute and the continuum environment in the total ground state energy and, at the same time, considering the intermolecular dispersion interaction between the QM molecules resulted in an unbalanced description of the relative stability of the more compact anion-π conformer and the halogen-bonded one in favor of the anion-π structure (cmp. Chapter 4). However, to achieve a more consistent evaluation of the relative stability of these conformers, in addition to the dispersion interaction between the QM molecules, the dispersion interaction between the QM system and the continuum environment should be included in the total energy. In doing so, the COSMO model needs to be extended to treat also non-electrostatic effects. This modification has already been done for the PCM model. [16]

With respect to the subjects discussed in chapter 5, the comparison of the performance of PTE, PTED and post-SCF reaction field schemes for the calculation of solvatochromic shifts can be further developed, in particular for $n\pi^*$ states, by taking the specific solute-solvent interactions into account via adding some explicit solvent molecules to the QM system. This procedure may improve the computed solvent shifts specially for cases which show a significant deviation from the experiment.

Appendices

Electronic Supplementary Material (ESI) for Physical Chemistry Chemical Physics.
This journal is © the Owner Societies 2018

Supporting Information: COSMO-RI-ADC(2) Excitation Energies And Excited State Gradients†

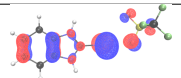
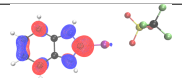
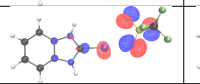
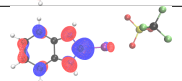
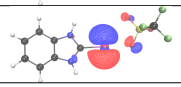
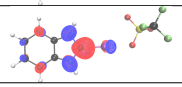
Sarah Karbalaei Khani,*[a] Alireza Marefat Khah,[a‡] and Christof Hättig[a‡]

[a]Arbeitsgruppe Quantenchemie, Ruhr-Universität, Bochum 44780, Germany.

* Corresponding author: E-mail: Sarah.KarbalaeiKhani@rub.de

1 Natural Transition Orbitals

Table 1: Vertical excitation energies (VEE), transition moments (OS), dipole moments (μ) and NTOs of 2-Iodobenzimidazolium.otf complex calculated in vacuum at ADC(2)/def2-TZVPP level of theory (The isosurface chosen to visualize is 0.05).

EEL	VEE	OS	μ	OCC	VIR	Contrib.
1	4.55	0.41	12.59			91.54%
2	4.67	0.08	1.08			96.89%
3	5.15	0.00	10.23			99.76%

2 Cartesian coordinates of the studied molecules

- **DMABN** MP2/def2-TZVPP optimized geometry of the ground state in vacuum:
  C -0.8614494 -1.9266209 0.7585447
  C 0.0756059 -2.5988760 -0.0317852
  C 0.9323351 -1.8547817 -0.8484680
  C 0.8502980 -0.4711480 -0.8779105
  C -0.1011966 0.2231015 -0.1029742
  C -0.9432094 -0.5429704 0.7288794
  H -1.5215945 -2.4905026 1.4031153
  H 1.6691444 -2.3627162 -1.4553781
  H 1.5342083 0.0677134 -1.5146653
  H -1.6737161 -0.0607953 1.3592987
  N -0.2121943 1.5966106 -0.1655166
  C 0.1627977 -4.0239660 0.0018321
  N 0.2342548 -5.1945397 0.0292641
  C -0.9636589 2.2692168 0.8748552
  H -0.5504525 2.0921931 1.8741168
  H -0.9511072 3.3368334 0.6766942
  H -2.0027079 1.9455420 0.8690906
  C 0.8728198 2.3427348 -0.7700960
  H 0.9942642 2.0657372 -1.8155376
  H 0.6274084 3.4000412 -0.7368242
  H 1.8281503 2.1871926 -0.2565355

- **DMABN** COSMO-MP2/def2-TZVPP optimized geometry of the ground state in acetonitrile solution:
  C -0.6707951 -0.8134369 0.7798387
  C 0.2661211 -1.4824523 -0.0170481
  C 1.1295705 -0.7413339 -0.8329054
  C 1.0539517 0.6422266 -0.8538808
  C 0.1020854 1.3382622 -0.0740591
  C -0.7448580 0.5701873 0.7574283
  H -1.3344092 -1.3756681 1.4232028
  H 1.8655386 -1.2475170 -1.4432617
  H 1.7407564 1.1815051 -1.4876921
  H -1.4728464 1.0527896 1.3909534

N -0.0014627 2.7028673 -0.1286447
C 0.3466662 -2.9055808 0.0092139
N 0.4127013 -4.0764341 0.0305139
C -0.7766460 3.3842812 0.8939528
H -0.3706925 3.2207313 1.8970631
H -0.7660672 4.4483983 0.6806468
H -1.8118949 3.0496393 0.8795863
C 1.0679927 3.4581649 -0.7585265
H 1.1808318 3.1696771 -1.8015872
H 0.8078754 4.5114692 -0.7290566
H 2.0274068 3.3166378 -0.2513178

- **DMABN** COSMO-ADC(2)/def2-TZVPP optimized geometry of the ICT state in non-equilibrium solution limit (acetonitrile):
C -0.1898504 -0.8001372 1.1529399
C 0.1436617 -1.4585007 -0.0851161
C 0.6267677 -0.6712921 -1.1734917
C 0.8434708 0.6791602 -1.0265310
C 0.6229528 1.3125293 0.2537931
C -0.0028468 0.5480552 1.2961759
H -0.5927830 -1.3847658 1.9707602
H 0.8563837 -1.1525640 -2.1169409
H 1.1985544 1.2707657 -1.8622357
H -0.2750925 1.0417840 2.2224480
N 0.2808921 2.6886716 0.1406608
C -0.0473507 -2.8373214 -0.2333872
N -0.2067448 -4.0062563 -0.3546624
C -1.1050865 3.1424278 0.1347440
H -1.1899714 4.0003519 0.7975361
H -1.3578425 3.4441128 -0.8830255
H -1.7387172 2.3219865 0.4561855
C 1.3438523 3.6551116 -0.0541287
H 2.0096594 3.2816935 -0.8306384
H 0.9291396 4.6207680 -0.3215367
H 1.9027773 3.7078333 0.8808708

- **DMABN** COSMO-ADC(2)/def2-TZVPP optimized geometry of the ICT state in equilibrium solution limit (acetonitrile):
C -0.2533603 -0.8080496 1.1187412
C 0.1436584 -1.4573983 -0.1093495
C 0.7027775 -0.6690960 -1.1574789
C 0.9270848 0.6771855 -0.9835970
C 0.6128657 1.3102230 0.2803138
C -0.0675760 0.5369787 1.2811454
H -0.6975656 -1.4003686 1.9085980
H 0.9875049 -1.1471790 -2.0870716
H 1.3421947 1.2663942 -1.7918993
H -0.3801353 1.0195615 2.2002274
N 0.2738454 2.6821757 0.1397024
C -0.0535476 -2.8313484 -0.2825931
N -0.2195436 -3.9976850 -0.4244692
C -1.0932336 3.1647158 0.2639118
H -1.0945859 4.0571393 0.8855575
H -1.4570955 3.4190266 -0.7337029
H -1.7061971 2.3788871 0.6937174
C 1.3223647 3.6342528 -0.1680536
H 2.0581003 3.1577962 -0.8107927
H 0.8996664 4.5172161 -0.6355860
H 1.8046039 3.8939864 0.7770989

- **2-Iodobenzimidazolium** · **OTF** MP2/def2-TZVPP optimized geometry of the ground state in vacuum:
S 4.9201145 1.1182332 0.1209306
O 6.1465768 1.6225221 0.6695918
O 4.5123334 -0.2290496 0.4525769
O 3.7910406 2.0877204 0.1847409
C 5.2149435 1.0480287 -1.6925832
F 4.1010525 0.6553112 -2.3345727
F 5.5636269 2.2403289 -2.1783619
F 6.1825274 0.1784169 -1.9861722
N -0.6671093 -0.9118184 0.4185568
N -1.5228679 1.0644022 0.3192845
C -2.0376874 -1.0941013 0.4473133

C -2.5954836 0.1923779 0.3827111
C -2.8332124 -2.2355639 0.5219549
C -3.9738116 0.3956716 0.3898848
C -4.2056839 -2.0319474 0.5290365
C -0.3555174 0.3948395 0.3409758
C -4.7649979 -0.7418393 0.4642565
H 0.0424144 -1.6299892 0.4488826
H -2.4048248 -3.2261810 0.5716012
H -4.4046154 1.3852594 0.3401027
I 1.5604660 1.1686525 0.2685158
H -4.8640891 -2.8867536 0.5857357
H -5.8401731 -0.6352754 0.4726743
H -1.5650220 2.0707547 0.2623632

- **2-Iodobenzimidazolium** · **OTF** COSMO-MP2/def2-TZVPP optimized geometry of the ground state in aqueous solution:

S 5.0878680 1.6044945 0.0472828
O 6.2448479 2.4456389 0.2821679
O 4.8947847 0.5174363 0.9872068
O 3.8687100 2.3312745 -0.2999819
C 5.4984233 0.7404988 -1.5202462
F 4.5047981 -0.0755555 -1.8884640
F 5.7021756 1.6144132 -2.5110511
F 6.6067386 0.0053679 -1.3841091
N -0.8270236 -0.9475282 0.0002959
N -1.6036133 1.0089523 0.5215236
C -2.1807936 -1.1159243 0.2048593
C -2.6837758 0.1512721 0.5424311
C -3.0032411 -2.2396974 0.1276206
C -4.0347232 0.3592206 0.8197318
C -4.3462210 -2.0319877 0.4034017
C -0.4945335 0.3346512 0.1938775
C -4.8516349 -0.7585727 0.7425557
H -0.1658203 -1.6684237 -0.2578275
H -2.6126658 -3.2128660 -0.1320416
H -4.4177909 1.3355805 1.0785509

I 1.3709904 1.1235692 0.0166583
H -5.0276927 -2.8697657 0.3578141
H -5.9075625 -0.6528995 0.9480235
H -1.6222443 2.0008509 0.7197199

- **2-Iodobenzimidazolium** · **OTF** COSMO-ADC(2)/def2-TZVPP optimized geometry of the first excited state in aqueous solution:

S 2.7575975 1.5520718 0.4125927
O 3.0323106 1.7874511 1.8099013
O 1.4519414 2.1537239 0.0039281
O 3.8231717 1.7558164 -0.5365386
C 2.4022949 -0.2500063 0.3235939
F 2.0687415 -0.6020079 -0.9200078
F 3.4814032 -0.9480823 0.6813310
F 1.4004512 -0.5745863 1.1381920
N -0.7138502 -0.0210757 -2.0006968
N -1.3597924 1.5499567 -0.6520714
C -1.1164795 -0.6548884 -0.8437565
C -1.5269130 0.3679268 0.0360415
C -1.1625071 -1.9987595 -0.4788100
C -1.9911765 0.0883842 1.3200131
C -1.6140334 -2.2733878 0.8060676
C -0.8865104 1.3170770 -1.8986515
C -2.0174873 -1.2510299 1.6881584
H -0.3482365 -0.4728629 -2.8275412
H -0.8528264 -2.7833851 -1.1547257
H -2.3040997 0.8728904 1.9947169
I 1.0145825 2.7259226 -2.4359985
H -1.6564455 -3.3010706 1.1401670
H -2.3596309 -1.5176754 2.6787913
H -1.5225056 2.4775972 -0.2846968

Supporting information for: UV Absorption and Magnetic Circular Dichroism Spectra of Purine, Adenine, and Guanine: a Coupled Cluster Study in Vacuo and in Aqueous Solution

Sarah Karbalaei Khani,* Rasmus Faber, Fabrizio Santoro, Sonia Coriani,* and Christof Hättig*

Arbeitsgruppe Quantenchemie, Ruhr-Universität, Bochum 44780, Germany

E-mail: Sarah.Karbalaeikhani@rub.de; soco@kemi.dtu.dk; Christof.Haettig@rub.de

*To whom correspondence should be addressed

Table S1: Purine. Vertical excitation energies ω_j (eV), oscillator strengths f (adim), Faraday $\mathcal{B}$ terms (a.u.) obtained in vacuo and in solution by using COSMO solvent model at the indicated level of theory. ($\varepsilon = 80.4$ and $n^2 = 1.78$)

State	ω_j	$f(0 \to j)$	$\mathcal{B}(0 \to j)$
CC2/aug-cc-pVDZ (B3LYP geometry)			
1	4.43	0.003	−0.933
2	5.24	0.096	−17.120
3	5.48	0.002	−0.250
4	5.66	0.000	0.309
5	5.69	0.057	35.680
6	5.96	0.013	1.290
7	6.31	0.001	0.724
CCSD/aug-cc-pVDZ (B3LYP geometry)			
1	4.73	0.003	−1.192
2	5.25	0.084	−8.055
3	5.70	0.002	−0.006
4	5.89	0.059	21.750
5	6.01	0.000	0.003
6	6.45	0.001	0.669
7	6.67	0.017	−0.207
CCSD/aug-cc-pVDZ (MP2 geometry)			
1	4.73	0.0030	−1.312
2	5.20	0.0900	−6.958
3	5.73	0.0021	0.291
4	5.85	0.0604	19.580
5	6.02	0.0001	−0.005
6	6.36	0.0010	0.661
7	6.69	0.0208	−0.367
8	6.84	0.0073	0.934
9	6.91	0.0021	6.421
RI-CC2/aug-cc-pVTZ (MP2 geometry)			
1	4.39	0.003	−0.93
2	5.14	0.102	−12.90
3	5.44	0.002	−0.13
4	5.63	0.000	3.09
5	5.63	0.052	27.05
COSMO-RI-CC2/aug-cc-pVTZ (COSMO-MP2 geometry)			
1	4.58	0.004	−2.23
2	5.01	0.228	−24.04
3	5.45	0.057	69.28
4	5.61	0.002	−0.52
5	5.79	0.000	0.11

Table S2: Adenine. Vertical excitation energies ω_j (eV), oscillator strengths f (adim), Faraday $\mathcal{B}$ terms (a.u.) calculated in vacuo and in solution by using COSMO solvent model at the indicated level of theory. $\varepsilon = 80.4$ and $n^2 = 1.78$.

COSMO-RI-CC2/aug-cc-pVDZ (MP2 geometry)			
state	ω_j	$f(0 \to j)$	$\mathcal{B}(0 \to j)$
1	5.04	0.468	79.09
2	5.27	0.017	−76.71
3	5.40	0.006	−3.45
4	5.55	0.011	−0.91
5	5.99	0.025	1.03
RI-CC2/aug-cc-pVDZ (COSMO-MP2 geometry)			
1	5.11	0.010	0.74
2	5.25	0.204	175.59
3	5.29	0.069	−168.27
4	5.39	0.020	−4.78
5	5.71	0.006	−0.46
COSMO-RI-CC2/aug-cc-pVDZ (COSMO-MP2 geometry)			
1	5.02	0.465	75.78
2	5.26	0.021	−73.58
3	5.37	0.006	−4.02
4	5.54	0.011	−0.90
5	5.96	0.017	0.23
RI-CC2/aug-cc-pVTZ (MP2 geometry)			
1	5.10	0.009	0.78
2	5.24	0.155	313.14
3	5.27	0.126	−310.06
4	5.56	0.011	−0.746
5	5.73	0.003	−0.706
COSMO-RI-CC2/aug-cc-pVTZ (COSMO-MP2 geometry)			
1	4.99	0.452	77.13
2	5.23	0.026	−75.7
3	5.32	0.007	−4.55
4	5.68	0.010	0.71
5	5.89	0.011	−0.11

Table S3: Adenine: Vertical excitation energies ω_j (eV), oscillator strengths f (adim), Faraday $\mathcal{B}$ terms (a.u.) and NTOs at the CCSD/aug-cc-pVDZ level of theory using the RI-MP2/cc-pVTZ geometry. NTO Isosurface is 0.05, except for the two last virtual NTOs.

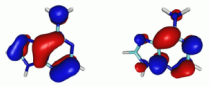
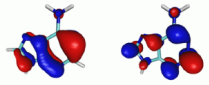
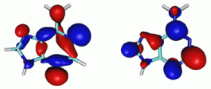
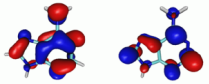
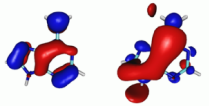
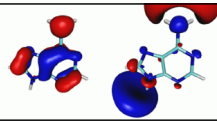
ω_j	$f(0\to j)$	$\mathcal{B}(0\to j)$	NTO pair	NTO e.v.
5.34	0.030	24.48		0.50
				0.27
5.46	0.064	-3.12		0.75
5.55	0.174	-13.35		0.71
5.61	0.023	-5.52		0.82
5.95	0.005	-0.35		0.80

Table S4: Adenine: Vertical excitation energies ω_f (eV), oscillator strengths f (adim), Faraday $\mathcal{B}$ terms (a.u.) and NTOs at the CCSD/aug-cc-pVDZ level of theory using the planar B3LYP geometry. NTO Isosurface is 0.05, except for the two last virtual NTOs.

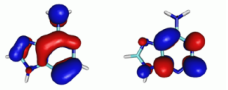
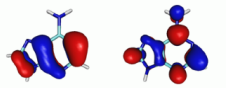
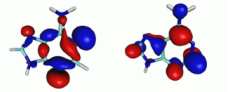
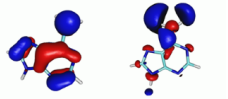
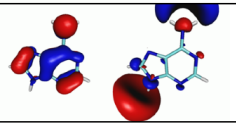
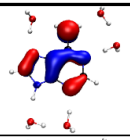
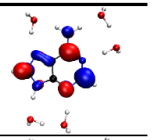
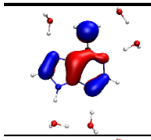
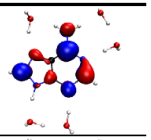
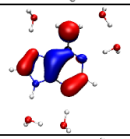
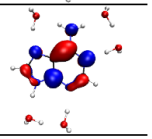
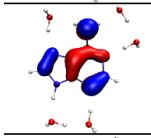
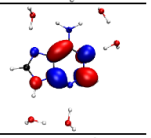
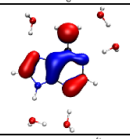
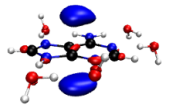
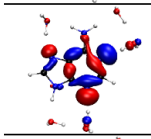
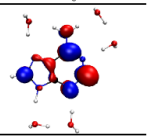
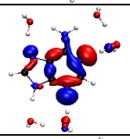
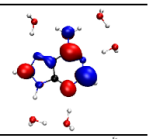
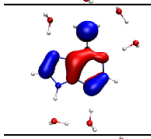
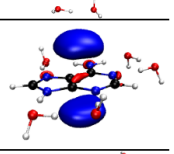
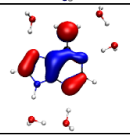
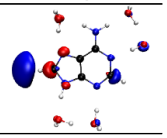
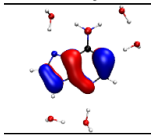
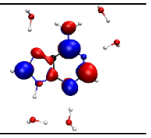
ω_j	$f(0\to j)$	$B(0\to j)$	NTO pair	NTO e.v.
5.36	0.008	40.72		0.50
				0.27
5.49	0.280	-11.95		0.73
5.50	0.002	-11.68		0.78
5.54	0.009	-16.31		0.82
5.89	0.001	-0.41		0.80

Table S5: Adenine: Natural transition orbitals (NTOs) for vertical singlet excitation energies of adenine including 5 H_2O molecules in vacuum and in aqueous solution modeled by COSMO solvent model at the corresponding ground-state optimized geometries.(ε = 80.4 and n^2 = 1.78).

	Adenine+5H_2O (Vacuo)		Adenine+5H_2O (COSMO)	
	occ	vir	occ	vir
state 1				
state 2				
state 3				
state 4				
state 5				

Sum-Over-State expression of the $\mathcal{B}$ term

In order to express the MCD Faraday $\mathcal{B}$ term approximately as a sum over states with products of one-photon transition moments in a way that accounts for the non-hermitian structure of coupled cluster theory, we started with defining the $\mathcal{B}$ term as the derivatives of

one-photon transition strengths:

$$B(0 \to j) = \frac{1}{2}\sum_{\alpha\beta\gamma}\epsilon_{\alpha\beta\gamma}\mathcal{I}\Big\{\frac{dS_{0j}^{d_\alpha d_\beta}}{dB_\gamma}\Big\} = \frac{1}{4}\sum_{\alpha\beta\gamma}\epsilon_{\alpha\beta\gamma}\mathcal{I}\Big\{\frac{d\big(S_{0j}^{d_\alpha d_\beta} - S_{0j}^{d_\beta d_\alpha}\big)}{dB_\gamma}\Big\}\,, \tag{1}$$

$$= \frac{1}{2}\mathcal{I}\Big\{\frac{d\big(S_{0j}^{d_x d_y} - S_{0j}^{d_y d_x}\big)}{dB_z} + \frac{d\big(S_{0j}^{d_z d_x} - S_{0j}^{d_x d_z}\big)}{dB_y} + \frac{d\big(S_{0j}^{d_y d_z} - S_{0j}^{d_z d_y}\big)}{dB_x}\Big\}\,, \tag{2}$$

and the transition strengths in CC theory are defined as:

$$S_{0j}^{d_\alpha d_\beta} = \frac{1}{2}\Big\{M_{0\leftarrow j}^{d_\alpha} M_{j\leftarrow 0}^{d_\beta} + (M_{0\leftarrow j}^{d_\beta} M_{j\leftarrow 0}^{d_\alpha})^*\Big\}\,, \tag{3}$$

where $M_{0\leftarrow j}^{d_\alpha}$ and $M_{j\leftarrow 0}^{d_\alpha}$ are, respectively, the left and right transition moments (which for CC are not the complex conjugates of each other). The first derivatives of the transition strengths are:

$$\frac{dS_{0j}^{d_\alpha d_\beta}}{dB_\gamma} = \frac{1}{2}\Big\{\tfrac{dM_{0\leftarrow j}^{d_\alpha}}{dB_\gamma} M_{j\leftarrow 0}^{d_\beta} + M_{0\leftarrow j}^{d_\alpha}\tfrac{dM_{j\leftarrow 0}^{d_\beta}}{dB_\gamma} + (\tfrac{dM_{0\leftarrow j}^{d_\beta}}{dB_\gamma} M_{j\leftarrow 0}^{d_\alpha})^* + (M_{0\leftarrow j}^{d_\beta}\tfrac{dM_{j\leftarrow 0}^{d_\alpha}}{dB_\gamma})^*\Big\}\,. \tag{4}$$

By inserting the sum-over-state formula for the derivative of a wavefunction with respect to the strength of the static magnetic field,

$$|0\rangle = \sum_{k\neq 0}|k\rangle\frac{\langle k|\hat{m}_\gamma|0\rangle}{-\omega_k}, \tag{5}$$

$$|j\rangle = \sum_{k\neq j}|k\rangle\frac{\langle k|\hat{m}_\gamma|j\rangle}{\omega_j - \omega_k}, \tag{6}$$

we arrived for the derivative of the left and right transition moments at the expressions:

$$\tfrac{dM_{0\leftarrow j}^{d_\alpha}}{dB_\gamma} = \frac{d\langle 0|\hat{d}_\alpha|j\rangle}{dB_\gamma} = \sum_{k\neq 0}\frac{M_{0\leftarrow k}^{m_\gamma} M_{k\leftarrow j}^{d_\alpha}}{-\omega_k} + \sum_{k\neq j}\frac{M_{0\leftarrow k}^{d_\alpha} M_{k\leftarrow j}^{m_\gamma}}{\omega_j - \omega_k} \tag{7}$$

$$\tfrac{dM_{j\leftarrow 0}^{d_\alpha}}{dB_\gamma} = \frac{d\langle j|\hat{d}_\alpha|0\rangle}{dB_\gamma} = \sum_{k\neq 0}\frac{M_{j\leftarrow k}^{d_\alpha} M_{k\leftarrow 0}^{m_\gamma}}{-\omega_k} + \sum_{k\neq j}\frac{M_{j\leftarrow k}^{m_\gamma} M_{k\leftarrow 0}^{d_\alpha}}{\omega_j - \omega_k} \tag{8}$$

where $d_\alpha^{(j)}$ is the expectation value for the electric dipole moment for state j.

For a non-hermitian (CC) parameterization we need to include both terms in eq. 3:

$$\frac{d\big(S_{0j}^{d_\alpha d_\beta} - S_{0j}^{d_\beta d_\alpha}\big)}{dB_\gamma} = \frac{1}{2}\Big\{\tfrac{dM_{0\leftarrow j}^{d_\alpha}}{dB_\gamma} M_{j\leftarrow 0}^{d_\beta} + M_{0\leftarrow j}^{d_\alpha}\tfrac{dM_{j\leftarrow 0}^{d_\beta}}{dB_\gamma} - \tfrac{dM_{0\leftarrow j}^{d_\beta}}{dB_\gamma} M_{j\leftarrow 0}^{d_\alpha} - M_{0\leftarrow j}^{d_\beta}\tfrac{dM_{j\leftarrow 0}^{d_\alpha}}{dB_\gamma} \tag{9}$$
$$+ \big(\tfrac{dM_{0\leftarrow j}^{d_\beta}}{dB_\gamma} M_{j\leftarrow 0}^{d_\alpha}\big)^* + \big(M_{0\leftarrow j}^{d_\beta}\tfrac{dM_{j\leftarrow 0}^{d_\alpha}}{dB_\gamma}\big)^* - \big(\tfrac{dM_{0\leftarrow j}^{d_\alpha}}{dB_\gamma} M_{j\leftarrow 0}^{d_\beta}\big)^* - \big(M_{0\leftarrow j}^{d_\alpha}\tfrac{dM_{j\leftarrow 0}^{d_\beta}}{dB_\gamma}\big)^*\Big\}\,.$$

Since the wavefunctions and the electric dipole operator are real and the magnetic dipole operator is purely imaginary, the complex conjugation (only) inverts the sign of the last four terms and leads to:

$$\frac{d\big(S_{0j}^{d_\alpha d_\beta} - S_{0j}^{d_\beta d_\alpha}\big)}{dB_\gamma} = \tfrac{dM_{0\leftarrow j}^{d_\alpha}}{dB_\gamma} M_{j\leftarrow 0}^{d_\beta} + M_{0\leftarrow j}^{d_\alpha}\tfrac{dM_{j\leftarrow 0}^{d_\beta}}{dB_\gamma} - \tfrac{dM_{0\leftarrow j}^{d_\beta}}{dB_\gamma} M_{j\leftarrow 0}^{d_\alpha} - M_{0\leftarrow j}^{d_\beta}\tfrac{dM_{j\leftarrow 0}^{d_\alpha}}{dB_\gamma}\,. \tag{10}$$

To evaluate the SOS expression with transition moments computed with CC2 response theory, we used Eqs. (7), (8), and (10) with the respective left and right transition moments from a CC2 response calculation, carried out with the same basis sets, structure and solvent contributions as the MCD calculation with which it is compared.

Coordinates

```
Purine: PTE-COSMO-MP2/cc-pVTZ
13
N     0.0000370    1.4452239    0.8922467
N     0.0000050    1.1499715   -1.5265454
N     0.0000179   -1.1019670   -1.6144999
N    -0.0000447   -0.6697866    2.0550867
C     0.0000614    0.7257008   -0.2283937
C     0.0000361   -0.6818691   -0.3036003
C     0.0000324   -1.3614603    0.9118197
```

```
C    -0.0000326    0.6786684    1.9872246
C     0.0000119    0.0300450   -2.3025439
H     0.0000888   -2.4428431    0.9719460
H     0.0001164    2.1042166   -1.8563766
H    -0.0001280    1.1997708    2.9349652
H    -0.0002016    0.0973690   -3.3780891
```

Adenine: PTE-COSMO-MP2/cc-pVTZ

```
15
N    -1.2879227    1.4543816   -0.0118765
N     0.0454944   -1.8721592    0.0139474
N     1.9306011   -0.3621440   -0.0300390
N    -2.0740547   -0.6528050   -0.0010290
N     1.7241299    1.9538444   -0.1870793
C    -0.2442729    0.5550526    0.0024255
C    -0.7089233   -0.7630874   -0.0028828
C     1.1494376    0.7270546   -0.0489931
C     1.3453996   -1.5775886    0.0054451
C    -2.3638944    0.6789990   -0.0077067
H     1.1678087    2.7421218    0.1121751
H    -2.7449012   -1.4103421    0.0093312
H     2.0274763   -2.4194731    0.0254678
H     2.6994977    2.0084601    0.0717568
H    -3.3824061    1.0333652   -0.0094326
```

Adenine+5H2O: PTE-COSMO-MP2/cc-pVTZ

```
30
N     2.2533842    0.9846421    0.0213155
N     0.3691517    2.2060711    0.0126523
```



```
N    -1.1335668   -1.1663459   -0.0125047
N     1.2711908   -1.2524398    0.0064366
N    -2.3587681    0.8096090   -0.0165406
C     1.2171971    0.0939846    0.0108305
C     0.0561286    0.8679324    0.0047666
C     1.6992773    2.2233064    0.0224494
C    -1.1812350    0.1838749   -0.0069513
C     0.0566506   -1.7924838   -0.0053589
O    -3.3046788   -2.9163560   -0.0478142
O    -4.8900856   -0.6739476   -0.0789948
O    -1.9625517    3.7492155    0.0360743
O     3.8057416   -2.4541273   -0.0377646
O     4.8560002    0.0647051    0.0058309
H     3.2609697    0.7470693    0.0334129
H     0.0116261   -2.8742702   -0.0110520
H    -3.2282742    0.2807873   -0.0281731
H    -2.3863275    1.8238544   -0.0097274
H     2.3006746    3.1168929    0.0308700
H    -3.3206755   -3.3315202    0.8209541
H    -2.5209680   -2.3174728   -0.0175119
H    -5.3082211   -0.5745021    0.7821997
H    -4.4640428   -1.5539164   -0.0377849
H     2.8761693   -2.1317087   -0.0289747
H     3.9090588   -2.8604353   -0.9047352
H    -1.0460122    3.4022575    0.0127439
H    -2.1006648    4.1028426   -0.8485810
H     5.3161246    0.1911891    0.8421706
```

```
H     4.6161798   -0.8873160   -0.0034029

Guanine: PTE-COSMO-MP2/cc-pVTZ
16
O    -0.2760266   -2.4737758   -0.0145416
N    -0.9501453    1.6284235    0.0397713
N    -1.6339751   -0.6338429    0.0360256
N     2.0239708   -0.4033003   -0.0379211
N     1.4723017    1.7685160   -0.0041198
N    -3.1992135    1.0720871    0.1575833
C     0.6569236   -0.2574852   -0.0086063
C     0.2924955    1.0858764    0.0134098
C    -0.3740075   -1.2478589    0.0013180
C    -1.8888266    0.7115755    0.0550626
C     2.4749390    0.8424343   -0.0340223
H    -2.4205353   -1.2713643    0.0629012
H     1.5849141    2.7717032    0.0041325
H     3.5117826    1.1323576   -0.0520764
H    -3.3786677    2.0363735   -0.0747726
H    -3.8821997    0.4285703   -0.2101341
```

Supporting information for:

Solvent Effects on the Absorption and Fluorescence of Halogen-bonded Ion Pairs

Sarah Karbalaei Khani* and Christof Hättig

Arbeitsgruppe Quantenchemie, Ruhr-Universität, Bochum 44780, Germany

E-mail: Sarah.Karbalaeikhani@ruhr-uni-bochum.de

Table S1: 2-Iodo-imidazolium · OTf: Vertical excitation energies (ω), oscillator strengths (f) and NTOs for the ground state equilibrium structure (S_0-eq) in vacuum at the ADC(2)/def2-TZVPP level.

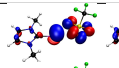
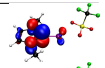
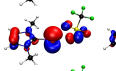
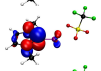
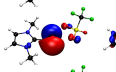
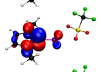
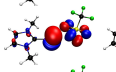
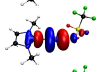
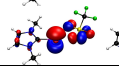
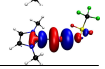
State	ω	f	occ	vir
1	5.22	0.104		
2	5.33	0.221		
3	5.59	0.000		
4	6.06	0.131		
5	6.17	0.136		

Table S2: 2-Iodo-imidazolium cation: Vertical excitation energies (ω), oscillator strengths (f) and NTOs for the ground state equilibrium structure (S_0-eq) in acetonitrile solution at the COSMO-RI-ADC(2)/def2-TZVPP(post-SCF) level.

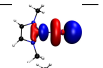
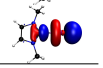
State	ω	f	occ	vir
1	5.06	0.000		
2	5.59	0.388		
3	5.83	0.001		
4	6.72	0.000		
5	6.95	0.000		

Table S3: 2-Iodo-imidazolium cation: Vertical excitation energies (ω), oscillator strengths (f) and NTOs for the S_1 equilibrium structure (S_1-eq) in acetonitrile solution at the COSMO-RI-ADC(2)/def2-TZVPP(post-SCF) level.

State	ω	occ	vir
1	2.58		
2	2.96		
3	3.54		
4	4.38		
5	5.98		

Table S4: 2-Iodo-benzimidazolium · OTf: Vertical excitation energies (ω), oscillator strengths (f) and NTOs for the ground state equilibrium structure (S_0-eq) in vacuum at the ADC(2)/def2-TZVPP level.

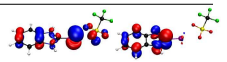
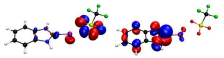
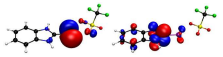
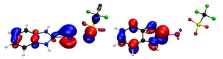
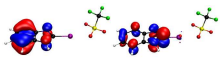
State	ω	f	occ	vir
1	4.55	0.411		
2	4.67	0.073		
3	5.15	0.000		
4	5.33	0.024		
5	5.44	0.061		

Table S5: 2-Iodo-benzimidazolium cation: Vertical excitation energies (ω), oscillator strengths (f) and NTOs for the ground state equilibrium structure (S_0-eq) in acetonitrile solution at the COSMO-RI-ADC(2)/def2-TZVPP(post-SCF) level.

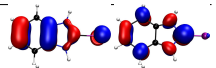
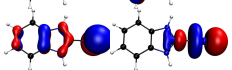
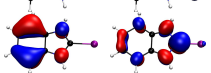
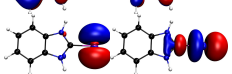
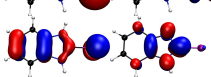
State	ω	f	occ	vir
1	4.73	0.445		
2	5.10	0.000		
3	5.14	0.093		
4	5.71	0.001		
5	5.82	0.429		

Table S6: 2-Iodo-benzimidazolium cation: Vertical excitation energies (ω), oscillator strengths (f) and NTOs for the S_1 equilibrium structure (S_1-eq) in acetonitrile solution at the COSMO-RI-ADC(2)/def2-TZVPP(post-SCF) level.

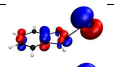
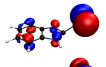
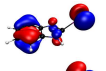
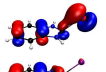
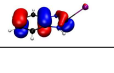
State	ω	occ	vir
1	2.58		
2	2.86		
3	3.17		
4	3.39		
5	5.05		

Table S7: Bis(2-Iodo-benzimidazolium) · Cl: Vertical excitation energies (ω), oscillator strengths (f) and NTOs for the ground state equilibrium structure (S_0-eq) in vacuum at the ADC(2)/def2-TZVPP level.

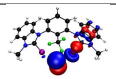
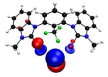
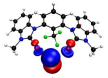
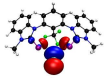
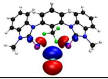
State	ω	f	occ	vir
1	4.30	0.189		
2	4.31	0.197		
3	4.45	0.012		
4	4.48	0.024		
5	4.54	0.003		

Table S8: Bis(2-Iodo-benzimidazolium) dication: Vertical excitation energies (ω), oscillator strengths (f) and NTOs for the ground state equilibrium structure (S_0-eq) in acetonirile solution at the COSMO-ADC(2)/def2-TZVPP(post-SCF) level.

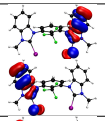
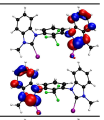
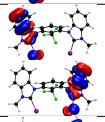
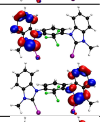
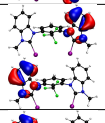
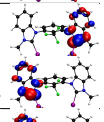
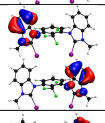
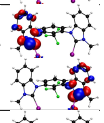
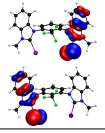
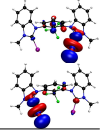
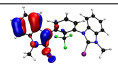
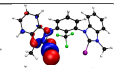
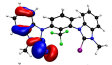
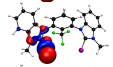
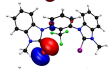
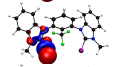
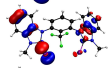
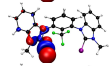
State	ω	f	occ	vir
1	4.54	0.120		
2	4.58	0.605		
3	4.81	0.302		
4	4.83	0.059		
5	5.00	0.004		

Table S9: Bis(2-Iodo-benzimidazolium) dication: Vertical excitation energies (ω), oscillator strengths (f) and NTOs for the S_1 equilibrium structure (S_1-eq) in acetonitrile solution at the COSMO-RI-ADC(2)/def2-TZVPP(post-SCF) level.

State	ω	f	occ	vir
1	2.30	0.061		
2	2.83	0.115		
3	3.25	0.012		
4	3.62	0.087		
5	3.73	0.028	